EVIDENCE FOR ADSORBED HYDROCARBON INTERMEDIATES DURING THE INITIAL STAGES OF CO HYDROGENATION ON IRON

H.P. Bonzel and H.J. Krebs

Institut für Grenzflächenforschung und Vakuumphysik, Kernforschungsanlage Jülich, D-5170 Jülich, Germany

1. Introduction

Surface science techniques have been applied to the study of the surface properties of the transition metals Fe, Co, Ni and Ru /1-12/ and it is natural to extend the same approach to the study of Fischer-Tropsch synthesis (FTS) reactions on the same metal surfaces. However, reaction products in the adsorbed or gaseous phase apparently cannot be detected under vacuum conditions. Therefore, in order to utilize surface analytical techniques for the study of FTS, a combination of a surface analysis ultra-high vacuum system and an atmospheric reaction chamber has to be used, such as pioneered by Somorjai and coworkers /13, 14/.

In this paper we report on the use of such a combination apparatus of novel design with Auger electron (AES) and X-ray photoelectron spectroscopy (XPS) as analytical capabilities and a differential microreactor. The analysis of the reaction products is performed by gas chromatography (GC). Using this system we studied the hydrogenation of CO on polycrystalline iron foils and a Fe(110) single crystal at a total pressure of 100 kPa (= 1 bar ≅ 1 atm) /15/.

2. Experimental

The experimental system, sketched in Fig. 1, consisted of a stainless steel ultra-high-vacuum (UHV) chamber pumped by an ion pump, and an attached sample transfer system containing a small micro-reactor. The UHV chamber shown on the left hand side of Fig. 1 operates at a base pressure of 1×10^{-8} Pa. This system (Leybold-Heraeus) features an ion sputter gun for surface cleaning, an electron gun, X-ray source and high resolution electron spectrometer for Auger electron (AES) and photoelectron (XPS) spectroscopies, and a quadrupole mass spectrometer for residual gas analysis. The sample is either a polycrystalline iron foil about 0.1 mm thick, or a Fe(110) single crystal, with an active area of 0.35 cm^2. It is situated at a cutout portion of a stainless steel rod of 2 cm diameter. This rod serves as a transfer mechanism between UHV chamber, micro-reactor and atmosphere. The Fe sample can be heated resistively up to 1400 K in vacuum and about 900 K in 100 kPa of a H_2/CO mixture. The temperature of the sample is measured by a sheathed Chromel-Alumel thermocouple attached to the underside of the sample.

The micro-reactor of about 4 cm^3 total volume is a small section of the sample transfer system, Fig. 1. A mixture of CO and H_2 was passed continuously through this reactor at a rate of 50 cm^3/min. The partial pressure ratio of CO to H_2 was fixed by adjusting the individual flow rates of these two gases before entering the mixing stage. Partial pressure ratios of CO to H_2 from 1:100 to 1:4 could be easily chosen.

The transfer of the Fe-foil from the UHV system into the micro-reactor was accomplished by pulling the sample rod until the sample was located inside the reactor. The sample could be moved to the atmospheric loading position in a similar way, and also back into the UHV chamber. The transfer time from the reactor into the UHV position including pump-down to 10^{-6} Pa was 45 seconds. The sample rod itself is water cooled such that during heating of the Fe sample inside the micro-reactor no parts other than the sample and the tip of the thermocouple get hot. During the catalytic rate measurements the hydrocarbon products were analyzed by gas chromatography. A 0.5 cm^3 sample (loop volume) of the gas mixture was taken by the GC sample valve and passed over a 8 ft. Porapak Q column. The separated products were analyzed by a flame ionization detector.

The Fischer-Tropsch measurements were carried out in the following way: The

cleaned Fe sample was transfered from UHV into the micro-reactor where a steady state gas flow was already established. As soon as the sample came to a halt, the temperature was raised to the desired value as measured by the thermocouple. From this point on the time was measured and GC samples were taken periodically. At a later time the reaction was stopped by turning off the heating current. About 4 sec later the sample was transfered back to UHV for surface analysis by AES or XPS.

3. Results and Discussion

The measurements of FTS from CO and H_2 on Fe were carried out at a total pressure of 100 kPa (=1 atm) and CO/H_2 ratios of 1:100, 1:20 and 1:4. The temperature range investigated was 460-750 K. In all cases methane was the dominant product and its rate of formation time dependent. In order to check this time dependence, a series of GC reactivity measurements with a cycle of approximately 100 sec was carried out at the same temperature. Three examples of such curves are shown in Fig. 2 for a CO/H_2 ratio of 1:20 and different temperatures where the logarithm of the turnover number for methane is plotted as a function of time. These curves exhibit several interesting features: First, there is a strong rise in the methane rate of formation within the first 40-60 sec after reaching the reaction temperature. This rise signals the start of the reaction, and the apparent delay of about 30 sec prior to the rise (which is more obvious in a linear plot of rate versus time) represents the time it takes for the gas to flow from the reactor to the GC sampling valve. Second, there is a maximum in the rate of methane formation followed by a steady decline; both the position of the maximum and the slope of the decline depend on the temperature of the Fe-foil and the CO/H_2 ratio.

The occurence of the maximum in these curves of Fig. 2 is connected with the known pehnomenon of carbon accumulation on the Fe surface as a function of time /14,15/. The rate of carbon accumulation is faster, the higher the temperature or the higher the ratio of CO/H_2. However, the influence of the rate of carbon accumulation on the rate of CO hydrogenation is complicated due to different kinds of chemically bound carbon. We have measured the relative carbon concentration by XPS and present as an example the data in Fig. 3. This figure shows the carbon (1s) signal at different reaction times for similar experimental conditions as those of Fig. 2. In these experiments the Fe sample was moved into the micro-reactor for reaction for a short time, then into the UHV chamber for surface (AES or XPS) analysis, and back into the reactor for a continuation of the reaction.

The data in Fig. 3 illustrate the rapid increase in surface carbon concentration as a function of the reaction time and also a shift in the binding energy E_B of the C1s level from about 283.9 eV to 284.6 eV. Figure 4a shows the shift in E_B(C1s) versus time for a particular run at 530 K and CO/H_2 = 1:20. Figure 4b shows the corresponding integrated C1s peak area versus time. Note in Figs. 4a and 4b that the initial change in the plotted quantities, i.e. during the first 50 sec, is very rapid followed by a slower increase. It is tempting to associate this behaviour with the presence of different chemical carbonaceous species on the iron surface and with the rate of CH_4 formation.

Therefore we performed a number of experiments which were aimed at identifying the chemical nature of the carbonaceous surface phases after the CO/H_2 reaction. The procedure consists essentially in comparing the carbon Auger peak shapes and C1s binding energies of carbonaceous surface layers of known chemical origin (composition) with those of the surface phases generated by the hydrogenation of CO.

A total of three significantly different carbonaceous layers were observed after the hydrogenation reaction. Figure 5 shows the carbon Auger spectra of these three layers which we call the surface phases I, II and III, respectively. These spectra were obtained for CO/H_2 = 1:20. In comparing the Auger spectra of Fig. 5 one should in particular pay attention to the relative heights of the peaks labelled A, B and C. Other differences can be noted in the negative peak excursion at 270 - 285 eV. These, however, will not be referred to in this paper.

The carbon 1s spectra corresponding to the AES spectra in Fig. 5 showed different binding energies similar to those of Fig. 3. These measured C1s binding energies are listed in Table I together with the data for adsorbed acetylene, segregated carbidic and graphitic carbon.

Table I
C1s Binding Energies

Species	Binding Energy (eV)	
CO	285.9	produced in UHV
C_2H_2	283.9	
carbidic C	283.3	
graphitic C	285.0	
Phase I-CH_x	283.9	after reaction
Phase II	284.2	
Phase III	284.7	

Surface phase I

The C1s binding energies of this surface phase and chemisorbed molecular acetylene are identical within experimental error. This fact suggests that surface phase I is a heavily hydrogenated carbon layer. A comparison of Auger data, Fig. 6, shows, however, a substantial difference for surface phase I and acetylene. On the other hand, a very good simulation of the surface phase I Auger spectrum is obtained when a carbidic surface carbon produced in UHV by heating the sample to 720 K for about 2 min is exposed to C_2H_2 at 400 K for 5 min (2×10^{-5} Pa). It is likely that under these conditions some decomposition of C_2H_2 into CH species will occur /16,17/. We propose therefore that the surface phase I consists mainly of carbidic carbon and CH species.

Surface phase II

At first sight the Auger spectrum of surface phase II, Fig. 5, appears to be identical to the spectrum of carbidic carbon segregated under UHV conditions. However, this is not the case. Figure 7 shows both spectra for a direct comparison, and it can be noted that the peaks B and C of these two spectra are shifted against each other by about 2 eV. The reason for this shift is presumably bonded hydrogen in the case of the surface phase II, as expected from the shift of 0.9 eV for the C1s spectra of UHV carbidic carbon and surface phase II carbon (see Table I). The fact that some hydrogen is necessary in order to generate the Auger peak of surface phase II is illustrated by the following experiment: Fe(110) with segregated carbidic carbon was exposed to C_2H_2 at 475 (2×10^{-5} Pa, 5 min). The Auger spectrum taken subsequently is shown as trace (c) in Fig. 7 and it has features identical to those of the surface phase II spectrum.

The amount of bonded hydrogen in the surface phase II is presumably less than in the CH_x layer, mainly for two reasons: (1) There is no shape change in the Auger peak relative to carbidic carbon, only an energetic shift; (2) the procedure of simulating phase II involves an C_2H_2 exposure at higher temperatures (475 K compared to 400 K for CH_x simulation) facilitating the dehydrogenation of C_2H_2. The surface phase II can thus be characterized as a carbidic carbon layer with bonded hydrogen.

Surface phase III

The carbon Auger peak of the surface phase III has a great similarity with that of graphitic carbon /18,19/. Figure 8 shows an Auger trace of graphitic

carbon on Fe(110) which was segregated to the surface by heat treating the crystal in UHV (625 K, 25 min). Looking at the relative peak heights A, B and C one can notice the same sequence as in the spectrum of phase III. In a procedure equivalent to those discussed in the previous sections we can also produce a phase III type carbonaceous layer by exposing the Fe crystal with carbidic carbon to C_2H_2 at about 580 K (2×10^{-5} Pa, 20 min). The Auger peak of this layer is shown as trace (b) in Fig. 8. For comparison the phase III peak is included as trace (c). All three traces (a) - (c) have very similar shapes but from a closer inspection of the energetic positions of the peaks it is apparent that peak B for the traces (b) and (c) is shifted to lower kinetic energies relative to that of trace (a). Since both layers characterized by (b) and (c) are originating from gas phase reactions involving hydrogen, it is reasonable to assume that this peak shift is indicative of bonded hydrogen.

Hydrogenation behavior

An interesting observation was made when the various carbonaceous layers were subjected to hydrogen atmosphere at elevated temperature. It was seen that the CH_x layer and the hydrogen containing carbidic carbon layer (phases I and II, respectively) could be readily removed by hydrogenation but that the graphitic layer was quite inert towards H_2. An example of a hydrogenation of a mixed phase II/phase III layer is presented in Fig. 9. The total amount of carbon is seen to decrease but the binding energy shift from 284.4 eV to 284.9 eV indicates that carbidic carbon (phase II) is removed and graphitic carbon left behind on the surface.

The fast hydrogenation of surface phases I and II relative to the much slower removal of small amounts of graphitic carbon creates a possibility to separate the different phases in a mixed layer. Experiments of this kind showed that the total amount of carbon plotted for example in Fig. 4b could be broken up into a portion representing CH_x and carbidic carbon and a portion representing graphitic carbon. The first portion plotted versus time yields a maximum at about 30 - 50 sec similar to the maximum in Fig. 2. The second portion, graphitic carbon, increases steadily with time. We conclude that the maximum in reactivity is linked to the maximum in CH_x and carbidic carbon on the surface whereas the graphitic carbon acts as an inhibitor on the methanation as well as the Fischer-Tropsch reaction.

4. Conclusions

1. Layers of (UHV segregated) carbidic and graphitic carbon, molecularly adsorbed CO and C_2H_2 can be fairly well characterized by their respective carbon Auger peak fine structure and C(1s) binding energies.

2. Carbonaceous layers deposited by the CO hydrogenation reaction at 1 bar were analyzed by AES and XPS and could be classified by a comparison of carbon Auger line shapes and C(1s) binding energies with those of layers of known chemical composition.

3. A carbonaceous layer of particular interest formed in the initial phase of CO hydrogenation on Fe(110) was found to correspond to heavily hydrogenated carbidic carbon, most likely a CH_x phase. This phase is suggested to consist mostly of CH radicals.

4. The CH_x phase and carbidic carbon can be easily removed from the surface by hydrogenation; graphitic carbon is quite stable towards hydrogen at 1 bar and elevated temperatures.

5. The maximum in the time dependent methanation rate correlates with the maximum in CH_x and carbidic carbon; these latter species are important intermediates for the formation of methane and probably higher molecular weight products.

References

/1/ K. Kishi and M.W. Roberts, J. Chem. Soc. Faraday Trans. I 71 (1975) 1715

/2/ R.W. Joyner and M.W. Roberts, J. Chem. Soc. Faraday Trans. I 70 (1974) 1819

/3/ K.Y. Yu, W.E. Spicer, I. Lindau, P. Pianetta and S.F. Lin, Surface Sci. 57 (1976) 157

/4/ C.R. Brundle, IBM J. Res. Develop 11 (1978) 235

/5/ G. Brodén, G. Gafner and H.P. Bonzel, Appl. Phys. 13 (1977) 333

/6/ T.N. Rhodin and C.F. Brucker, Solid State Comm. 23 (1977) 275

/7/ W. Erley and H. Wagner, Surface Sci. 74 (1978) 333

/8/ G. Wedler, K.G. Colb, G. McElhiney and W. Heinrich, Appl. Surface Sci. 2 (1978) 30

/9/ K.A. Prior, K. Schwaha and R.M. Lambert, Surface Sci. 77 (1978) 193

/10/ R. Ku, N.A. Gjostein and H.P. Bonzel, Surface Sci. 64 (1977) 465

/11/ H.P. Bonzel and T.E. Fischer, Surface Sci. 51 (1975) 213

/12/ K.J. Singh and H. Grenga, J. Catal. 47 (1977) 328

/13/ B.A. Sexton and G.A. Somorjai, J. Catal. 46 (1977) 167

/14/ D.J. Dwyer and G.A. Somorjai, J. Catal. 52 (1978) 291 and J. Catal. 56 (1979) 249

/15/ H.J. Krebs, H.P. Bonzel and G. Gafner, Surface Sci. (to be published)

/16/ C.F. Brucker and T.N. Rhodin, J. Catal. 47 (1977) 214

/17/ T.N. Rhodin, C.F. Brucker and A.B. Anderson, J. Catalysis (to appear)

/18/ J.P. Coad and J.C. Rivière, Surface Sci. 25 (1971) 609

/19/ C.C. Chang, Surface Sci. 25 (1971) 53

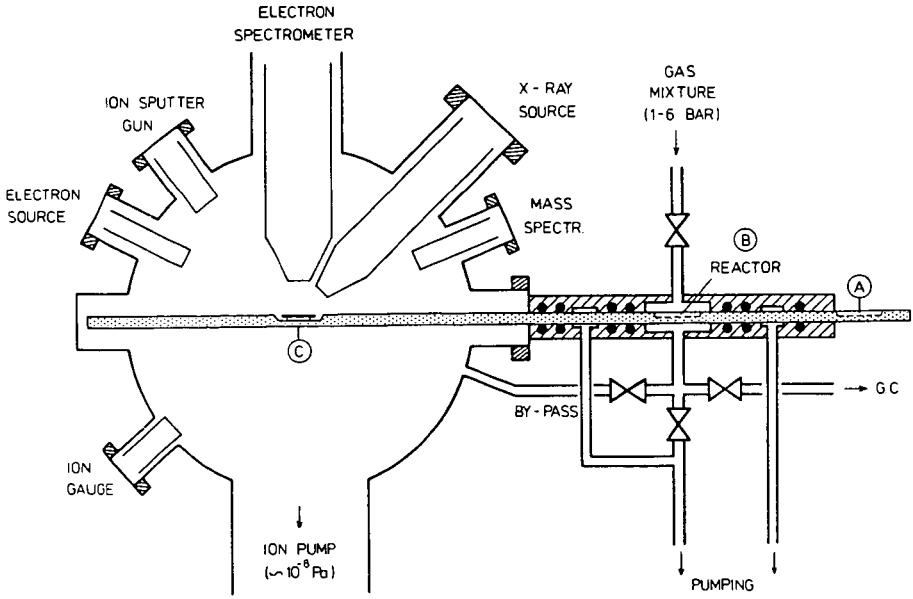

Figure 1: Schematic of UHV apparatus with attached sample transfer system and micro-reactor for catalytic rate measurements. The sample, located at the surface analysis position "C" in the center of the UHV chamber, can be moved by pulling the stainless steel rod, to the position "B" (reactor for chemical reaction) or position "A", the atmospheric loading position.

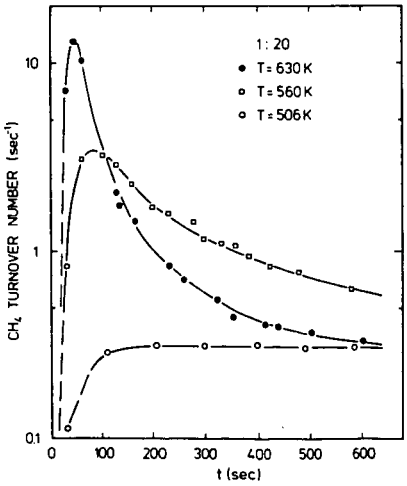

Figure 2: Semilog-plot of methane turnover number versus time for a CO/H_2 ratio of 1:20.

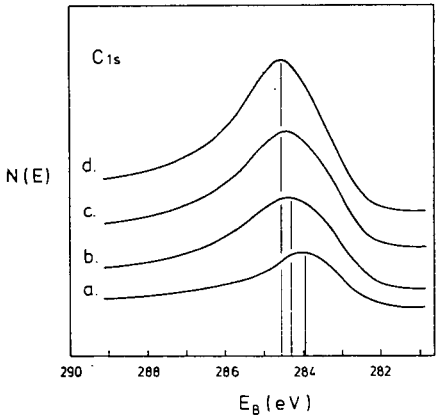

Figure 3: Carbon 1s XPS data after reaction, CO/H_2 = 1:20, T = 530 K, reaction times a) 3 sec, b) 23 sec, c) 83 sec and d) 600 sec. Note shift in maximum.

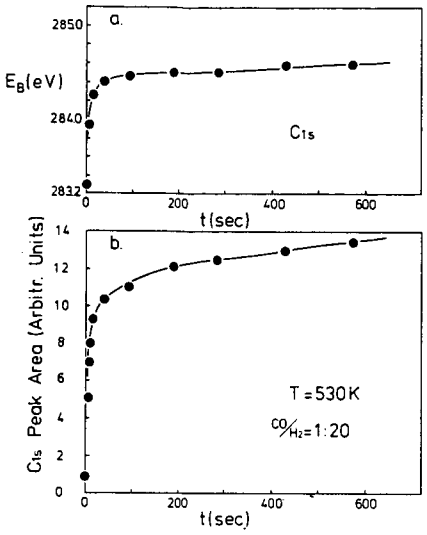

Figure 4: Same reaction data as in Fig. 3. (a) C1s binding energy as a function of reaction time. (b) Integrated C1s peak area (as a measure of surface carbon concentration) versus reaction time.

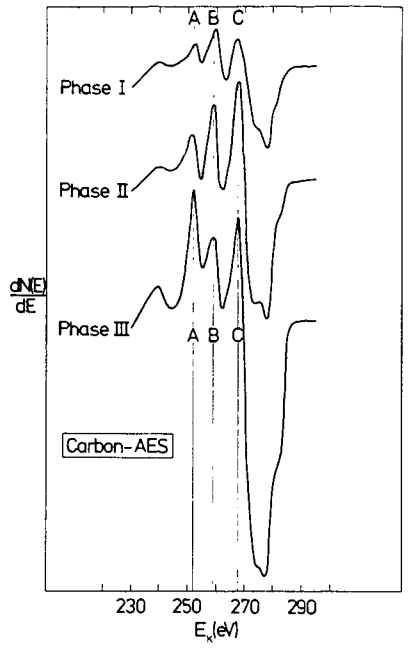

Figure 5: Carbon Auger spectra of the three carbonaceous surface phases formed after the CO/H_2 reaction at 1 bar and CO/H_2 = 1:20. Reaction conditions: Surface phase I - T = 565 K, t = 15 sec; surface phase II - T = 615 K, t = 15 sec; surface phase III - T = 615 K, t = 90 min.

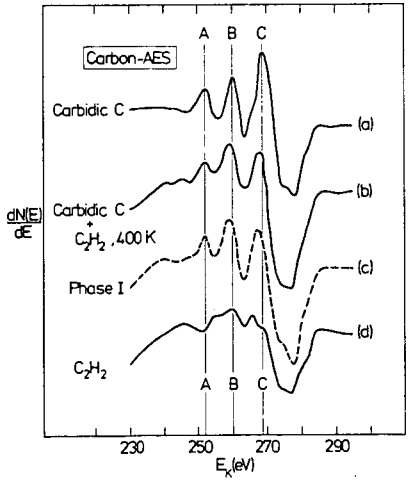

Figure 6: Carbon Auger spectra. (a) After heating the Fe(110) crystal in UHV at 720 K for about 3 min; (b) after exposure of the carbidic carbon on Fe (110) to 2×10^{-5} Pa C_2H_2 for 5 min at 400 K; (c) after reaction at 1 bar; (d) after exposing the clean Fe(110) crystal to C_2H_2 at room temperature (2×10^{-5} Pa, 5 min).

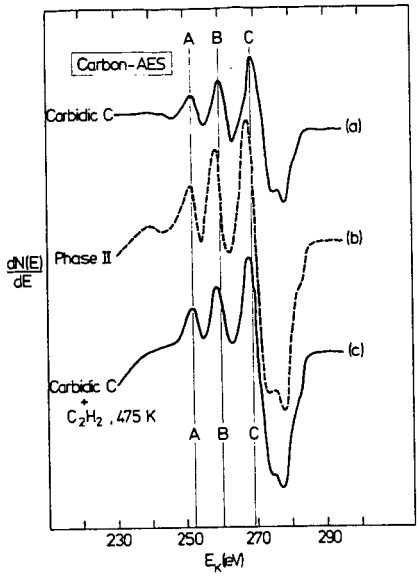

Figure 7: Carbon Auger spectra. (a) Fe(110) crystal was heated in UHV to 720 K for about 3 min; (b) after CO/H_2 reaction at 1 bar; (c) after exposing the surface produced under (a) to C_2H_2 at 475 K (2×10^{-5} Pa, 5 min).

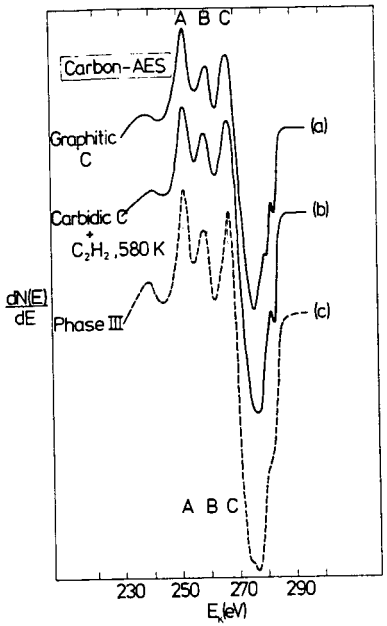

Figure 8: Carbon Auger spectra. (a) Fe(110) crystal was heated in UHV to 625 K for about 25 min; (b) after exposure of the Fe surface to C_2H_2 at 580 K (2×10^{-5} Pa, 20 min); after CO/H_2 reaction at 1 bar.

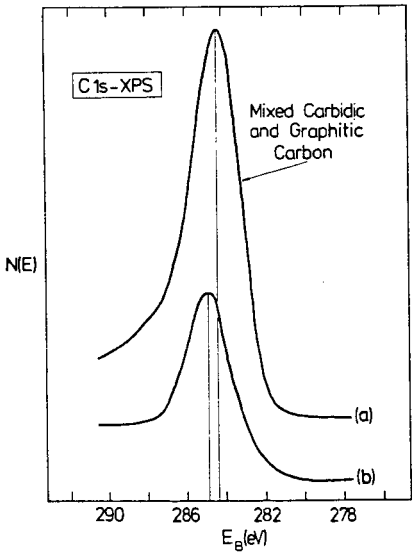

Figure 9: C1s spectra. (a) After CO/H_2 reaction at 1 bar and 630 K (CO/H_2 = 1:20, 10 min reaction time); (b) after hydrogenation of the surface under (a) at 1 bar, 630 K for 60 min.

CO HYDROGENATION OVER RHODIUM FOIL AND SINGLE CRYSTAL CATALYSTS: CORRELATIONS OF CATALYST ACTIVITY, SELECTIVITY, AND SURFACE COMPOSITION

D. G. Castner,* R. L. Blackadar, and G. A. Somorjai

Materials and Molecular Research Division, Lawrence Berkeley Laboratory
and Department of Chemistry, University of California,
Berkeley, California 94720

*Present address: Chevron Research Company, P.O. Box 1627, Richmond,
California,94802

ABSTRACT

CO hydrogenation at 6 atm over polycrystalline Rh foil and single crystal Rh (111) catalysts was investigated in a system where the surface structure and composition of the catalysts could be characterized both before and after the reaction. The reaction conditions (H_2:CO ratio, reaction temperature, and surface pretreatment) were systematically varied to determine the optimum conditions for formation of oxygenated hydrocarbons. Initially clean Rh catalysts showed no structure sensitivity, primarily produced methane (90 wt%) at an initial rate of 0.15 molecules $site^{-1}sec^{-1}$ at 300°C, and did not produce detectable amounts of oxygenated hydrocarbons. Preoxidation of the Rh catalysts (800 Torr O_2, 600°C, 30 min.) resulted in dramatically increased initial rates, a larger fraction of higher molecular weight hydrocarbons, some structure sensitivity, and formation of methanol, ethanol, and acetaldehyde. The different Arrhenius parameters over the clean and preoxidized foils indicate that the methanation mechanism is different on these two surfaces. Decreasing the reaction temperature or H_2:CO ratio increased the C_2H_4 to C_2H_6 ratio and shifted the product distribution towards higher molecular weight hydrocarbons.

INTRODUCTION

Reaction of H_2-CO mixtures over the Group VIII metals usually yields a wide range of products, including alkanes, alkenes, and oxygenated hydrocarbons. In recent studies,[1,2] Rh supported on SiO_2 showed a unique selectivity for production of the two-carbon oxygenated species acetaldehyde, acetic acid, and ethanol. Similar selectivity was shown at 1 atm on catalysts prepared by depositing Rh clusters on basic metal oxides.[3,4] This contrasts with results for Rh foil[5] and Rh supported on Al_2O_3,[6] over which no oxygenated hydrocarbons were formed at 1 atm. A need therefore exists for studying CO hydrocarbons over well-characterized Rh at elevated pressures, under a variety of reaction conditions and surface pretreatments, to determine the conditions necessary for oxygenated product selectivity. We have measured reaction rates and product distributions over clean and preoxidized Rh foil and Rh(111) crystal surfaces at 6 atm and 250-400°C, with H_2:CO ratios of 3:1 to 1:3. Surface structure and chemical composition were characterized using low-energy electron diffraction (LEED) and Auger electron spectroscopy (AES). The results will be compared to previous results on Rh catalysts.

EXPERIMENTAL

The apparatus and technique employed in these experiments are described elsewhere.[5,7] Briefly, the reaction cell is located inside an ultra-high vacuum (UHV) chamber to allow ion sputter cleaning and surface characterization by LEED and AES immediately before and after reaction. After closing the cell, first the H_2 (99.9995% purity) and then the CO (99.99% purity,

Fe and Ni carbonyls removed in a dry ice trap) were admitted and circulated in the closed loop. Allowing a few minutes for mixing at room temperature, the reaction was then started by heating the Rh sample resistively. The buildup of products was monitored by a gas chromatograph using a Chromasorb 102 column and flame ionization detector. The reaction was stopped after times ranging up to 3 hr, by cooling to room temperature and pumping down to UHV, to measure changes in surface composition.

For preoxidized samples, the surface was heated to 600°C in 1 atm O_2 for 30 minutes inside the reaction cell. During this treatment, an epitaxial oxide was formed, and oxygen also dissolved into the bulk. The oxide layer was amorphous and had an O_{510}/Rh_{302} AES peak intensity ratio of 0.5 to 0.6, although ratios up to 2.6 were obtained by oxidizing carbon-covered surfaces.

The initial turnover numbers (TN) were determined from a least squares fit to the initial slope of the product concentration vs. time curves. In the calculation, the atom density of the Rh(111) surface (1.6×10^{15} atoms cm^{-2}) was used as the active site density. The same figure was also used for preoxidized samples, thus ignoring possible increases in surface area as well as a reduced Rh surface density on the oxide.

RESULTS

Fig. 1 shows the buildup of products during a typical run on clean Rh at 300°C and $3H_2$:1CO. Results on the clean Rh foil and Rh(111) were identical. Under the above conditions, CH_4 was the main product (90 wt%) with initial TN 0.15 molecules $site^{-1} sec^{-1}$. C_2 and C_3 hydrocarbons were formed, but no oxygenated hydrocarbons were detected. All rates of product formation, ex-

cept C_2H_6, declined over the course of three hours. The AES spectra before and after reaction, in Fig. 2, show that small amounts of S and Cl and a monolayer of C built up on the surface during CO hydrogenation. AES peak intensities for these impurities remained nearly constant after the first 30 minute minutes, although the reaction rates continued to decline. The proximity of the Rh_{256} and Rh_{302} peaks prevented AES lineshape analysis to determine whether the carbon state was changing during this time.

Preoxidation of the Rh(111) crystal (see Figs. 3 and 4) greatly increased the initial TN's, shifted product distribution slightly to higher molecular weight, and resulted in the appearance of the oxygenated products methanol, ethanol, and acetaldehyde. The marked decrease in TN's during the first 30 minutes coincided with rapid loss of the epitaxial oxide. After this period, the near-surface oxygen concentration reached a low steady-state value, as shown in Fig. 5. Methane was still formed at a higher rate on the steady-state surface with oxygen than on the clean surface. Oxygenated products were formed during the entire three hours. Decreasing the temperature led to a further shift toward higher molecular weight and an increase in the C_2H_4 to C_2H_6 ratio, as shown in Figs. 6 and 7. During the CO-rich reactions acetaldehyde was the only oxygenated hydrocarbon produced. Also, two to four monolayers of carbon were deposited on the preoxidized Rh during CO-rich runs at 300°C, probably accounting for the increased poisoning rate (Fig. 6).

Results for preoxidized Rh foil were similar to those for preoxidized Rh(111) except for a small structure sensitivity shown in a lower CH_4 TN and larger C_2H_4 to C_2H_6 ratio. Also, ethanol formed a smaller fraction of the oxygenated products. In CO-rich runs, more carbon was deposited on the preoxidized foil than on preoxidized Rh(111), giving a faster poisoning rate.

The activation energy for methanation was found to be 12 kcal/mole on preoxidized foil, half the value (24 kcal/mole) found on clean Rh foil.[5]

DISCUSSION

Preoxidation of the Rh surfaces markedly changes their activity and selectivity, indicating that the chemical environment of the Rh atoms is important in determining their catalytic properties. This is consistent with the variability of supported Rh catalysts depending on their preparation.[1-4] The CH_4 formation rate depends directly on the oxygen concentration in the near-surface region, as shown in Table I. The lowest initial CH_4 production rate is obtained during CO hydrogenation over clean catalysts and the highest over the catalyststwith an epitaxial oxide. An intermediate value is given by peroxidized surface which are flashed in vacuum prior to CO hydrogenation,[5] resulting in a low near-surface oxygen concentration.[10] The fact that CO_2 hydrogenation gives a higher CH_4 TN than CO hydrogenation under the same reaction conditions suggests that CO_2 oxidizes the catalysts during hydrogenation. CO_2 has been shown to dissociatively adsorb on Rh surfaces,[8,9,11] and an oxygen AES signal was detected in the early stages of CO_2 hydrogenation over Fe.[12]

The changes in Arrhenius parameters, shown in Table II, strongly indicate that a change in mechanism is the cause of the increased CH_4 TN on preoxidized surfaces. In particular, a simple effect of surface area or active site density can be ruled out. The activation energy on the oxygen-treated surface is 12kcal/mole, half that on the clean surface, 24 kcal/mole,[5] and within experimental error of the value for CO_2 hydrogenation on clean Rh. This again

suggests oxidation by the CO_2. Preexponential factors show a similar trend.

The effect of increasing pressure from 1 atm [5] to 6 atm (this study) was minor. The C_2H_4 to C_2H_6 ratio was smaller, presumably the result of the higher H_2 partial pressure increasing olefin hydrogenation. Also, the poisoning observed in this study at 6 atm was not observed at 1 atm. Possibly the effect of S and Cl impurities, or deactivation of C overlayers, is enhanced at high pressure. Behavior at 6 atm is in other respects similar to that at 1 atm[5] and agrees well with findings for supported Rh catalysts which produce hydrocarbons.[1,2,6] This indicates that metallic Rh or a complex of Rh and C is active in hydrocarbon formation, but that these surfaces do not provide the conditions necessary for oxygenated hydrocarbon formation, suggesting that a higher Rh oxidation state may be crucial to this process. Production of oxygenated hydrocarbons after the near-surface oxygen concentration reaches steady-state indicates that CO is the source of oxygen in these products, but bulk oxygen diffusing into the near-surface reagion is another possible source. We are undertaking isotopic labeling studies to resolve this question.

Varying the temperature and H_2:CO ratio produces results that follow the trends predicted for a mixture of products in equilibrium,[13] that is, higher molecular weight and more unsaturated or oxygenated products are favored at low temperature, and the hydrogen-poor species C_2H_4 and CH_3CHO are favored at low H_2:CO ratio. Thus thermodynamics seems to have relevance even though the overall CO-H_2 conversion to any of the products is far from equilibrium in our experiments. A possible explanation is that an initial slow step in the mechanism is followed by rapid combination and partial equilibration of hydrocarbon fragments.

REFERENCES

1. M. Ichikawa, Bull. Chem. Soc. Japan 51, 2268 (1978).
2. M. Ichikawa, Bull. Chem. Soc. Japan 51, 2273 (1978).
3. M. M. Bhasin, W. J. Bartley, P. C. Ellgen, and T. P. Wilson, J. Catal. 54, 120 (1978).
4. P. C. Ellgen, W. J. Bartley, M. M. Bhasin, and T. P. Wilson, 175th ACS Meeting, Los Angeles, Calif., Div. Petrol. Chem. Preprints 23, 616 (1978).
5. B. A. Sexton and G. A. Somorjai, J. Catal. 46, 167 (1977).
6. M. A. Vannice, J. Catal. 37, 449 (1975).
7. D. W. Blakely, E. I. Kozak, B. A. Sexton, and G. A. Somorjai, J. Vac. Sci. Technol. 13, 1091 (1976).
8. D. G. Castner, B. A. Sexton, and G. A. Somorjai, Surface Sci. 71, 519 (1978).
9. D. G. Castner and G. A. Somorjai, Surface Sci. 83, 60 (1979).
10. D. G. Castner and G. A. Somorjai, LBL-9288.
11. L. H. Dubois and G. A. Somorjai, LBL-8976 and LBL-9280.
12. D. J. Dwyer and G. A. Somorjai, J. Catal. 52, 291 (1978).
13. D. J. Dwyer, K. Yoshida, and G. A. Somorjai, 175th ACS Meeting, Los Angeles, Calif., Div. Petrol. Chem. Preprints 23, 521 (1978).

Table I. Comparison of initial methanation TN for CO and CO_2 hydrogenation in a batch reactor at 300°C over Rh and Fe catalysts. Methane TN is in molecules $site^{-1} sec.^{-1}$

Catalyst	Reaction Conditions	Surface Pretreatment	Initial CH_4 TN at 300°C	Ref.
Rh foil	0.92 atm $3H_2:1CO$	clean	0.13	(5)
		preoxidized[a]	0.33	(5)
Rh foil	0.92 atm $3H_2:1CO_2$	clean	0.33	(5)
		preoxidized[a]	1.7	(5)
Rh foil	6 atm $3H_2:1CO$	clean	0.15	this study
		preoxidized[b]	1.7	
Rh(111)	6 atm $3H_2:1CO$	clean	0.15	this study
		preoxidized[b]	4.6	
Fe foil	6 atm $3H_2:1CO$	clean	1.9	(12)
		preoxidized[c]	18.7	(12)
Fe foil	6 atm $3H_2:1CO_2$	clean	10.9	(12)

(a) 15 min at 300°C in 700 Torr O_2, then heated to 1000°C in vacuum.

(b) 30 min at 600°C in 800 Torr O_2.

(c) 20 min at 300°C in 4 atm O_2.

Table II. Comparison of the Arrhenius methanation parameters ($TN = A\,e^{-E_a/RT}$) for CO and CO_2 hydrogenation over polycrystalline Rh foils. Units for TN and A are molecules $site^{-1}sec^{-1}$. E_a is in kcal/mole.

Reaction Conditions	Surface Pretreatment	CH_4 TN at 300°C	A	E_a	Ref.
0.92 atm $3H_2$:1CO	clean	0.13 ± 0.03	10^8 (a)	24 ± 3	(5)
0.92 atm $3H_2$:1CO_2	clean	0.33 ± 0.05	10^5 (a)	16 ± 2	(5)
6 atm $3H_2$:1CO_2	preoxidized(b)	1.7 ± 0.4	10^5	12 ± 3	this study

(a) determined from data in Ref. (5).
(b) 30 min. at 600°C in 800 Torr O_2.

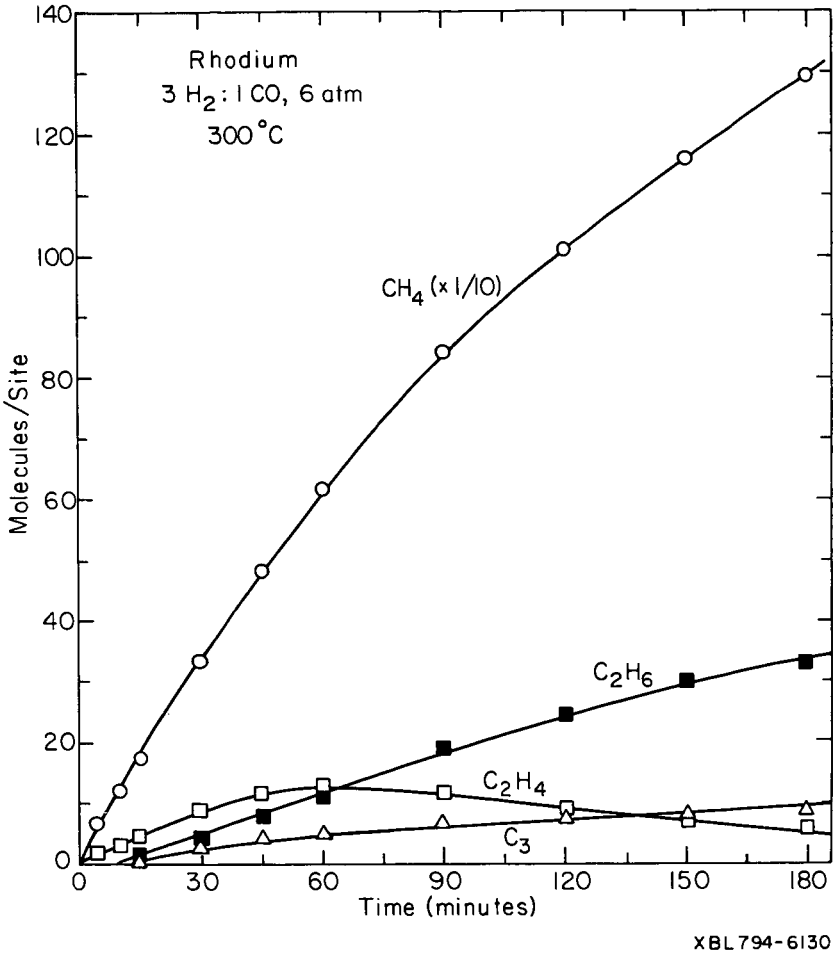

Fig. 1. Buildup of the C_1 to C_3 hydrocarbon products during CO hydrogenation over initially clean Rh foil or Rh(111) catalysts at 6 atm, 300°C, and $3H_2$:1CO.

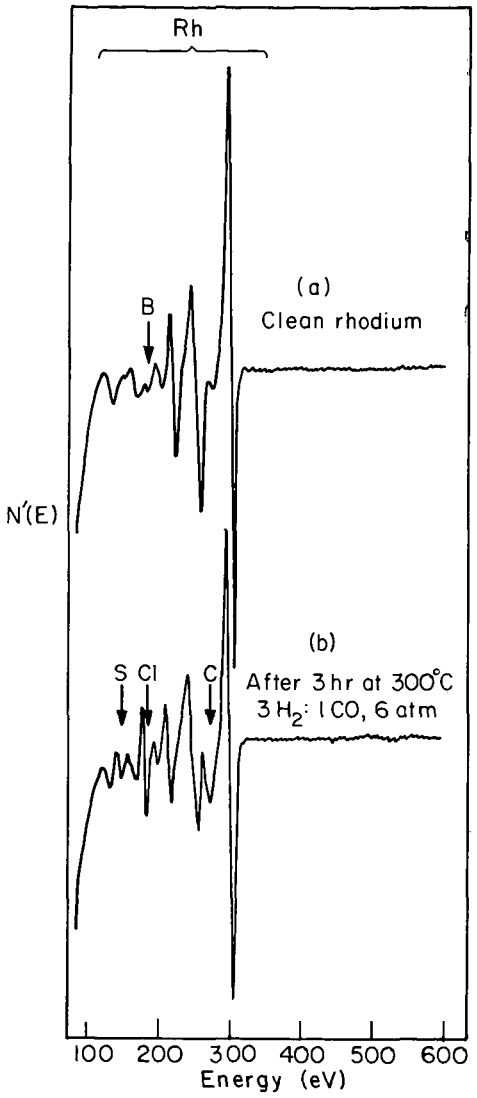

XBL 797-6655

Fig. 2. AES spectra of the initially clean Rh catalysts (a) before and (b) after 3 hr of CO hydrogenation at 6 atm, 300°C, and $3H_2$:1CO.

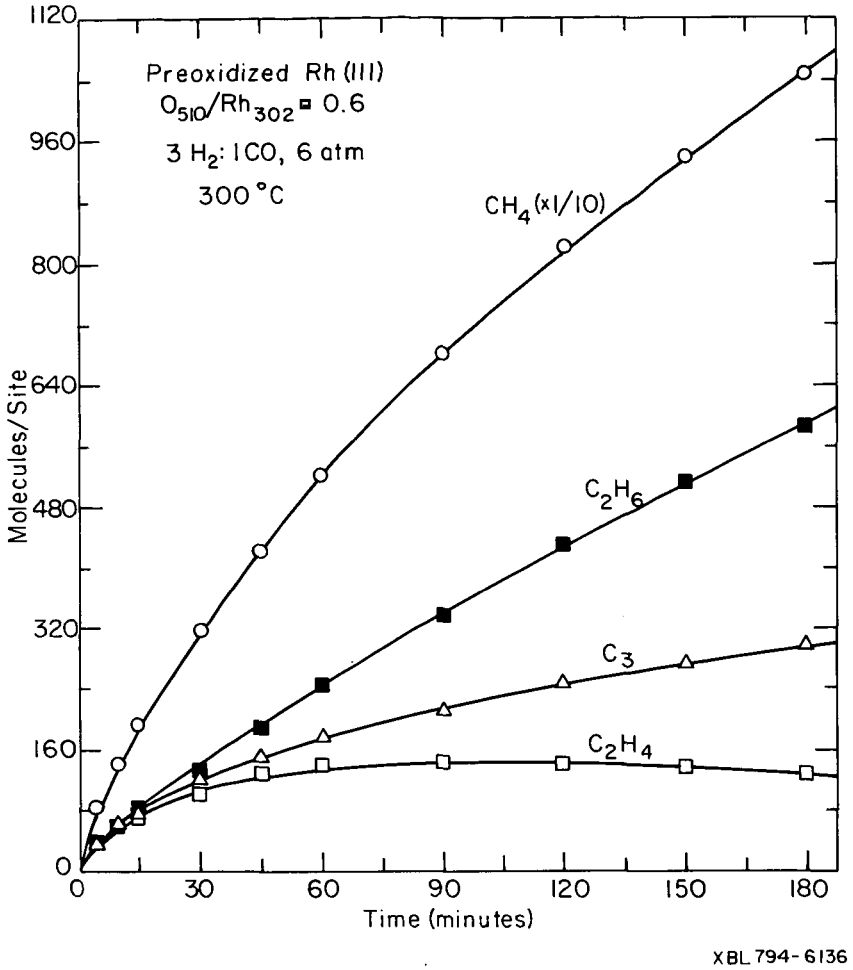

Fig. 3. Buildup of the C_1 to C_3 hydrocarbon products during CO hydrogenation over a preoxidized Rh(111) catalyst at 6 atm, 300°C, and $3H_2$:1CO.

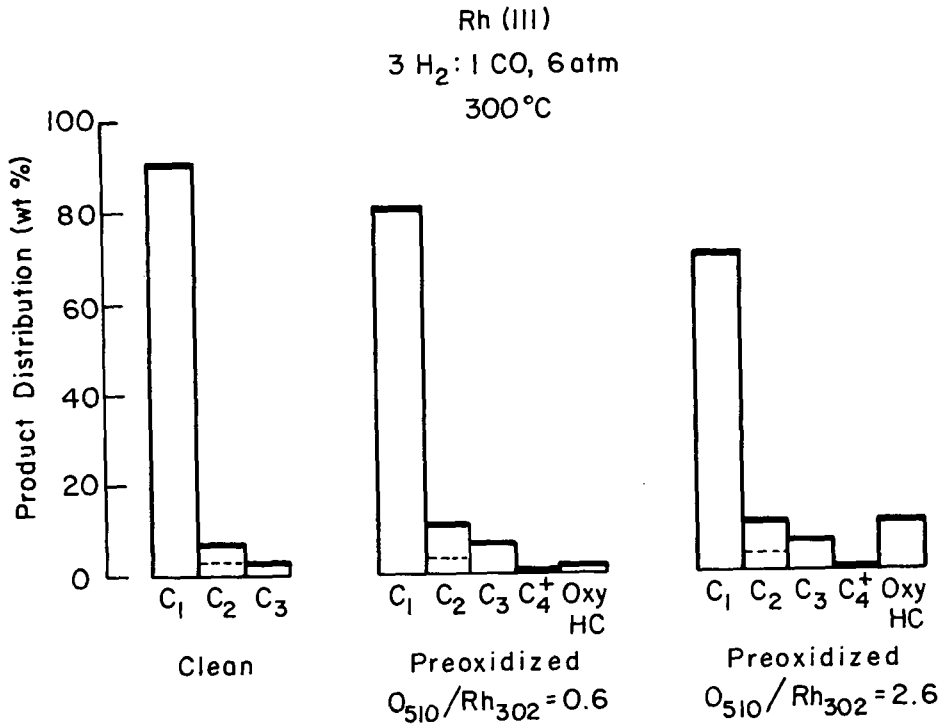

Fig. 4. The product distributions in weight percent after 2 hr of CO hydrogenation over pretreated Rh(111) catalysts at 6 atm, 300°C, and $3H_2$:1CO. Oxy HC is the sum of the CH_3OH, CH_3CH_2OH, and CH_3CHO fractions. In the C_2 fraction the areas above and below the broken line represent the C_2H_6 and C_2H_4 fractions.

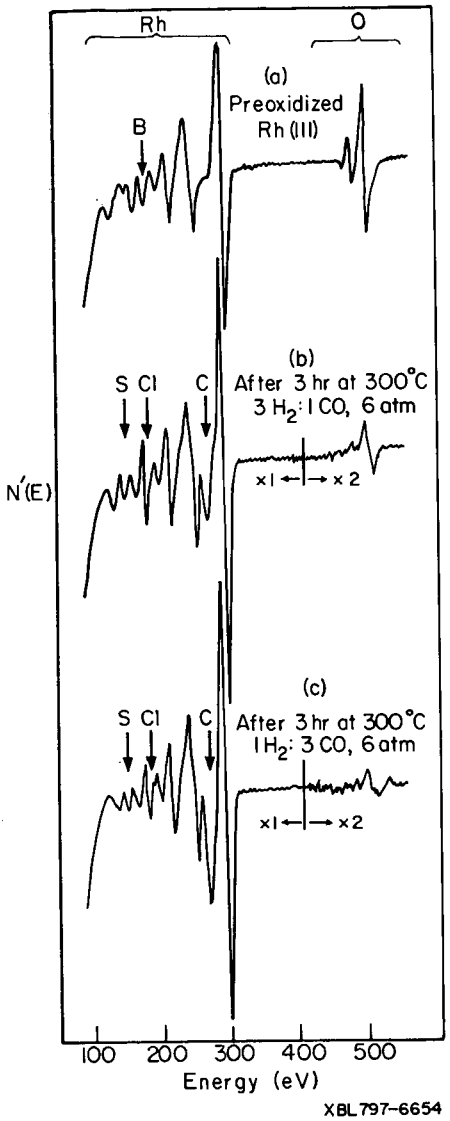

Fig. 5. AES spectra of the preoxidized Rh(111) catalyst (a) before and (b) after 3 hr of CO hydrogenation at 6 atm, 300°C, $3H_2$:1CO, or (c) after 3 hr of CO hydrogenation at 6 atm, 300°C, $1H_2$:3CO.

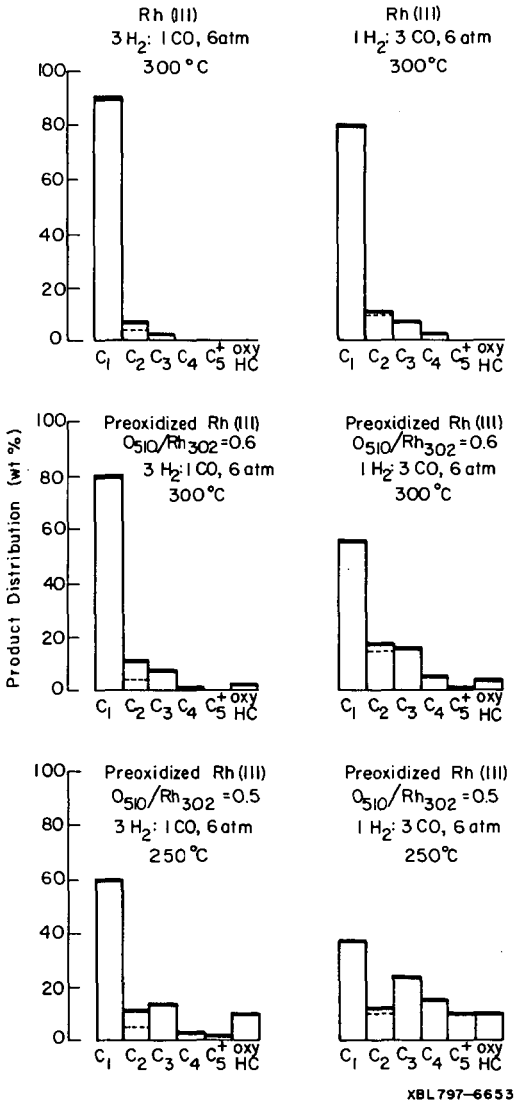

Fig. 6. Buildup of C_1 to C_4 hydrocarbon products during CO hydrogenation over a preoxidized Rh(111) catalyst at 6 atm, 250°C, and $1H_2$:3CO.

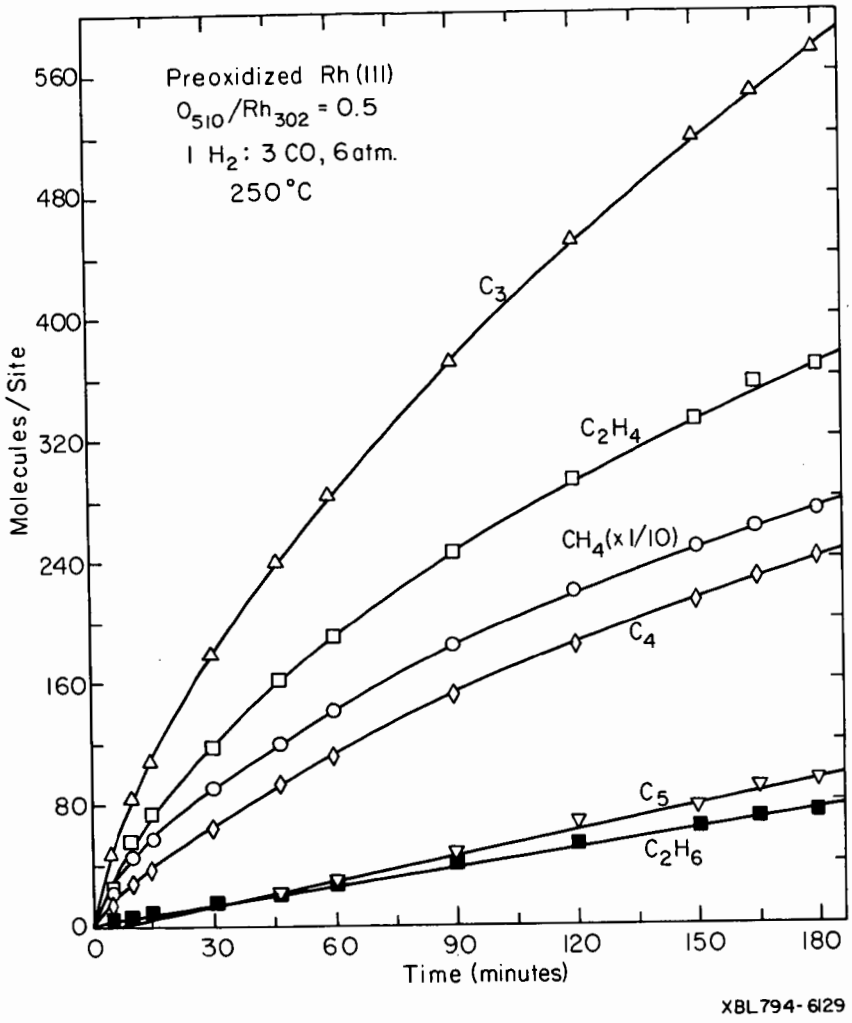

Fig. 7. The product distributions in weight percent after 2 hr of CO hydrogenation over pretreated Rh(111) catalysts at various reaction conditions. See Fig. 4 for explanation of symbols.

CATALYTIC METHANATION OVER SINGLE CRYSTAL NICKEL AND RUTHENIUM: REACTION KINETICS ON DIFFERENT CRYSTAL PLANES

R. D. Kelley and D. Wayne Goodman

Surface Science Division

National Bureau of Standards

Washington, D.C. 20234

Introduction

A specially designed ultrahigh vacuum system has been used to study the kinetics of the hydrogenation of CO over low surface area, single crystal catalysts. In a recent publication (1), we have reported reaction rate measurements for a Ni(100) catalyst and compared those results with kinetic data, derived from the literature, for small particle Ni supported on Al_2O_3. There was remarkable agreement between the two catalyst systems in regard to specific reaction rates (the rate normalized to the number of surface metal atoms), the activation energy, and the product distribution. In the present report, we compare reaction rates measured on two crystal planes of Ni--the (100) and the close-packed (111)--and two crystal planes of Ru--the zig-zag, open (110) and the close packed (001). We also report the variation of the reaction rate and the surface carbon concentration with total pressure and with the H_2:CO ratio. The surface carbon concentration (an active "carbidic" carbon species) varies with the total pressure and with the reactant gas ratio. A striking correlation has been found between the surface carbide level and the catalytic reaction rate.

Experimental

The apparatus used for these studies consists of two connected ultrahigh vacuum chambers--one for surface analysis (Auger Electron Spectroscopy (AES)) and the other suitable for high pressure catalytic rate studies. A detailed description of the apparatus, the crystal cleaning procedure, and the techniques used to obtain kinetic rate data have been published (1). It should be noted that the number of metal surface atoms exposed to the reactant gas (used to normalize reaction rate data) is derived from the geometrical surface area of the annealed crystal and the appropriate surface atom density [Ni(100): 1.62×10^{15} atoms/cm^2; Ni(111): 1.86×10^{15} atoms cm^{-2}; Ru(110): 1.00×10^{15} atoms/cm^2; Ru(001): 1.58×10^{15} atoms cm^{-2}]. The Ru samples were cleaned using high temperature oxidation at 10^{-6} torr O_2 followed by heating in vacuum to 1570K. (2)

Results and Discussion

The observation (1) that the rate of the reaction

$$3\ H_2 + CO \rightarrow CH_4 + H_2O$$

(expressed as CH_4 molecules/surface site/sec) measured over a low surface area, single crystal catalyst is nearly identical to that measured over a supported small particle Ni catalyst (2) is a strong indication that there is little reactivity difference between those crystal planes commonly found in polycrystalline material (i.e., the low index planes). This expectation is confirmed in the data presented in Fig. 1, which is a plot of the specific rate (or turnover number) of CH_4 production versus the reciprocal temperature. The similarity between the open (100) and the close-packed (111) crystal planes of Ni is evident in both the value of the specific rate and the activation energy (24.7 kcal $mole^{-1}$ derived from the Ni(100) data). For comparison three sets of data for nickel (supported on alumina) catalysts are replotted from the literature. Thus for the H_2 + CO reaction over Ni, there is essentially no variation in the reaction rate as the catalyst changes from small metal particles to bulk single crystal planes.

Analysis of an active crystal catalyst surface with AES indicates a low level of a carbon species and the absence of oxygen (1). Measurements of the rate of production of this surface carbon species (in pure CO) and the rate of reaction (in pure H_2) have indicated that both processes (i.e., the production and the removal of the surface carbon species) proceed at very similar rates. (3) A mechanism for the H_2 + CO reaction consistent with the kinetic data and the finite surface carbon level during reaction was developed which involves the hydrogenation of an active carbon species formed from the dissociation of CO. Fig. 2a shows the changes in the reaction rate as the pressure is increased from 1-120 torr at a fixed H_2:CO ratio. At low temperatures the rates fall on the same straight line at all pressures. As the temperature is increased a deviation from linearity is seen--the higher the pressure the higher the deviation temperature. Accompanying this non-linear rate behavior is an increase in the active carbon level on the surface of the catalyst crystal. We have proposed that this behavior (the departure from the linearity of the rate in Fig. 2a and the accompanying increase in the surface carbon level) is due to a decrease in the surface coverage of hydrogen and thus a decrease in the rate of hydrogenation of surface carbon. Fig. 2b shows similar data for a Ru(110) crystal. The variation of the reaction rate with pressure is very similar to the Ni(100) crystal--i.e., a departure from linearity of the rate and accompanying this departure an increase in the surface carbon level (see reference (4) for details of the AES measurement of carbon on Ru). We presume that the explanation of this behavior is the same offered for the Ni crystal. In fact, since the binding energy of H on Ru is lower than on Ni (2) the deviation from linearity should be expected at a lower temperature. This is particularly evident in the 1 torr data of Fig. 2a and 2b.

In addition to the rate data for the Ru(110) crystal, Fig. 2b also contains limited data for the basal plane of ruthenium, Ru(001). While the comparison is limited, it is clear that the H_2 + CO reaction is quite similar in regard to the specific reaction rate and the activation energy for these two crystal planes of ruthenium.

The data of Fig. 2 indicate that the effect of the total pressure on the reaction rate is dependent on the temperature at which the measurements are made. Fig. 3 shows the variation of the specific rate as a function of pressure at two temperatures over a Ni(100) catalyst with the $H_2/CO = 4$. Many authors (5) have fitted reaction rate variation with pressure to a power rate law of the form

$$R_{CH_4} = A\, e^{-E/RT}\, P_{H_2}^{x}\, P_{CO}^{y} \qquad 1)$$

The exponents, fitted from experimental data, have been used to derive information about the reaction mechanism (6). It is clear from Fig. 3 that, while power rate law exponents can be derived and used to scale rate data at fixed reaction conditions, such exponents are very sensitive to the reaction temperature. It is doubtful that any fundamental significance can be attached to values of the exponents derived at one temperature.

We have attempted to determine the dependence of the methanation rate on the partial pressure of both H_2 and CO. In conducting this study, we have measured the rate of CH_4 production with H_2:CO ratios which varied from 0.1 to 1000 and with a total pressure which varied from 1 to 1500 torr. The results of this study indicate that even at one temperature a power rate law such as equation 1 is not adequate to describe the partial pressure dependence of the reaction rate. However, <u>all</u> reaction rate data measured over a Ni(100) catalyst can be correlated, on a smooth curve, with the concentration of "active" carbon on the Ni surface. Figure 4 is a plot of the measured carbon surface coverage and the measured specific reaction rate for various H_2:CO ratios and total pressures at a temperature of 625K. It should be noted that the reaction rates are steady-state rates with no evidence for deactivation and that the carbon AES lineshape is always that of a "carbide" with no evidence for graphite formation. The estimate of carbon surface coverage from the AES carbon intensity is based on AES data obtained from a CO monolayer (4).

Since there is no pressure effect--in the pressure range of these measurements--in the rate of carbide production from pure CO (3) and since

at any H_2:CO ratio an increase in pressure results in a decrease in surface carbon, we conclude that the data of Figure 4 is a manifestation of the change in the hydrogenation rate of the surface carbide with total pressure and with the H_2:CO ratio. We have previously concluded (1) that the methanation reaction rate is determined by a delicate balance of the formation and removal of surface carbide and that neither of these processes are rate determining in the usual sense. Thus, as indicated in Figure 4 under reaction conditions unfavorable for the hydrogenation rate (e.g., low partial pressure of H_2 at a high temperature) the reaction rate should decrease and be accompanied by an increase in the surface carbon level. At lower temperatures the surface concentration of hydrogen (and thus the hydrogenation rate) becomes less strongly dependent on pressure. For example, the rate of CH_4 production for a 4:1 H_2:CO ratio at 503K (plotted in Fig. 3) is only slightly dependent on pressure (from 1-1500 torr). The measured surface carbon level under these conditions is approximately 10% of a monolayer and does not change significantly over the entire pressure range.

Thus it appears that changes in temperature, H_2/CO ratio, and total pressure have a common effect on the methanation rate--namely, to change the surface concentration of hydrogen. Although these effects have been observed predominately on the Ni(100) crystal, the similarities between Ni and Ru with regard to reaction rate variation with pressure and with surface carbide level (Fig. 2) strongly suggest a similar explanation for ruthenium.

The results of these pressure studies suggest considerable caution in drawing the conclusion that crystallographic effects are absent in the methanation reaction over Ni or Ru. While this result appears valid under reaction conditions in which surface carbide level is low, as reaction conditions change effects due to diffusion of carbon, stability of the surface carbide, hydrogen surface concentation and other effects which can have a strong crystallographic dependence can become dominant factors influencing the reactivity.

FIGURE CAPTIONS

Figure 1. Arrhenius plot comparing CH_4 synthesis on Ni(100), Ni(111), and supported Ni catalysts. Reaction conditions: 120 torr, $H_2/CO = 4$. Ni(111) - this work; Ni(100) - ref. (1); supported Ni - ref. 7.

Figure 2. a.) Arrhenius plot of CH_4 synthesis on a Ni(100) catalyst at total reactant pressures of 1, 10, 120 torr. $H_2CO = 4$.

b.) Arrhenius plot of CH_4 synthesis on a Ru(110) catalyst at total reactant pressures of 1, 10, 120 torr. $H_2CO = 4$. Data at two temperatures for a Ru(001) catalyst at 120 torr is plotted with the symbol, x.

Figure 3. Methane production rate (molecules/surface site/sec) versus pressure at 503K and 625K over a Ni(100) catalyst.

Figure 4. Methane production rate (molecules/surface site/sec) at 625K over a Ni(100) catalyst versus surface carbon concentration (under steady state reaction conditions). The H_2:CO ratio and the total pressure (torr) for each point plotted is indicated in the insert.

REFERENCES

1. D. W. Goodman, R. D. Kelley, T. E. Madey, and J. T. Yates, Jr., accepted for publication in J. Catalysis.

2. D. W. Goodman, T. E. Madey, M. Ono, and J. T. Yates, Jr., J. Catal., 50 279 (1977).

3. D. W. Goodman, R. D. Kelley, T. E. Madey, and J. M. White, accepted for publication in J. Catalysis.

4. D. W. Goodman and J. M. White, accepted for publication in Surface Science.

5. For example, M. A. Vannice, J. Catl., 37, 449 (1975).

6. D. F. Ollis and M. A. Vannice, J. Catal., 38, 514 (1975).

7. M. A. Vannice, Catal. Rev. Sci. Eng. 14(2), 153 (1976).

Fig. 1

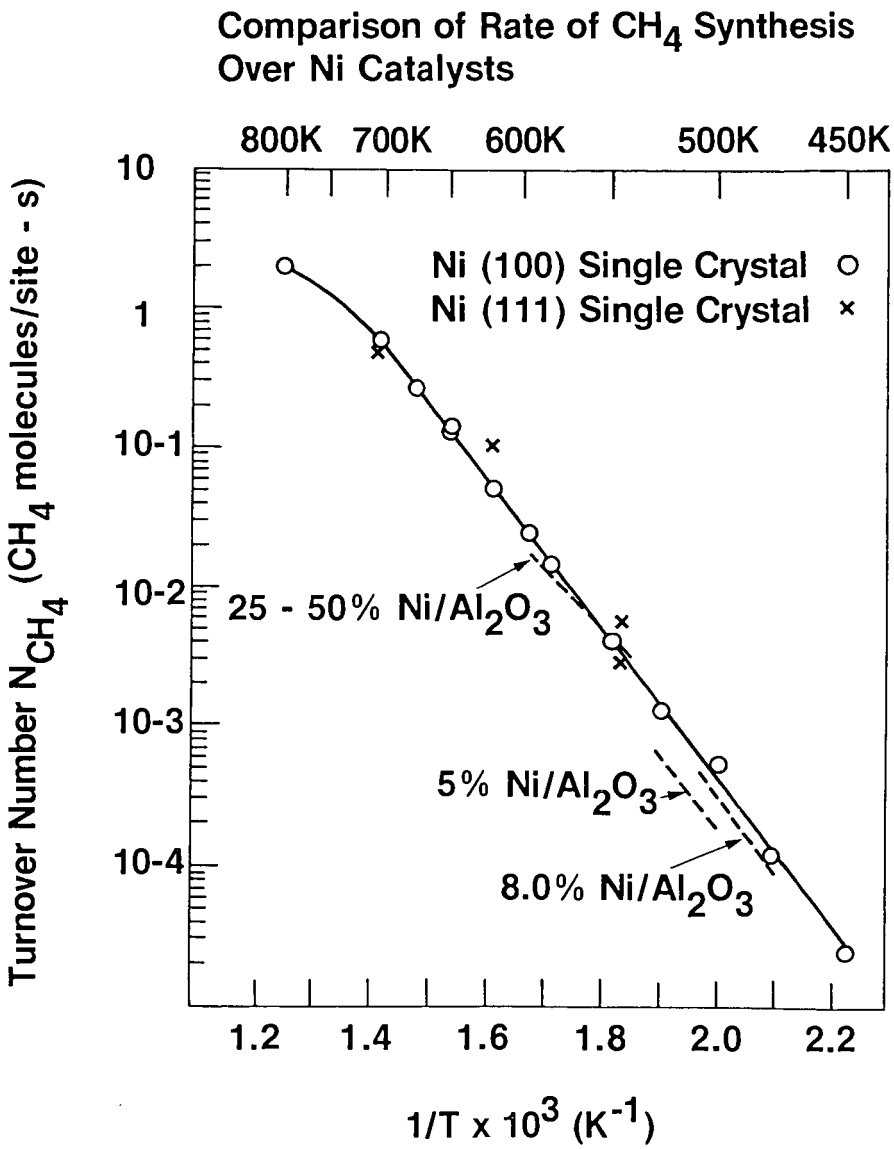
Comparison of Rate of CH_4 Synthesis Over Ni Catalysts
800K
700K
600K
500K
450K
10
1
10-1
10-2
10-3
10-4
Turnover Number N_{CH_4} (CH_4 molecules/site - s)
Ni (100) Single Crystal
Ni (111) Single Crystal
25 - 50% Ni/Al_2O_3
5% Ni/Al_2O_3
8.0% Ni/Al_2O_3
1.2
1.4
1.6
1.8
2.0
2.2
$1/T \times 10^3$ (K^{-1})

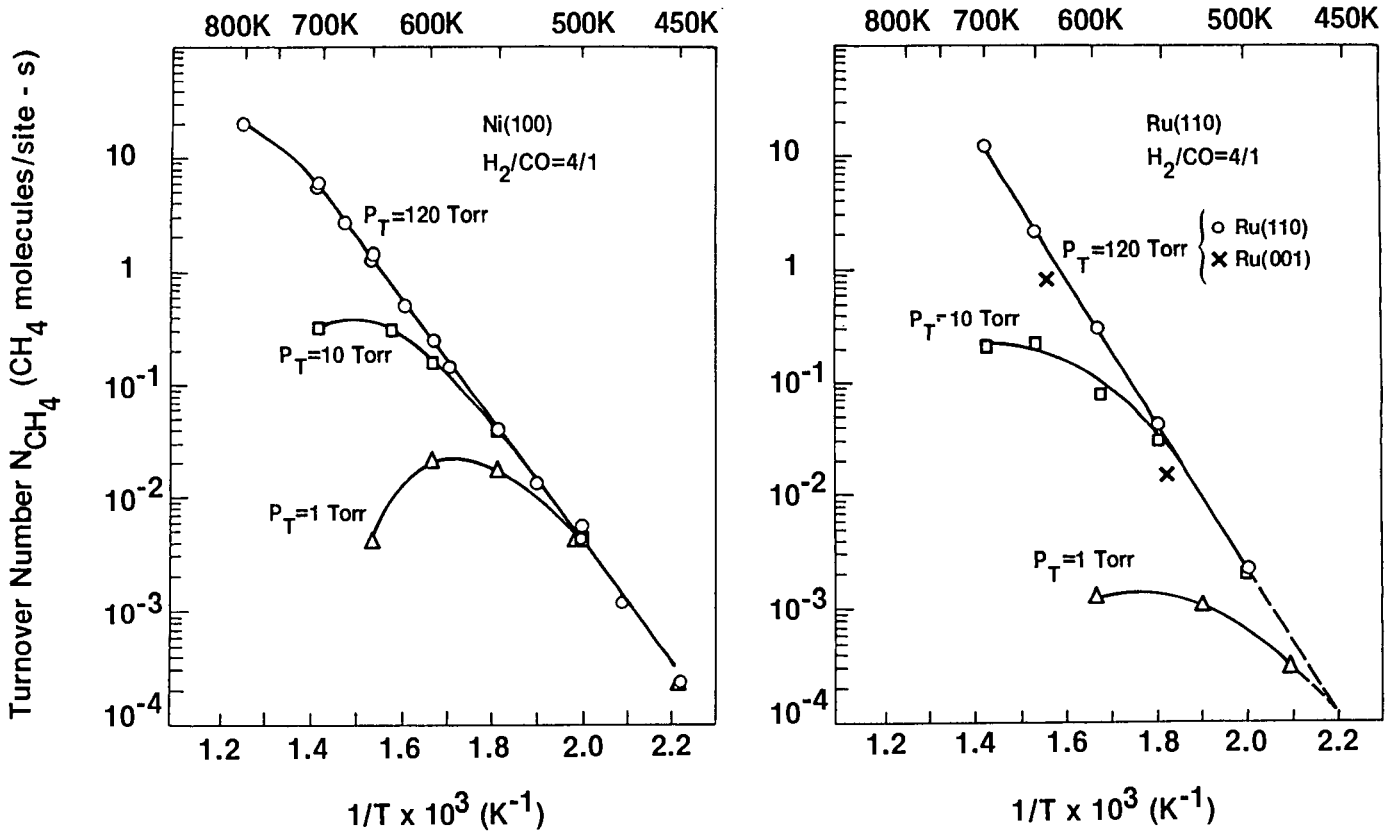
Turnover Number N_{CH_4} (CH_4 molecules/site - s)
800K 700K 600K 500K 450K
Ni(100)
H_2/CO=4/1
P_T=120 Torr
P_T=10 Torr
P_T=1 Torr
10
1
10^{-1}
10^{-2}
10^{-3}
10^{-4}
1.2 1.4 1.6 1.8 2.0 2.2
1/T x 10^3 (K^{-1})
800K 700K 600K 500K 450K
Ru(110)
H_2/CO=4/1
P_T=120 Torr
o Ru(110)
× Ru(001)
P_T=10 Torr
P_T=1 Torr
10
1
10^{-1}
10^{-2}
10^{-3}
10^{-4}
1.2 1.4 1.6 1.8 2.0 2.2
1/T x 10^3 (K^{-1})

Fig. 2

Fig. 3

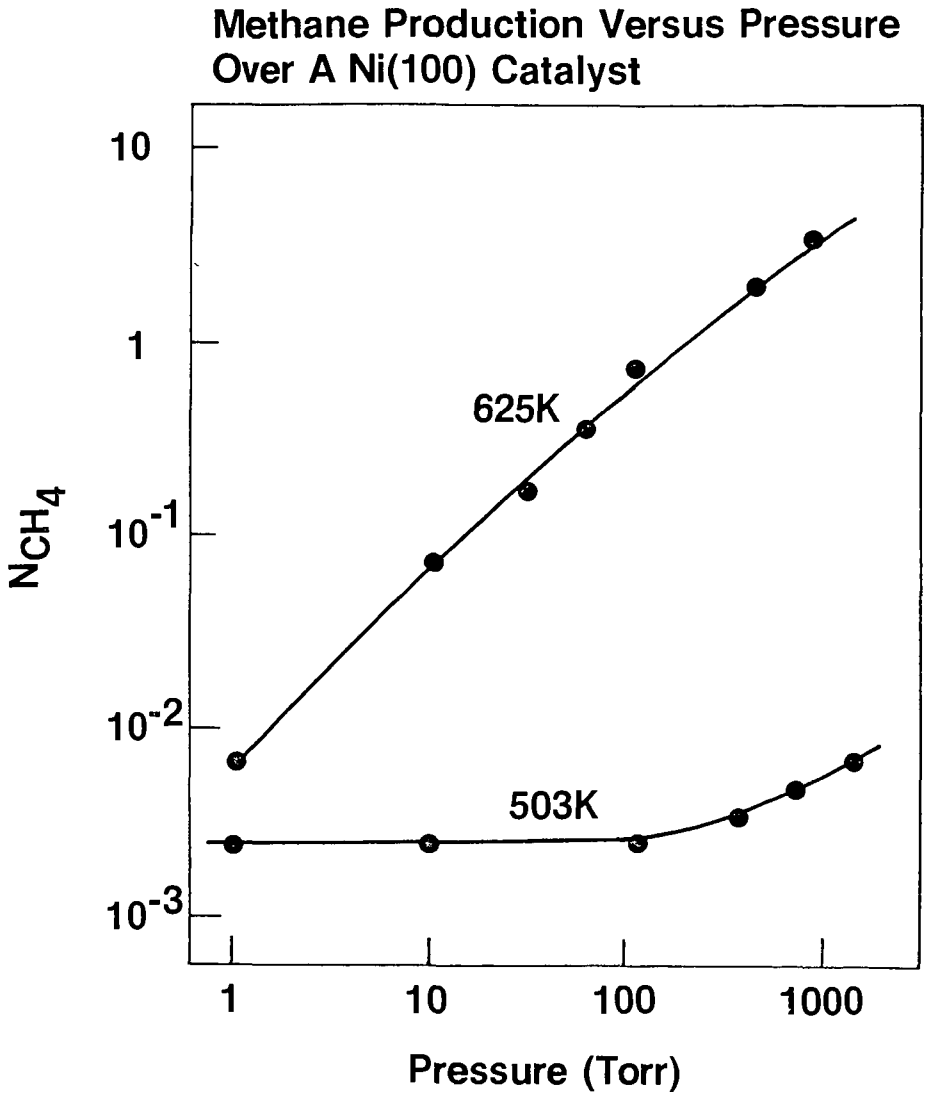
Methane Production Versus Pressure
Over A Ni(100) Catalyst
10
1
10^{-1}
10^{-2}
10^{-3}
N_{CH_4}
625K
503K
1
10
100
1000
Pressure (Torr)

Fig. 4

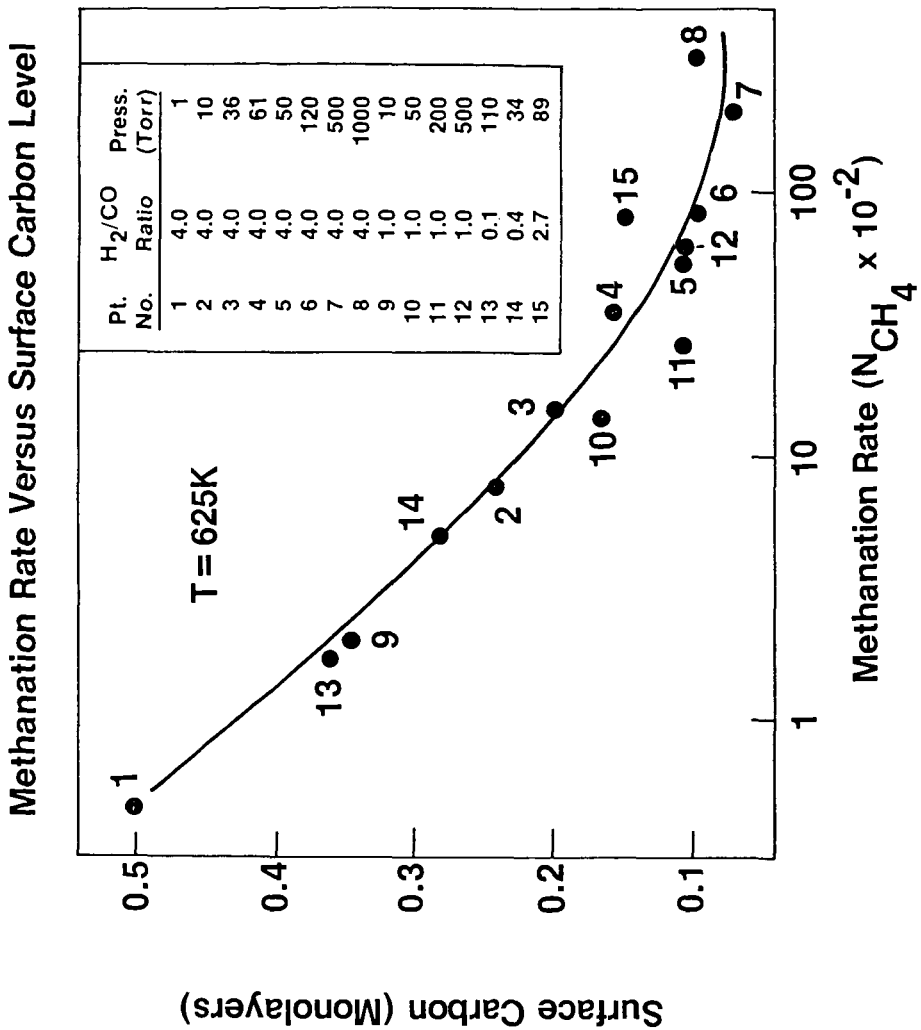
Methanation Rate Versus Surface Carbon Level
T = 625K
Pt. No. | H_2/CO Ratio | Press. (Torr)
1 | 4.0 | 1
2 | 4.0 | 10
3 | 4.0 | 36
4 | 4.0 | 61
5 | 4.0 | 50
6 | 4.0 | 120
7 | 4.0 | 500
8 | 4.0 | 1000
9 | 1.0 | 10
10 | 1.0 | 50
11 | 1.0 | 200
12 | 1.0 | 500
13 | 0.1 | 110
14 | 0.4 | 34
15 | 2.7 | 89
Surface Carbon (Monolayers)
0.5
0.4
0.3
0.2
0.1
1
10
100
Methanation Rate (N_{CH_4} x 10^{-2})

THE EFFECTS OF POTASSIUM PROMOTION ON THE CHARACTERISTICS OF IRON FISCHER-TROPSCH CATALYSTS. H. Arakawa and A. T. Bell. Materials and Molecular Research Division, Lawrence Berkeley Laboratory and Department of Chemical Engineering, University of California, Berkeley, CA 94720.

The addition of potassium is well known to alter the performance of iron catalysts used for Fischer-Tropsch synthesis. The objectives of this investigation were to characterize the dependence of the activity, selectivity, and stability of alumina-supported iron catalysts on the K/Fe ratio and to seek explanations for the influence of potassium on the catalysts performance. Experiments were conducted with 20% Fe/Al_2O_3 catalysts containing 0 to 1 % of potassium. With increasing potassium content the catalyst activity decreased, the olefin to paraffin ratio of the product increased substantially, the methane selectivity decreased, and the catalyst stability was enhanced. The interpretation of these results will be discussed in terms of the influence of potassium on the adsorption of H_2, CO, and CO_2, and infrared observations obtained under reaction conditions.

DEACTIVATION BY CARBON OF NICKEL AND NICKEL-MOLYBDENUM METHANATION CATALYSTS

A. Douglas Moeller and Calvin H. Bartholomew

Brigham Young University
Department of Chemical Engineering
Provo, Utah 84602

INTRODUCTION

A serious problem in the catalytic methanation of coal synthesis gas is fouling of the catalyst by carbon deposition. This problem can be avoided by increasing the hydrogen content of the feed stream so that thermodynamic equilibrium is unfavorable toward carbon deposition (1); however, process economics favor minimizing hydrogen usage. Since most gasifiers produce a hydrogen deficient gas the application of a methanation catalyst which deposits carbon at negligible rates would be highly desirable, since it would eliminate the need for the shift reactor prior to methanation. Except for a few recent studies in this laboratory (2-5) there has been very little research to determine the effects of carbon deposition on activity or the kinetics and mechanism of carbon deposition on various catalysts during methanation. Such information would be valuable in determining the best catalysts and optimum operating conditions for methanation of hydrogen-poor synthesis gas.

A previous study in this laboratory (6) showed that Ni-Mo catalysts are promising for use in the BI-GAS process since they are as active as Ni but more resistant to sulfur poisoning. The present study was undertaken to determine the behavior of Ni and Ni-Mo catalysts under reaction conditions which are characteristic of combined shift/methanation and which favor massive carbon formation. The objectives of this study were to:

1. Determine the effects of carbon deposition on the activity of these catalysts under high temperature conditions (both low and high pressures) which promote carbon formation.

2. Determine if the carbon fouled catalysts could be regenerated by treatment in air or O_2 at high temperatures.

The results of activity, adsorption, carbon deposition and regeneration tests to accomplish these objectives are presented and discussed in this paper.

EXPERIMENTAL METHODS

Materials

Catalyst composition and suppliers are listed in Table 1. Catalyst preparation and pretreatment was the same as described previously (6).

Hydrogen gas (99.99% Whitmore) was purified using a Pd catalyst followed by a molecular sieve trap. Gases for the reaction mixtures, N_2 (99.99% Whitmore), CO (99.99% Matheson) CH_4 (99.97% Matheson), CO_2 (99.8% Whitmore) were used as delivered. The reaction mixture for the carbon deposition runs was passed through an activated charcoal trap heated to 473 K and a ZnO/molecular sieve trap heated to 353 K to remove any iron carbonyl and sulfur impurities before undergoing methanation. Catalyst presulfiding treatments were carried out using a 66 ppm H_2S in H_2 mixture prepared in this laboratory diluted to 9 ppm with hydrogen.

Procedure

H_2 Chemisorption. Prior to each test series, small samples (0.2-0.5 g) of reduced catalysts were rereduced at 773 K as previously described (6). H_2 adsorption isotherms were then measured at 298 K following procedures reported previously (7-9). H_2 chemisorption measurements were also performed following each series of tests to detect any changes in the catalyst surface area, and in the case of catalysts analyzed for carbon content H_2 chemisorption measurements were made directly after carbon deposition.

Specific Rate Measurement. Except for the fluidized bed tests specific rates were measured in a Pyrex, fixed-bed reactor at 498 K before and after the steady state carbon deposition runs and after regeneration in the same manner as in our previous study (6). Specific rate measurements for catalysts deactivated in the fluidized bed reactor were performed only after regeneration. Except for the measurements before and after high pressure carbon deposition these tests were performed with 0.2 to 0.6 gram samples and a reactant mixture consisting of 1% CO, 4% H_2 and 95% N_2. To avoid lengthy reduction and passivation steps, the specific rate measurements before and after the high pressure carbon deposition runs were carried out in the stainless steel high pressure reactor described previously (6) using 1 ml samples. The reactant mixture for these measurements was 4.3% CO, 5.6% H_2 and 90.1% N_2.

Steady State (24 h) Carbon Deposition Runs. After initial specific rate measurements, each catalyst was operated in a fixed bed for approximately 24 hours under steady state conditions at 723 K and pressures of 138 kPa or 2600 kPa to observe its behavior under severe carbon deposition conditions. Two samples of each catalyst were run at the lower pressure. One was used for regeneration tests and one was analyzed for carbon content. The space velocity for all steady state carbon deposition runs was 100,000 h^{-1}. Operation in the carbon deposition region of the equilibrium diagram was ensured by using a 4.2% CO mixture (in a N_2 diluent) and a H_2/CO ratio of 1.3. Figure 1 shows this composition on a carbon-hydrogen-oxygen triaxial plot along with our 1% CO mixture (H_2/CO = 4) and the BI-GAS nominal feed gas composition (H_2/CO = 1.4). Sample sizes were again 0.2-0.6 g for low pressure runs and 1 ml for high pressure runs. Reactant and product sampling was performed in the same way as in our previous in situ deactivation measurements (6).

Ni-Mo-Cu (0.57 g) and Ni-Mo (0.51 g) were operated in a fluidized bed reactor (6) for 24 hours at 723 K and 138 kPa. A fluidized bed was used in order to simulate more closely the BI-GAS process. The reaction mixture was a dilute BCR mixture of the following composition: 5.3% CO, 6.5% H_2, 1.6% CH_4, 3.6% CO_2, 83.0% N_2. These runs were repeated using fresh samples (0.5-0.6 g) and a 4.2% CO, 5.5% H_2, 90.3% N_2 mixture to obtain samples for carbon analysis.

Regeneration Tests and Passivation. Regeneration tests were performed with a 1-3% air in N_2 mixture at 138 kPa for catalysts deactivated at low pressure and a 1-4% O_2 in N_2 mixture at 2600 kPa for those deactivated at high pressure. In both cases the temperature was 573 K. Catalysts deactivated in a fluidized bed were also regenerated in a fluidized bed. During regeneration CO and CO_2 concentrations in the product stream were monitored continuously with the chromatograph for 15 to 30 minutes. After 30 minutes the CO_2 concentration was negligible indicating completion of carbon removal. The catalysts which had undergone either high pressure regeneration or low pressure fluidized bed regeneration were passivated with a dilute air/N_2 mixture and transferred to the fixed bed reactor cell to facilitate subsequent specific rate and H_2 chemisorption measurements.

Regeneration of the Ni catalyst was attempted using a 50% H_2O/H_2 mixture at 723 K and 2600 kPa for 6.5 hours, but it resulted in severe attrition and there was not enough catalyst left in the reactor to perform any meaningful tests. For this reason a dilute O_2/N_2 mixture at high pressure was used for regeneration of catalysts deactivated at high pressure.

Pre-sulfiding Runs. 0.5 ml samples of the Ni and Ni-Mo-Cu catalysts were loaded into the Pyrex fluidized bed reactor and re-reduced as discussed previously. The fluidized bed was used to assure uniform poisoning of the catalyst particles. These catalysts were then exposed to 375 ml/min of a gas mixture of 9 ppm H_2S in H_2 at 725 K for sufficient time to sulfide 50% of the catalyst surface (6). After exposure for the required time, the catalysts were cooled to room temperature and passivated. Activity tests were then run as described below.

RESULTS

Specific Rate and H_2 Chemisorption Measurements

Reaction rates per active site of catalyst, i.e. methane turnover numbers (N_{CH_4}), and product yields (fractions of converted CO occurring as various products) obtained in differential reactor tests of Ni, Ni-Mo, and Ni-Mo-Cu catalysts are presented in Table 2 along with H_2 chemisorptive uptakes.

The data in Table 2 show that all three catalysts suffered significant decreases in metal surface area measured by H_2 adsorption after carbon deposition at either low or high pressure. However, there were significant variations in the magnitude of changes observed for turnover numbers after carbon deposition at low pressure. The CH_4 turnover numbers of Ni and Ni-Mo-Cu did not change significantly while that of Ni-Mo dropped over 90%. CH_4 yield dropped for Ni and Ni-Mo but remained unchanged for Ni-Mo-Cu. Ni-Mo-Cu and Ni-Mo exhibited significant increases in CO_2 yield after carbon deposition, whereas Ni showed no significant CO_2 yield either before or after carbon deposition.

The catalysts also responded differently to regeneration. Ni and Ni-Mo regained activity after regeneration having CH_4 turnover numbers near those for the fresh catalysts; CH_4 yield was almost completely restored for Ni but only in part for Ni-Mo. Regeneration did not improve the activity or selectivity of Ni-Mo-Cu, but rather caused decreases in CH_4 and CO_2 yields. All of the sulfur-free catalysts apparently suffered a decrease in surface area after regeneration.

The results of differential runs for catalysts subjected to carbon deposition at high pressure demonstrated similar trends. That is, CH_4 turnover numbers as well as CH_4 yields decreased for all catalysts. In fact N_{CH_4} decreased by a factor of 2 for Ni and a factor of 10 for Ni-Mo-Cu and Ni-Mo.

Despite a decrease in surface area the regeneration treatment at high pressure with a dilute O_2 mixture seemed to greatly improve catalyst performance for all catalysts. CH_4 turnover numbers for the three catalysts ranged from 1.5 to 8 times the value before carbon deposition and CH_4 yields were 37 to 66 percent higher than pre-carbon deposition values. To determine if this effect was permanent the Ni catalyst was tested for an additional 20 hours at 623 K and space velocity of 100,000 h^{-1} with 1% CO and H_2/CO = 4, after which the turnover number reverted to the pre-carbon deposition value.

Table 2 also shows the results of differential tests on two catalysts, Ni-Mo-Cu and Ni, which were pre-sulfided and exposed to carbon depositing environment at low pressure. These results show that carbon deposition is extremely detrimental to Ni-Mo-Cu when it has been previously exposed to H_2S. On the other hand Ni is

relatively unaffected showing similar activity performance to the non-sulfided catalyst. Both catalysts showed little change in H_2 uptake as a result of carbon deposition and/or regeneration. However, regeneration apparently caused a significant increase in CH_4 yield for pre-sulfided Ni.

Steady State (24 h) Carbon Deposition Tests

Values of CO conversion, rates of methane production and normalized activities are listed in Table 3 for Ni, Ni-Mo and Ni-Mo-Cu catalysts before and after 24 hour steady state tests at 773 K and 100,000 h^{-1}. Typical plots of normalized activity versus time are shown in Figures 2 and 3. Normalized activity is defined as the ratio of the instantaneous rate of methane production to the initial rate; the half life corresponds to a normalized activity of 0.5.

Based on the normalized activity after 24 hours the order of decreasing resistance to carbon deposition at low pressure was Ni, Ni (pre-sulfided), Ni-Mo-Cu, Ni-Mo, Ni-Mo-Cu (pre-sulfided). The order of increasing content of carbon deposited after 24 hours followed this same trend. However, when the Ni-Mo and Ni-Mo-Cu catalysts were operated in a fluidized bed, Ni-Mo maintained an activity of 0.38 compared to zero for Ni-Mo-Cu after the 24 hour carbon deposition test, even though 10 times more carbon was deposited on Ni-Mo compared to Ni-Mo-Cu. In fact, the Ni-Mo-Cu catalyst lost all measurable activity within 15 hours in the fluidized bed. The pre-sulfided Ni-Mo-Cu also deactivated very rapidly as shown in Figure 2. Figure 3 shows fairly significant fluctuations in the data at 8 hours for the Ni-Mo fluidized bed run. Maintenance of a steady flow during this run required constant attention, and this fluctuation can be attributed to flow variations during the evening and night hours when the run was unattended.

Data in Table 3 obtained at high pressure show that Ni-Mo lost no activity during the 24 hour period. Only a slight decrease in activity was observed for Ni, whereas the activity for Ni-Mo-Cu decreased by almost 40%.

For the low pressure fixed bed carbon deposition runs the decrease in normalized activity with time is represented best by the following expression:

$$a = \frac{a_0}{1+\exp(-ka_0\tau)[\exp(k_d[CO^o]t)-1]} \qquad 1)$$

where a = normalized activity at time t, a_0 = normalized activity at t = 0, k = reaction rate constant (h^{-1}), k_d = decay constant ($l\ mol^{-1}\ h^{-1}$), t = time (h), $[CO^o]$ = concentration of CO at bed entrance (mol l^{-1}), and τ = inverse space velocity (h). An expression for the half life ($t_{1/2}$) is obtained from Equation 1 by setting a/a_0 = 0.5 and rearranging. The result is

$$t_{1/2} = \frac{1}{k_d[CO^o]} \ln [\exp (ka_0\tau) + 1] \qquad 2)$$

Equations 1 and 2 were used to plot the solid lines in Figures 2 and 3 and to calculate the half lives shown in Table 3.

The data from the fluidized bed runs are correlated fairly well by the following expression after about 5 hours:

$$a = a_0 e^{-k_d t} \qquad 3)$$

where the symbols have the same meaning as before. From Equation 3 the half life can be obtained as follows:

$$t_{1/2} = 0.693\ (k_d)^{-1} \qquad 4)$$

This expression was used to calculate the half lives of Ni-Mo and Ni-Mo-Cu in a fluidized bed which are shown in Table 3.

DISCUSSION

Effects of Carbon Deposition on Methanation Activity

Effects on Intrinsic Activity/Selectivity Properties. Several recent investigations of methanation over Ni, and Ru catalysts (10-12) have provided evidence that adsorbed carbon is an active reaction intermediate. McCarty and Wise (11) reported four types of carbon which are adsorbed on the Ni surface after exposure to CO. Two species designated α'-carbon and α-carbon (both atomic carbon) were easily removed by H_2 and another designated β-carbon (polymerized carbon) was about 1/100 as active toward H_2. Graphitic carbon, the fourth type is apparently formed by high temperature conversion of the β-form. McCarty and Wise indicated that α-carbon (C_α) is slowly transformed to β-carbon (C_β) at temperatures above 600 K. Thus, carbon fouling of methanation catalysts is likely the result of C_β formation from C_α, the rate of transformation probably depending on the nature of the active site. The more active sites are more likely to promote both rapid deposition and gasification of C_α. If deposition occurs more rapidly than gasification, C_α will build up on the surface and C_β formation will be favored.

Assuming carbon is an active intermediate, the deactivation rate is then determined by the relative contributions of the rate of active carbon formation and the rate of gasification. The relationship between rates of carbon formation and gasification forms the basis of the following discussion of individual catalyst behavior under low pressure conditions. Apparently under the low pressure conditions of this study Ni shows very little deactivation and accumulates very little carbon. This behavior suggests that the rate of gasification equalizes the rate of deposition for nickel under these conditions. The small amount of carbon fouling that did occur appears to be mainly due to blockage or loss of sites since carbon deposition did not change the turnover number. The addition of Mo to Ni apparently favors the massive deposition of carbon as evidenced by the very significant loss of specific activity and greater carbon content of Ni-Mo. Indeed, recently obtained data from a gravimetric study in this laboratory (4,5) show that the rate of carbon deposition at 773 K on a 5.5% Ni-Mo/Al_2O_3 catalyst is 5 times greater than for a 3% Ni/Al_2O_3 catalyst. The major difference in behavior of these two catalysts appears to be the significantly higher rate of gasification of carbon for the 3% Ni/Al_2O_3. Perhaps Mo believed to be present as MoO_2 dissociates CO but not H_2, thus catalyzing formation but not removal of C_α.

The addition of Cu to Ni-Mo appears to cause a reduction in the amount of C_α formed as indicated by the significantly lower turnover number of Ni-Cu-Mo. Consequently little C_β is formed, resulting in the relatively long half-life of Ni-Mo-Cu relative to Ni-Mo. Ponec (10,12) suggests that in order to dissociate adsorbed CO and form the active surface carbon species an ensemble of active Ni sites is necessary, and that addition of Cu, itself inactive towards methanation, dilutes the active Ni sites causing lower methanation activity of Ni-Cu catalysts as compared to Ni catalysts.

The change in selectivity observed for all catalysts after low pressure carbon deposition suggests some type of modification of the active sites. It is also reasonable to expect that a carbon covered surface will behave catalytically more like a metal carbide than a clean metal surface. This is supported by previous work of McCarty et al. (13,14) and Sexton et al. (15). In addition, massive deposits of carbon in filamentous form have been shown by previous workers to separate and encapsulate metal crystallites. Thus formation of large amounts of C_β may place the metal crystallites in a new support environment, the subsequent change in metal-support interactions inducing changes in activity/selectivity properties. In the case of bimetallic catalysts metal-carbon interactions may induce changes in surface composition which affect selectivity. Ponec (12), for example, presents evidence for the surface modification of a Ni-Cu film by repeated adsorption and temperature programmed desorption of CO.

The data in Table 2 suggest that carbon deposition at high pressure may increase the amount of C_β formed in the case of Ni and Ni-Mo catalysts. That is, the percentage decrease in CH_4 turnover number observed after high pressure carbon deposition is equal to or greater than that observed in the low pressure runs. This observation can be explained on the basis of CO partial pressure. At high pressure the minimum partial pressure of CO was 10 kPa (assuming 90% conversion) whereas the maximum partial pressure of CO in the low pressure carbon deposition tests was 6 kPa. At a higher partial pressure of CO the adsorption and dissociation of CO on the catalyst surface proceeds at a much greater rate (4,5). If the carbon formation rate is greater than the gasification rate more C_β will result.

Effects of Carbon Deactivation on Apparent Activity/Selectivity Properties in a Fixed Bed at High Temperature, Conversion Conditions. Even though considerable carbon fouling was evident, relatively little deactivation was observed during steady state deposition tests for most catalysts except Ni-Mo-Cu (see Figs. 2 and 3). This was particularly true at high pressure. This behavior indicates that only a portion of the active sites are necessary to maintain a high reaction rate. It is therefore reasonable to assume that in a fixed bed reactor most of the reaction takes place in a small zone at the entrance to the bed, creating a large concentration gradient over the reactor. In this small zone, the CO partial pressure is large and the rate of formation of C_β is high; further downstream the catalyst is subjected to a lower CO partial pressure and less C_β is formed. Thus a reaction zone is created which gradually moves downstream as the catalyst becomes fouled. Therefore, at high temperature, high conversion conditions and especially at high pressure, we would expect to observe very little deactivation until the reaction zone reaches the end of the bed. The catalyst would then exhibit an extremely rapid deactivation similar to the depletion of an ion-exchange column. Thus, the true deactivation behavior in a fixed bed at high temperatures and especially at high pressures is masked by heat and mass transfer limitations.

Ni-Mo-Cu exhibits a different type of behavior from the other catalysts at high pressure. During the first three hours a very rapid deactivation occurs. After this time the deactivation rate is similar to that observed during the low pressure carbon deposition run. The turnover number data in Table 2 and the larger amount of carbon for Ni-Mo-Cu relative to Ni (Table 3) suggest that the rate of gasification of the deposited carbon is slower at high pressure resulting in more C_β formation and more rapid deactivation. The presence of Cu probably inhibits the gasification step by limiting the area available for H_2 to adsorb and since higher CO partial pressure increases the rate of C_α formation, a net increase in C_β occurs. Ponec (12) showed that for CO adsorption on Ni-Cu/SiO_2 powder the surface Ni concentration increased with time. Assuming such a change in Ni-Mo-Cu, the increasing concentration of Ni on the surface would increase the rate of gasification with the net effect of slowing down the rate of C_β formation, thus accounting for the lower deactivation rate observed after three hours.

Effects of Pre-sulfiding. Separate gravimetric studies in this laboratory (4,5) have shown that pre-sulfiding the catalyst substantially reduces the gasification rate without significantly affecting the rate of inactive carbon deposition. The result is increased C_β formation (4,5) and more rapid deactivation of pre-sulfided Ni-Mo-Cu and Ni relative to the fresh catalysts (see Table 3).

Carbon Deposition in a Fluidized Bed. As might be expected Ni-Mo-Cu and Ni-Mo deactivated more rapidly in a fluidized bed than in a fixed bed due to more uniform exposure to the reaction mixture. However, Ni-Mo-Cu deactivated more rapidly than Ni-Mo, a result opposite to that obtained in the fixed bed. Perhaps this can be accounted for by the lower space velocities and lower conversions associated with the fluidized bed reactor. The rate of carbon formation is proportional to the partial pressure of CO. The lower conversion would translate to a higher CO partial pressure at the catalyst surface which would affect each catalyst differently because of their different compositions. Careful examination of the low pressure fixed bed data of Tables 2 and 3 reveals that Ni-Mo and Ni-Mo-Cu suffered approximately the same percentage loss of surface area, but that Ni-Mo contained ten times more carbon after the steady-state carbon deposition run. Thus under the higher CO partial pressure Ni-Mo-Cu might be expected to deactivate more rapidly than Ni-Mo since increased carbon deposition would have more effect on Ni-Mo-Cu. A possible additional effect is that under uniform exposure to the reactant mixture a greater modification of the surface occurred for Ni-Mo-Cu than for Ni-Mo. Since large concentration and temperature gradients are absent in the fluidized bed, these results are much more indicative of the true deactivation behavior. Moreover, they model better the behavior anticipated in the BI-GAS process.

Regeneration of Carbon Fouled Catalysts in Air/Oxygen

The restoration of activity following regeneration provides strong evidence that carbon fouled catalysts can be regenerated with dilute mixtures of air or oxygen. In fact, this may be the only practical approach since in industrial equipment the regeneration temperature is usually limited to 700 K, and significant carbon gasification by steam, H_2 or CO_2 does not occur at temperatures below 800 K (16,17). The increase in CH_4 turnover number for the catalysts after the high pressure dilute O_2 treatment was more than could be accounted for by simple removal of the deposited carbon. This could be the result of a surface modification by the O_2 treatment and/or a modification which occurred during reaction as discussed previously.

Palmer and Vroom (18) showed that the activity of nickel is increased by high temperature treatment with O_2 as a result of incorporating dissolved O_2 just below the surface. Sexton and Somorjai (15) reported similar results. Unfortunately this effect appears to be only temporary, since the specific activity of regenerated Ni/Al_2O_3 returned to the same value as the fresh catalyst after 24 hours of reaction at 623 K $H_2/CO = 4$, a condition chosen to ensure that further deactivation did not occur.

Regeneration of methane activity by oxygen is not without a price, however. The results show an overall decrease in surface area after carbon deposition and regeneration of 18 to 71%. This surface area loss is undoubtedly a consequence of sintering and even loss of the catalyst crystallites themselves. Rostrup-Nielsen (19) reports that deposited carbon grows in long hollow filaments with the Ni crystallite at the end. Transmission electron microscopy studies in this laboratory (20) confirm this observation. The Ni crystallite is thus removed from the support by the carbon filament and when the carbon is removed by oxidation the crystallite is probably carried out of the reactor with the gas stream. In fact, chemical analysis of fresh and regenerated Ni/Al_2O_3 samples revealed a 7% loss of nickel. It may be, therefore, impractical to regenerate carbon-fouled catalysts with air or oxygen since after a few cycles of deactivation and regeneration a large part

of the active surface of the catalyst would be gone. It depends, of course, on how much Ni is removed per treatment and the frequency of treatments.

A Model for Deactivation by Carbon

We propose a model to account for deactivation of nickel by β-carbon in a fixed bed during methanation. The proposed model for deactivation is a modification of that proposed by Wise et al. (21) for interaction of sulfur with Ni. A modification in the reaction mechanism is also made to account for the transformation of C_α to C_β and the loss of activity for surface reaction between C and H as the number of available nickel sites diminishes. Our proposed model is

$$CO_s \longrightarrow C_{\alpha s} + O_s \qquad 5)$$

$$C_{\alpha s} + H_s \longrightarrow (CH_4)g \quad \text{stepwise} \qquad 6)$$

$$2C_{\alpha s} \longrightarrow C_{2\beta s} \qquad 7)$$

where the subscript "s" denotes an adsorbed species. Since the α state represents single carbon atoms which are easily gasified and the β state represents polyatomic carbon which is much less active it is reasonable to assume that the dimerization of single C_α atoms to C_β causes the deactivation observed for Ni and Ni bimetallic methanation catalysts.

According to our proposed model the rate of deactivation due to carbon fouling is proportional to the rate of C_β formation which is proportional to the net rate of C_α formation. The rate of C_α formation is in turn proportional to the partial pressure of CO and the activity of the catalyst. Assuming first order dependence on both of these variables, an expression for the deactivation rate can be written as $da/dt = -k_d[CO]a$ where k_d = deactivation rate constant, [CO] = concentration of CO, a = normalized activity at time t. The deactivation model proposed by Wise et al. for sulfur poisoning (21) can be adapted by assuming the reaction rate to be first order in CO concentration and that there are no radial concentration gradients. Simultaneous solution of the deactivation rate expression and the equation of continuity in the z direction (direction of flow) yields Equation 1. The following expression also results if $z/V \ll 1$, where V is the velocity in the z direction.

$$\ln[(\frac{1}{1-x_{CO}})-1] = \ln[\exp(ka_o z/V)-1]-k_d[CO^o]t \qquad 8)$$

By plotting $\ln[(\frac{1}{1-x_{CO}})-1]$ versus time t, values for k and k_d can be determined from the intercept and slope respectively.

Equation 1 is plotted as a solid line in Figure 2 using these parameters. It fits the data very well for the low pressure fixed bed runs. A similar development assuming no concentration gradient in the z direction leads to the exponential relationshp of Equation 3 for fluidized beds. Using Equations 1 and 3 we estimate that half of the active sites for Ni-Mo would be fouled in 37 days in a fixed bed and only 30 hours in a fluidized bed based on process conditions of $H_2/CO = 1.4$ and a space velocity of 3000 h^{-1}.

The fact that the proposed model for deactivation by carbon deposition predicts experimental behavior quite well indicates that it is consistent with the observed deactivation behavior -- i.e., the rate of deactivation increases as the partial pressure of CO is increased and decreases as the surface of the

catalyst is fouled by increasing accumulations of inactive carbon.

CONCLUSIONS

1. At 723 K and atmospheric pressure deactivation of nickel catalysts by carbon exhibited first order dependence on CO concentration (second order overall). Half-lives of Ni and Ni-Mo catalysts varied from 13-170 hours. Based on the specific intrinsic activities (CH_4 turnover numbers) after reaction under carbon depositing conditions the order of decreasing resistance to carbon deposition at low pressure was: Ni, Ni (pre-sulfided), Ni-Mo-Cu, Ni-Mo, Ni-Mo-Cu (pre-sulfided).

2. During reaction in a fixed bed at high temperatures and pressures little apparent deactivation was observed except in the case of Ni-Mo-Cu. The effects of deactivation were masked by the fast rate of reaction occurring in a portion of the bed. Thus the turnover numbers determined under reaction limited conditions reveal the true effects of deactivation.

3. Ni-Mo is more resistant to carbon deposition in a fluidized bed than Ni-Mo-Cu. The fluidized bed experiments provide more realistic indication of the true deactivation behavior because temperature and reactant concentrations are more uniform than in a fixed bed.

4. Pre-sulfiding the catalysts does not improve their tolerance to carbon deposition. In fact, pre-sulfiding Ni-Mo-Cu severely degraded its performance under severe carbon deposition conditions. It is believed that sulfur poisons the gasification of active carbon leading to a build up and transformation to inactive carbon.

5. A low pressure dilute air mixture at 573 K regenerates most carbon fouled catalysts. Using a dilute O_2 mixture at high pressure results in CH_4 turnover numbers and CH_4 yields which are temporarily higher than for fresh catalysts. Regeneration using air or O_2 results in a significant loss of surface area, but it may be the only practical method due to temperature limitations of industrial equipment.

ACKNOWLEDGEMENTS

The authors gratefully acknowledge financial support from Bituminous Coal Research, Inc. under their Contract No. EF-76-C-01-1207, U.S. Dept. of Energy; permission to publish catalyst data from the Climax Molybdenum Company of Michigan and the Harshaw Chemical Co.; and technical assistance from Dr. Robert Streeter of BCR.

REFERENCES

1. M.J. Whalen, "Carbon Formation in Methanators," Final Report to ERDA, FE-2240-10 (July 1976).

2. G.D. Weatherbee, G.A. Jarvi, and C.H. Bartholomew, Presented at the 85th National AIChE Meeting, June 4-8, 1978, Philadelphia.

3. C.H. Bartholomew, Final Report to DOE, FE-1790-9, Sept. 6, 1977.

4. D.C Gardner, M.S. Thesis, Brigham Young U., 1979.

5. D.C Gardner and C.H. Bartholomew, paper in preparation.

6. R.W. Fowler, Jr. and C.H. Bartholomew, I & EC Prod. Res. & Dev., in press.

7. C.H. Bartholomew, "Alloy Catalysts with Monolith Supports for Derived Gases," Quarterly Technical Progress Report to ERDA, FE-1790-1, (Aug. 6, 1975).

8. C.H. Bartholomew and R.J. Farrauto, J. Catal. 45, 41 (1976).

9. R.B. Pannell, K.S. Chung, and C.H. Bartholomew, J. Catal. 46, 340 (1977).

10. M. Araki and V. Ponec, J. Catal., 44, 439 (1976).

11. J.G. McCarty and H. Wise, J. Catal., 57, 406 (1979).

12. V. Ponec, Catal. Rev. - Sci. Eng., 18(1), 151 (1978).

13. J.G. McCarty and R.J. Madix, J. Catal. 38, 402 (1975).

14. J.G. McCarty and R.J. Madix, Surface Sci., 54, 121 (1976).

15. B.A. Sexton and G.A. Somorjai, J. Catal., 46, 167 (1977).

16. J.L. Figueirdo and D.L. Trimm, J. Catal., 40, 154 (1975).

17. D.L. Trimm, Catal. Rev. - Sci. Eng. 16(2), 155 (1977).

18. R.L. Palmer and D.A. Vroom, J. Catal. 50, 244 (1977).

19. J.R. Rostrup-Nielsen, J. Catal. 27, 343 (1972).

20. D. Mustard and C.H. Bartholomew, paper in preparation, (1979).

21. H. Wise, B.J. Gikis, W.E. Isakson, J.G. McCarty, K.M. Sancier, S. Schechter, P.R. Wentrcek, and B.J. Wood, SRI, Final Report PERC-0060-8 (ERDA), Sept. 30, 1977.

TABLE 1

CATALYST COMPOSITIONS AND SUPPLIERS

Catalyst	Metal Composition (wt.%)			Bulk Density (g/cm^3)	Support[b]	Supplier
	Ni	Mo	Cu			
Ni	14			0.54	γ-Al_2O_3[c]	BYU Catalysis Lab
Ni-Mo	10.9	19.8		0.91	Al_2O_3 - SiO_2[d]	Climax Moly. Corp.
Ni-Mo-Cu	10	9[a]	3	0.86	Al_2O_3	Harshaw Chem. Co.

a) wt.% MoO_3

b) Powder form

c) Kaiser SAS Medium; 0.32 cm spheres

d) Harshaw AL-1605P (91% Al_2O_3, 6% SiO_2)

TABLE 2

RESULTS OF DIFFERENTIAL REACTOR TESTS (498 K and 138 kPa)

Catalyst	Low Pressure Carbon Deposition[a]				High Pressure Carbon Deposition[b]			
	H_2 Uptake (μmol/g)	N_{CH_4}[c] (s^{-1})x10^3	Yield (%)[d]		H_2 Uptake (μmol/g)	N_{CH_4} (s^{-1})x10^3	Yield (%)	
			CH_4	CO_2			CH_4	CO_2
Ni								
Pre-Carbon Deposition	163	2.4	69	0	163	1.5	52	14
Post Carbon Deposition	142	2.6	43	0	---	0.8	31	1
Post Regeneration	135	2.1	68	0	147	2.7	86	14
Post Regeneration + 20 h at 623 K	---	---	---		148	2.7[a]	86[a]	
Ni (Pre-Sulfided)								
Pre-Carbon Deposition	89	2.0	66	19	---	---	---	---
Post Carbon Deposition	---	1.9	42	0	---	---	---	---
Post Regeneration	99	2.4	85	0	---	---	---	---
Ni-Mo								
Pre-Carbon Deposition	83	2.8	53	3	83	0.35	29	20
Post Carbon Deposition	51	0.16	13	26	---	0.04	6.5	71
Post Regeneration	24	2.5	23	21	22	2.6	40	42
Post Regeneration FBR	41	2.2	43	9	---	---	---	

TABLE 2 - Continued

Ni-Mo-Cu								
Pre-Carbon Deposition	52	0.11	28	31	52	0.11	21	69
Post Carbon Deposition	37	0.15	27	46		0.01	8.5	73
Post Regeneration	30	0.11	21	30	46	0.31	32	34
Post Regeneration FBR[f]	25	---[e]	---[e]	---[e]	---	---	---	
Ni-Mo-Cu (Pre-Sulfided)								
Pre-Carbon Deposition	20	0.22	25	15	---	---	---	---
Post Carbon Deposition	---	---[e]	---[e]	---[e]	---	---	---	---
Post Regeneration	18	---[e]	---[e]	---[e]	---	---	---	---

a) Conditions: 498 K, 138 kPa, 1% CO, $H_2/CO = 4$.

b) Conditions: 498 K, 138 kPa, 4.3% CO, $H_2/CO = 1.3$.

c) N_{CH_4} (turnover number) is the number of molecules produced per site per second.

d) Yield is percent CO converted which goes to CH_4/CO_2.

e) Too low to measure accurately.

f) FBR: Fluidized Bed Reactor run.

TABLE 3

RESULTS OF STEADY STATE (24 h) CARBON DEPOSITION TESTS (723 K, 138 or 2600 kPa, 100,000 h^{-1})

Catalyst	% CO Conversion		Initial CH_4 rate ($\mu mol/cm^3$ cat. s)	Normalized[a] Activity after 24 h	Half life[b] (h)	Carbon Content after 24 h (wt%)
	Initial	Final				
LOW PRESSURE						
Fixed Bed						
Ni	41	43	14	1.05	170	0.6
Ni (P)	33	34	11	0.93	134	---
Ni-Mo	43	31	9.0	0.67	50	16.8
Ni-Mo-Cu	33	27	9.6	0.81	107	1.7
Ni-Mo-Cu (P)	13	2	3.6	0.10	13	---
Fluidized Bed						
Ni-Mo	61	23	7.7	0.38	33	7.2
Ni-Mo-Cu	32	0	4.6	0	2[c]	0.6
HIGH PRESSURE						
Ni	94	91	36	0.99	---	---
Ni-Mo	81	83	21	1.05	---	---
Ni-Mo-Cu	81	52	25	0.63	---	---

a) Normalized activity = rate of CH_4 production divided by initial CH_4 production rate.

b) Half life = time at which normalized activity equals 0.5.

c) No activity after 15 h.

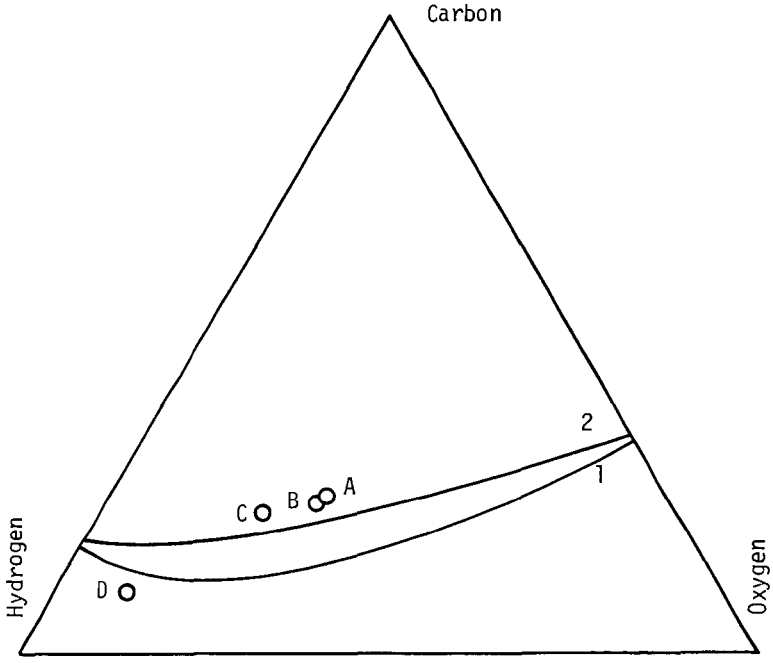

Figure 1. Equilibrium Diagram at 723 K and 138 kPa Showing BI-GAS and Test Feed Gas Compositions. A = BI-GAS, B = Fluidized Bed Runs, C = High and Low Pressure Runs plus some Differential Runs, D = Differential Runs. Curve 1 is the equilibrium curve based on graphite. Curve 2 is based on "non-ideal" carbon as reported by J.R. Rostrup-Nielsen in J. Cat. 27, 343-356 (1972).

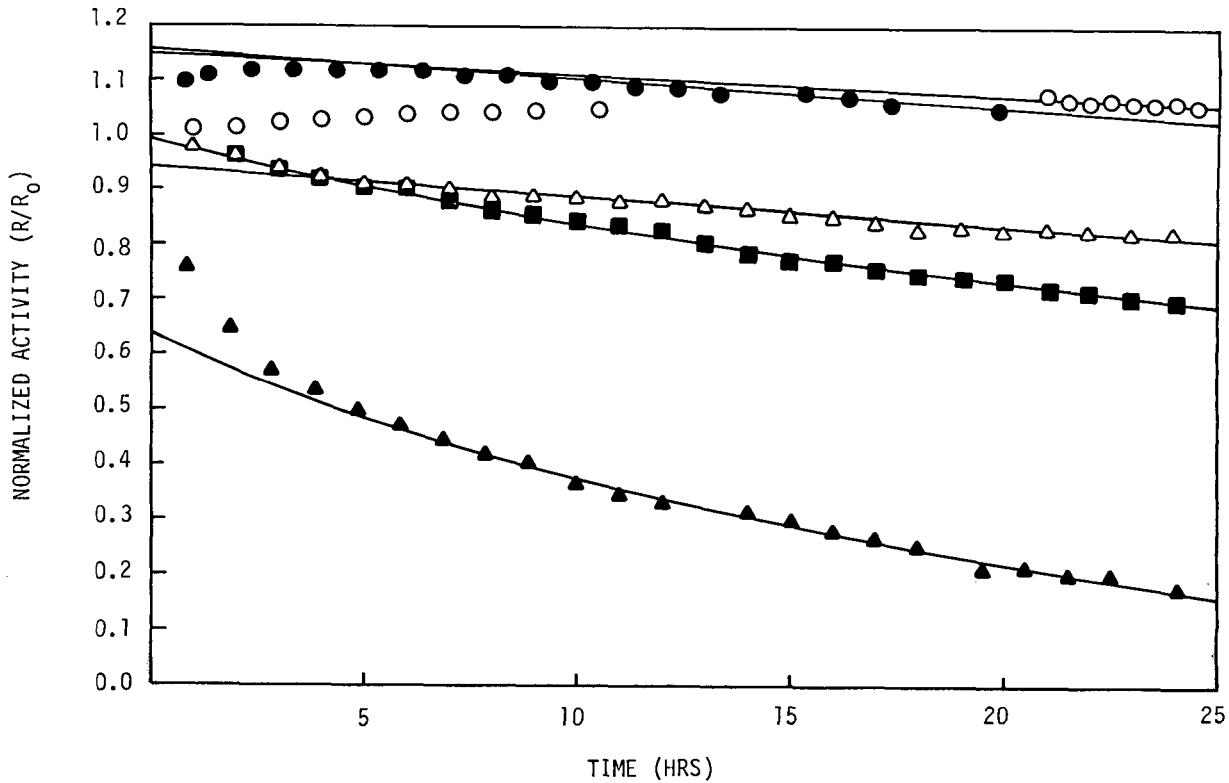

Figure 2. Variation of Normalized Activity with Time at Low Pressure: ○ = Ni, ● = Ni Pre-sulfided), △= Ni-Mo-Cu, ▲= Ni-Mo-Cu (Pre-sulfided), ■ = Ni-Mo. Solid lines represent correlation of data by expression:

$$a = \frac{a_0}{1+\exp(-ka_0\tau)[\exp(k_d[CO^\circ]t)-1]}$$

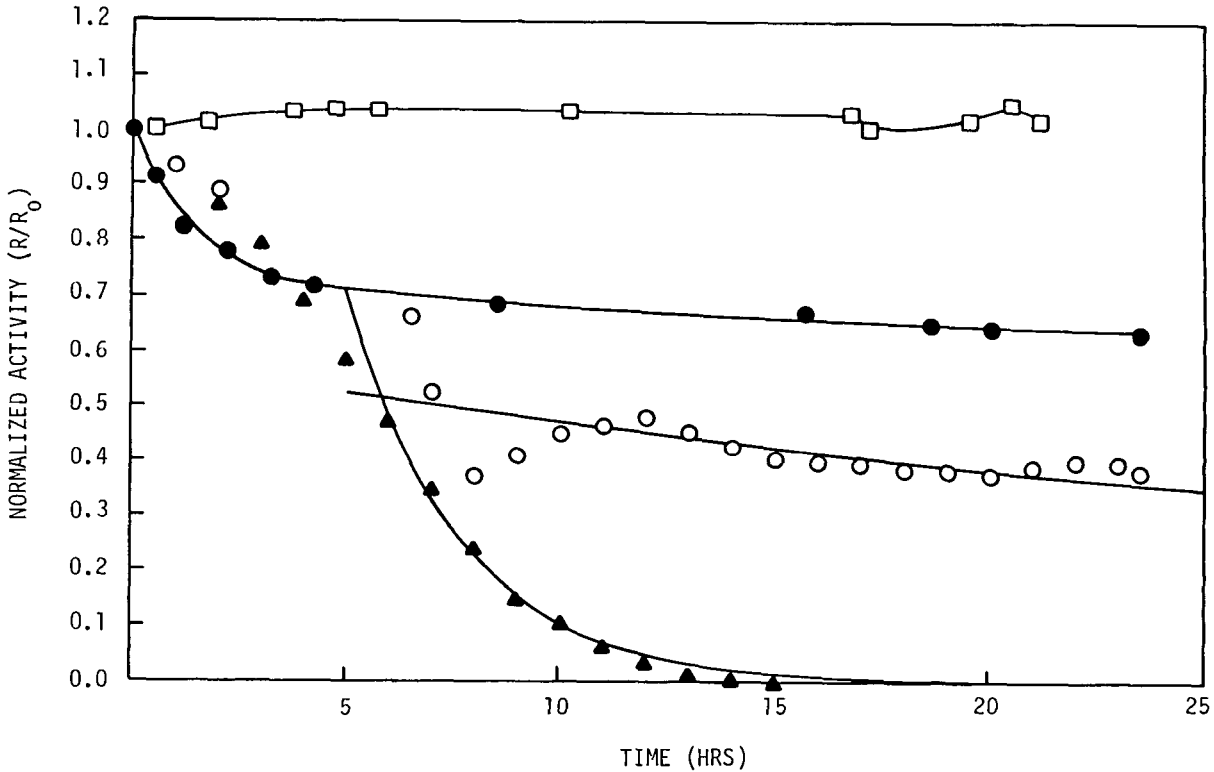

Figure 3. Variation of Normalized Activity with Time: □ = Ni-Mo high pressure run, ○ = Ni-Mo low pressure fluidized bed run, ● = Ni-Mo-Cu high pressure run, ▲ = Ni-Mo-Cu low pressure fluidized bed run. Fluidized bed data after 5 hours are correlated by the expression $a = a_0 \exp(-k_d t)$.

Further Results on the Reaction of H_2/CO on Fused Iron by the Transient Method

J. P. Reymond, P. Mériaudeau,
B. Pommier, and C. O. Bennett*

Laboratoire de Thermodynamique et Cinétique Chimiques
Université Claude Bernard, Lyon I
69621 Villeurbanne, France

Introduction

In a previous study (1) it has been proposed that the surface of a promoted fused iron catalyst is largely covered with carbon during the steady-state reaction of hydrogen and carbon monoxide (90% H_2, 10% CO) at atmospheric pressure and 250°C. This same catalyst, a commercial ammonia synthesis catalyst (CCI), was also evaluated (at 2.0 MPa) in a more applied way in connection with the study of a scheme for energy storage in a central power plant (2, 3). It is now clear that it is necessary to consider that each catalyst (i.e., even the same metal on different supports) may operate for reactions of H_2/CO through a unique sequence of steps, or at least with a particular rate-determining step. Thus although the hydrogenation of surface carbon seems to be rate-limiting on iron (1), on ruthenium the dissociation of adsorbed CO has been proposed as rate limiting (4). The present work is a continuation of that of reference (1); this time the role of CO_2 and H_2O has been investigated, and interesting information has been obtained on the chain growth process.

Experimental

The reactor was made of 1/4-inch stainless steel tube and filled with 100 mg of catalyst (particles of 300 μm) mixed with 500 mg of glass beads of the same size. The reactor and the glass beads were confirmed to produce no products at the reaction conditions. Feed rates of H_2/CO (9/1) between 20 and 120 ml/min were explored but if not otherwise noted, 40 ml/min was used; the conversion was always less than 5% of the CO fed.

Hydrogen (99.99%, Air Liquide) was purified by a molecular sieve (5A) trap, followed by a deoxo reactor, followed by a second molecular sieve 5A. Carbon monoxide (99.9%, Air Liquide) was passed through a glass tube heated to 220°C to decompose carbonyls and then through a trap of activated carbon at 25°C.

Analysis of the reaction products was by gas chromatography. For the separation of the hydrocarbons, a Poropak Q (80-100 mesh) 6-m, 1/8-inch stainless steel column was used with a flame ionization detector. Column temperature was 195°C, and the carrier gas (He) was used at 30 ml/min. The CO_2 and H_2O were measured by a second identical Poropak Q column at 175°C, leading to a thermal conductivity detector. For the reaction conditions used, only alkanes were found among the hydrocarbon products.

Results

The Basic Reaction

After an initial reduction in flowing hydrogen at 60 ml/min for 60 hours at 500°C, the reactor is cooled to 250°C, and the feed is switched at time zero to 10% CO in H_2. The curve 1 of Fig. 1 results. The deactivation is rapid and the production rate of methane passes through a maximum. A reactivation in H_2 at 500°C

*Now at University of Connecticut, Storrs, Connecticut 06268.

for 15 hours increases the activity of the catalyst to a level above what it was at the end of the first run, but below what it was at its maximum. This process continues with further reactivations, and Fig. 1 shows curves after 10 reactivations and after 20 reactivations. However, it was found that a short (30 min) treatment by oxygen at 500°C and 1 atm before the usual reduction by hydrogen produced a relatively stable catalyst, as shown by the curve O_2 of Fig. 1. The activity of the catalyst is obviously very sensitive to its state of oxidation and to the concentration of refractory carbon at or near its surface. It may be recalled that Matsumoto and Bennett (1) found that short treatments in helium at 250°C converted the active carbon intermediate to a form inactive at this temperature. Similar effects are observed for nickel (5).

Figure 2 shows the other hydrocarbons produced corresponding to the curve labelled O_2 on Fig. 1. The numbers by the curves are the steady-state rates of production divided by that for methane. These selectivities are insensitive to the activity level and are about the same for all the catalyst conditions of Fig. 1. Water and carbon dioxide are also produced, but these production rates are less reproducible. The catalyst has a fraction exposed of only about 5 percent, and it has been shown that the entire mass of iron is carburized (1). Thus small changes in carbon concentration in the bulk may produce CO_2 and H_2O at rates at least as high as the catalytic reaction. Figure 3 shows the history of a freshly reduced catalyst after exposure to CO/H_2 at 250°C, H_2 at 250°C, and finally H_2 programmed to 500°C. The first peak represents the removal of a surface carbon intermediate as methane, and the second large peak comes from the decarburization of the bulk of the catalyst. This result has already been discussed (1).

Another aspect of the reacting system can be seen in Fig. 4. Experiments were started with a feed rate of 120 ml/min, but the conversion (0.003 to CH_4) was not sufficient to obtain reliable analyses for H_2O and CO_2 by chromatography (thermal conductivity detector). The hydrocarbons, however, were analyzed correctly (flame ionization detector). When the conversion was increased (0.006 to CH_4) by reducing the feed rate to 20 ml/min, a much lower formation rate of methane was observed. This reduction in activity can only be explained by inhibition of the rates by products of the reaction; the reactant concentrations are of course almost unchanged. In other words, even at these low conversions the reactor is not truly differential.

We are thus led to investigate the effect of the products of reaction on the reaction rates, and these experiments will be described later. In order not to be mislead by secular changes in the catalyst, a steady state condition is first established with 10% CO + H_2 feed. The feed is then changed to one containing H_2O, CO_2, etc. as desired, and finally it is changed back to 10% CO + H_2.

The base reaction has been studied at several temperatures (230°, 250°, 270°, and 300°C), and an activation energy of 20.4 kcal/mole is observed, similar to the value found at 2.0 MPa (2).

Influence of CO_2

To the reaction mixture 10% CO + H_2 was added 5% CO_2. The CH_4 production diminished by about 8%, and when the CO_2 was removed the methane formation rate regained its initial value. This effect is not sufficient to explain Fig. 4.

If the CO in the feed gas is replaced by CO_2, the methanation reaction continues at a lower rate, as shown in Table 1. The formation of higher hydrocarbons, however, is drastically reduced. The CO_2 is dissociatively adsorbed, but the surface oxygen concentration is increased.

Influence of Water

A concentration of 0.6% water vapor was added to the 10% CO + H_2 feed mixture at steady-state reaction, and Fig. 5 shows the result. The inhibiting effect of water is clear, and it is probable that the lower rates at higher conversion shown in Fig. 4 are explained by the increased water concentration at higher conversion.

It is also interesting to evaluate the capability of the steady-state catalyst surface to catalyze the shift reaction. Figure 6 indicates that when the H_2 in the 10% CO + H_2 mixture is replaced by 0.6% water, all production of hydrocarbons stops, and a large rate of CO_2 formation is observed. These results are further evidence of the power of the iron catalyst to adsorb dissociatively H_2 as well as CO.

Influence of Ethane

The addition of 10% C_2H_6 to the reactants does not change the rates of reaction. However, iron has some activity for hydrogenolysis (6). If the 10% CO + H_2 mixture is changed to 10% C_2H_6 + H_2, methane is formed at 0.65 μ mole/g min (see Fig. 7), less than 10% of a typical methanation rate.

Influence of Olefins

When 10% C_2H_4 + H_2 is fed to the reactor just after the reduction of the catalyst at 500°C, the curves of Fig. 7 are obtained. There is immediate production of methane, propane, n-butane, and n-pentane. Ethane is confounded with the large ethylene peak in the analysis by chromatography. The rates do not increase from zero as in Fig. 2. A switch to hydrogen (not shown on Fig. 7) produces no methane peak at 250°C, and programming the temperature to 500°C results in the production of only 4 μ moles of CH_4/g of iron. Thus the C_2H_4/H_2 mixture does not carburize the iron at 250°C. The reaction rates after 4 hours with ethylene are about twice those with CO, and the initial rates are an order of magnitude higher. Figure 7 shows also the switch from C_2H_4/H_2 to CO/H_2 and then to C_2H_6/H_2.

Figure 8 shows the usual curves for CO/H_2 over a reduced catalyst, followed by a switch to C_2H_4/H_2 over the now carburized catalyst. These results are consistent with the idea that the rate-determining step with CO is the hydrogenation of surface carbon. Subsequent chain growth occurs through CH_2 groups (or CH), and if these groups are formed directly from ethylene, the production rates of the products are higher; the rate limiting step coming from CO is no longer relevant. The C_2H_4/H_2 reaction occurs on iron, and after exposure of the catalyst to CO/H_2, much of the surface is covered with carbon, so the rate of CH_4 production with C_2H_4/H_2 of Fig. 8 is lower than that of Fig. 7.

Figure 9 shows the reaction of 10% C_3H_6 + H_2 over the reduced catalyst. The results are qualitatively the same as with ethylene. Butene-2/H_2 reacts as shown in Fig. 10, and butene-1/H_2 (always 90% H_2) gives rates that are all a bit lower than for butene-2, as shown. All these results emphasize that on the iron surface the CH_2 or CH fragments come rapidly to a steady state; the rates of production of the alkane products (no olefins were observed) are not appreciably influenced by the source of the CH_2 groups on the surface. However, there are some differences, as shown in Table 2, which gives the ratios of the production rates after 4 hours. Starting from a given olefin, the products are mostly of shorter chain length, and close to the chain length of the reactant. In any event, we are justified in supposing that, starting from CO/H_2, all the steps after CH_2 or CH formation are rapid, and little of the surface is covered by chain fragments at 250°C and 100 kPa.

Discussion

The new results of the present study confirm most aspects of the sequence of steps proposed by Matsumoto and Bennett (1). CO is adsorbed as C + O, and the freshly formed surface carbon is the most abundant surface intermediate; its hydrogenation by adsorbed hydrogen present as H is the rate-determining process. Carbon dioxide added to CO/H_2 is not strongly enough adsorbed to affect the rate appreciably. However, in the absence of CO, CO_2/H_2 makes methane at a lower rate; the surface is more oxidized, and the active C is present in lower concentration than in the presence of CO.

However, water can compete with CO for the surface, and it oxidizes the surface while reducing the active C coverage by forming CO_2. The high reaction rate of CO/H_2O to CO_2 rather than CH_4 shows the strong affinity of the surface of the iron catalyst for oxygen (Figs. 5-6).

We recall that the rate of hydrocarbon production over a freshly reduced catalyst rises from an initial value of zero. The carbon formed from CO reacts with the bulk iron of the catalyst, and the surface carbon necessary for hydrocarbon production gradually increases in coverage as the bulk of the iron is carburized to Fe_2C at 250°C. However, when C_2H_4/H_2 is passed over the reduced catalyst, no active C intermediate seems to be necessary. The rate starts at a maximum value, and the iron is not carburized. Thus the observed formation of CH_4 and C_3H_8 shown in Fig. 7 arises through a CH_n fragment. No oxygen is present. Iron thus behaves differently from cobalt, for which oxygen is apparently necessary for chain growth (7, 8).

When a CO/H_2 feed is changed to C_2H_4/H_2 (Fig. 8), the rate of hydrocarbon production is higher from ethylene than from CO. Methane is an important product from C_2H_4/H_2. This result is not inconsistant with the lack of $^{14}CH_4$ formed when $^{14}C_2H_4$ is added in small quantity to CO/H_2 (9). With CO present the C_1H_n groups must originate principally from CO, so that the added ^{14}C will be concentrated principally in C_xH_y groups of $x \geq 2$.

It is clear that the reaction of ethylene takes place on the iron surface, since the rate decreases as the inert graphitic carbon builds up (Figs. 7 and 8). It was shown previously (1) that the reaction from CO also occurs on the iron part of the surface; after steady state under CO/H_2, a brief exposure to H_2 alone and then a switch back to CO/H_2 leads to a temporary increase in the rate. If the exposure to hydrogen is long enough to decarburize some of the bulk, the subsequent CO/H_2 reaction rate is lowered as recarburization lowers the concentration of the active surface carbon.

A freshly reduced catalyst is carburized by the H_2/CO mixture in about an hour (recall that carburization in CO alone is much slower (1)). During this period the hydrocarbon formation rate gradually increases as the surface carbon concentration rises, as influenced by the bulk carbon (carbide) concentration. A switch to pure H_2 gives a methane peak, meaning that hydrogen reacts as H on the surface and that the surface coverage by C is high. The rate-determining process is the formation of CH_n from the surface C; subsequent chain growth is rapid and occurs through these groups, and the product distribution is determined by the rate of propagation and termination (desorption) of chains arising from CH_n. The presence of H_2O and to some extent CO_2 in the gas phase increases surface O at the expense of C and/or H, inhibiting the reaction. However, active surface carbon is gradually converted to inert (at 250°C) graphite, and activity slowly declines as the part of the iron covered with labile C decreases. For a much regenerated catalyst, oxygen followed by hydrogen cleans off a higher fraction of inert graphite than H_2 alone.

References

1. Matsumoto, H., and Bennett, C. O., J. Catal. 53, 331 (1978).
2. Atwood, H. E., and Bennett, C. O., Ind. Eng. Chem. Process Des. Dev. 18, 163 (1979).
3. Borghard, W. G., and Bennett, C. O., Ind. Eng. Chem. Product Res. Dev. 18, 18 (1979).
4. Dalla Betta, R. A., and Shelef, M., J. Catal. 49, 383 (1977).
5. McCarty, J. G., and Wise, H., J. Catal. 57, 406 (1979).
6. Montarnel, R., and Martino, G., Rev. Inst. Français du Pétrole 32, 367 (1977).
7. Gibson, E. J., and Clarke, R. W., J. Appl. Chem. 11 293 (1962).
8. Eidus, YaT., Zelinskii, N. D., and Ershov, N. I., Dokl. Akad. Nauk SSSR 60, 599 (1948).
9. Hall, W. K., Kokes, R. J., and Emmett, P. H., J. Am. Chem. Soc. 82, 1027 (1960).

Table 1

Reaction of CO_2 and H_2

Formation Rate, μ mole/g min.	Feed		
	Before		After
CH_4	7.0	4.4	7.4
C_2H_6	3.2	0.52	3.5
C_3H_8	1.5	0.065	1.5

Table 2

Relative Production Rates

(4 hours on stream)

Feed Mixture	$\frac{C_2}{C_1}$	$\frac{C_3}{C_1}$	$\frac{C_4}{C_1}$	$\frac{C_5}{C_1}$
10% CO + H_2	0.6	0.29	0.10	0.02
10% C_2H_4 + H_2		0.15	0.06	0.001
10% C_3H_6 + H_2	0.49		0.087	0.002
10% butene-1 + H_2	0.19	0.76		0.08
10% butene-2 + H_2	0.20	0.92		0.09

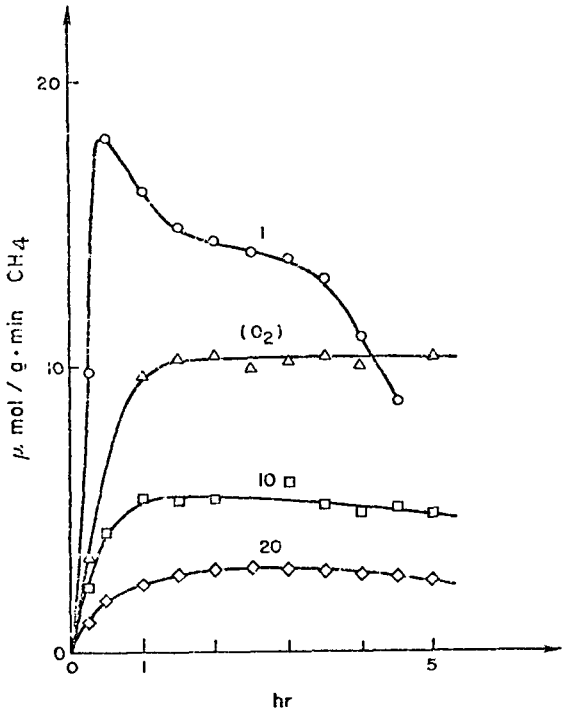

Figure 1

Rate of Reaction after Various Reactivations; Feed Rate, 120 mℓ/min.

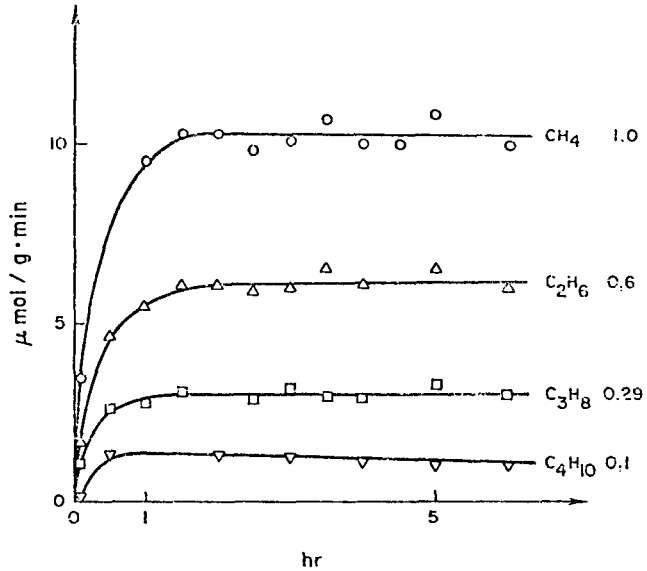

Figure 2

Formation Rates of Products.

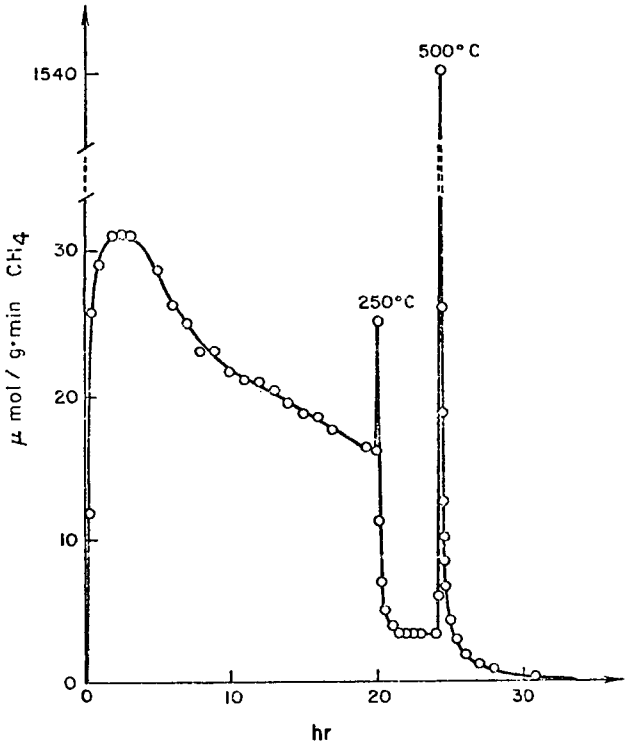

Figure 3

Hydrogenation of Surface Carbon.

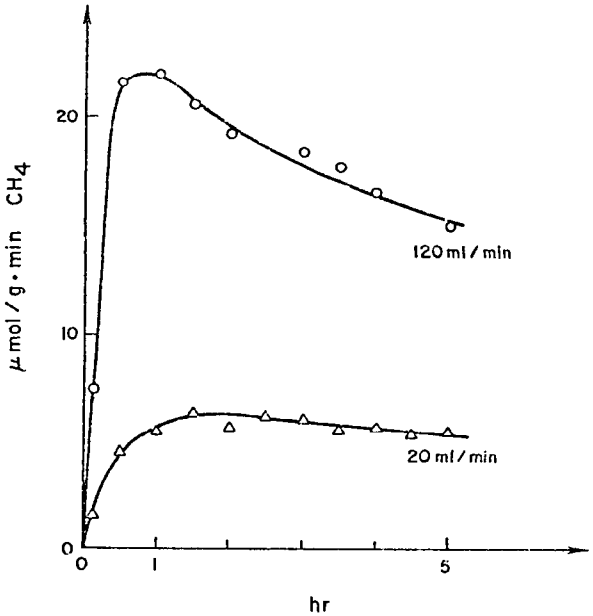

Figure 4

Effect of Flow Rate on Methane Formation.

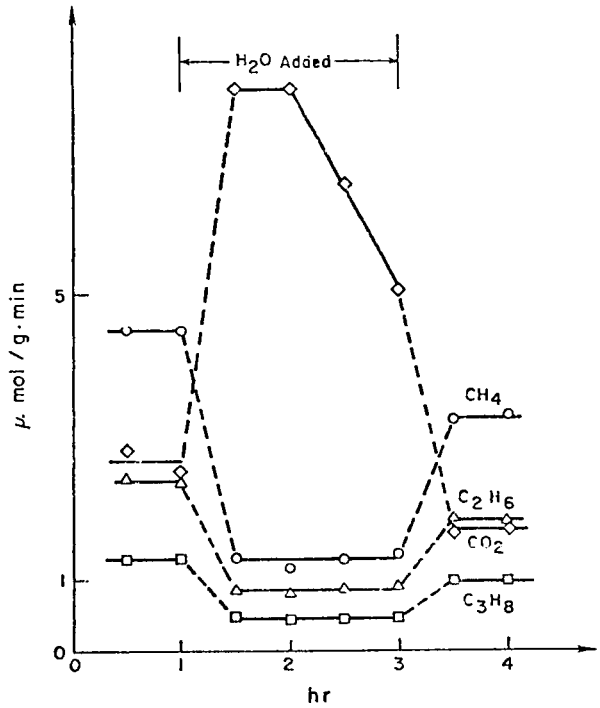

Figure 5

Effect of Water Vapor on the Reaction.

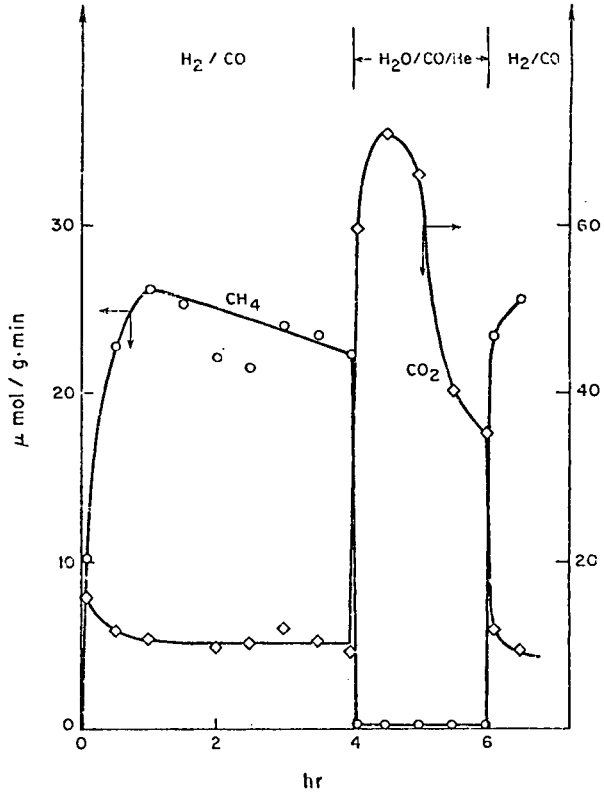

Figure 6

Reaction of Water and Carbon Monoxide.

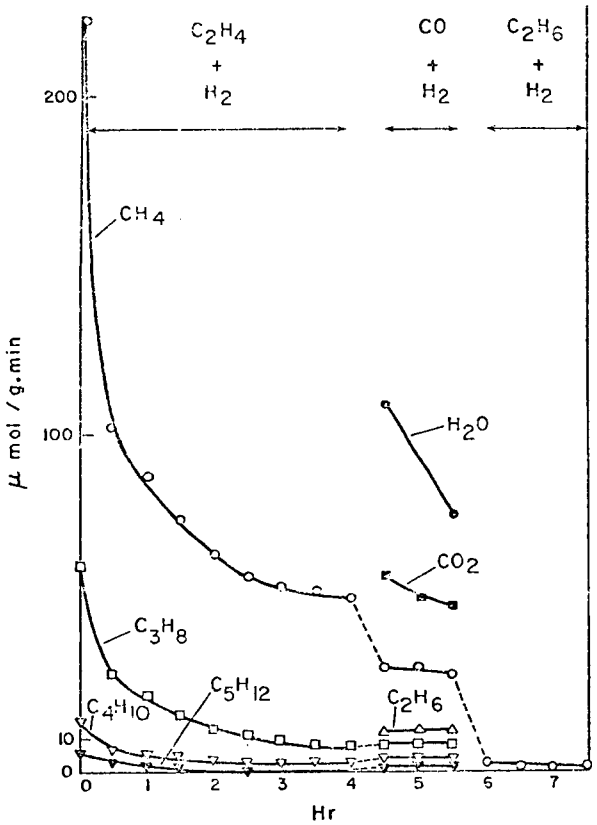

Figure 7

Reaction of Ethylene and Hydrogen on a Reduced Catalyst.

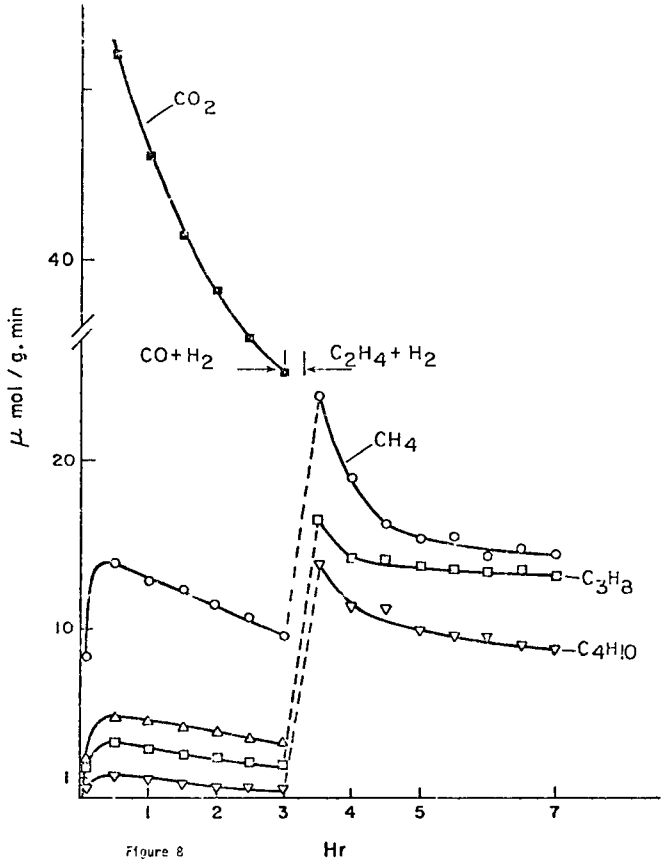

Figure 8

Reaction of Ethylene and Hydrogen on a Carburized Catalyst.

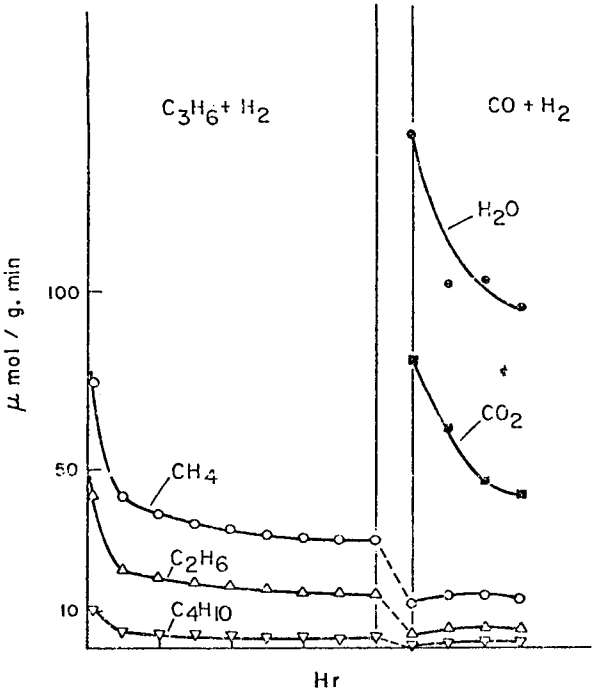

Figure 9

Reaction of Propylene and Hydrogen.

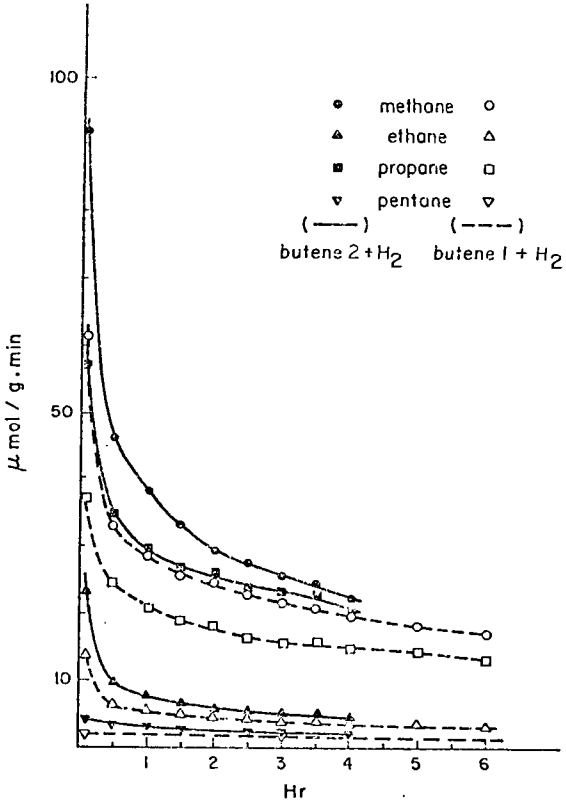

Figure 10

Reaction of Butene-1 and Butene-2 with Hydrogen.

Synthesis Gas Reactions Using Catalysts Formed by Oxidizing Ni-Containing Intermetallic Compounds

H. Imamura and W. E. Wallace

Department of Chemistry
University of Pittsburgh
Pittsburgh, PA. 15260

I. Introduction

Intermetallic compounds containing rare earths or actinides in chemical union with the transition metals Fe, Co or Ni are transformed when exposed to synthesis gas at elevated temperatures into mixtures of rare earth or actinide oxides and elemental Fe, Co or Ni. It has been found that these mixtures are exceptionally active for syngas conversion (1-12). The converted alloys have been characterized by Auger spectroscopy (1,13), x-ray diffraction, ESCA (14) and electron microscopy (7). These studies showed that the surface regions consisted of transition metal nodules growing out of or dispersed on a substrate of rare earth or actinide oxide. The decomposed materials rather than the original alloy appear to be the catalytically active species for the reaction.

Additionally, it has been found that thorium-containing intermetallics such as $ThNi_5$ readily reacted with elemental oxygen to form a mixture of metallic Ni and ThO_2 (12). The oxidation of $ThNi_5$ occurred with a predominant formation of ThO_2 because of the strong chemical affinity of thorium for oxygen. During the oxidation reaction metallic Ni aggregates precipitated out in a fashion similar to that observed when the intermetallic is exposed to syngas. The reaction of $ThNi_5$ with a stoichiometric amount of oxygen required for the formation of thoria-supported Ni catalysts (Ni/ThO_2) brought about complete transformation into a mixture of Ni and ThO_2. This mixture had higher activity for methane formation by an order of magnitude than oxide-supported catalysts (15) prepared by conventional wet chemical procedures. Accordingly, it appears that the oxidation treatment of intermetallics constitutes a novel way for forming oxide-supported catalysts with high activity for syngas conversion.

In this work, the character of catalysts formed by the oxidation of several rare earth-nickel intermetallic compounds was studied in the manner used earlier to study the Th intermetallics. They were evaluated using x-ray diffraction, ESCA and CO chemisorption techniques. The resulting materials, which are probably new supported catalysts, were examined as syngas conversion catalysts.

II. Experimental

The intermetallic compounds ($LaNi_5$, $CeNi_5$, $PrNi_5$, $NdNi_5$, $HoNi_5$, $ErNi_5$ and $ThNi_5$) were prepared by induction melting the metal components in a water-cooled copper boat under an atmosphere of purified helium. These intermetallics were subjected to remelting several times or annealing at a prescribed temperature to insure homogeneity. The formation of the desired compounds was established by x-ray diffraction analysis.

The oxidation treatment of the intermetallics, which had been previously powdered in a porcelain mortar followed by outgassing, was conducted in the presence of oxygen at 610 mmHg. The amount of oxygen uptake by the compound was determined by the pressure drop in a closed system.

To establish the nature of the sample thus treated x-ray diffraction, x-ray photoelectron spectroscopy (ESCA) and CO chemisorption techniques were used.

Powder x-ray diffraction patterns were obtained using a Picker model 3488K diffractometer with Cu radiation. ESCA spectra were recorded on an AEI ES200 electron spectrometer using Al Kα radiation (1486.6 eV). The spectrometer was operated at 12 KV and 25 mA with base pressure $<10^{-9}$ torr in the sample chamber. The binding energy was determined by reference to the contamination C 1s line at 285.0 eV. The CO chemisorption measurements were made at room temperature by means of an adsorption flow method (16). The procedures used have been described in detail previously (12).

III. Results and Discussion

1. Characterization of Catalysts Formed by Oxidation

X-RAY DIFFRACTION

The previous work (12) on the oxidation of thorium-containing intermetallic compounds showed that the oxidation reaction occurred in a stepwise fashion. At first, thorium in the alloy was oxidized largely to form the oxide, during which process finely divided Ni aggregates precipitated out on the resulting oxide surface. Accompanying this there was a remarkable enlargement in the surface area, by up to 200-fold. After completion of the oxidation of thorium further oxygen was taken up by the reaction of Ni to form NiO.

All the compounds studied in the present work readily reacted with considerable amounts of oxygen at 350°C. It was confirmed from x-ray diffraction studies that the oxidation steps approximated that of the thorium intermetallics just mentioned. For example, as depicted in Fig. 1, $CeNi_5$ was completely transformed into a mixture of Ni phase and CeO_2, i.e., Ni/CeO_2, when reacted with the stoichiometric amount of oxygen required to oxidize the Ce present in the alloy. When the CeO_2-Ni mixture was exposed to oxygen there was an additional uptake of oxygen. This occurred by the oxidation of Ni to form NiO. However, after reduction with hydrogen there was no evidence of NiO peaks in the pattern.

From x-ray line broadening measurements of the Ni (111) peak at $2\theta = 44.5$ (Cu Kα radiation) it was possible to establish the Ni particle sizes dispersed on the resulting oxide using the Sherrer equation (18). As shown in Table 1, the particle sizes ranged from 90 to 350 Å. The particle sizes usually but not always showed an increase with increasing oxygen uptake for $LaNi_5$, $CeNi_5$ and $ThNi_5$.

ESCA

X-ray diffraction studies in the preceding section provided an overall image of the alloy transformed by the oxidation. ESCA measurements were made on the oxidized $CeNi_5$ to examine the chemical state of the surface species participating in the reaction. ESCA spectra of the oxidized $CeNi_5$ showed Ni, Ce, O and C signals within the probing depth of ESCA (several atomic layers). Confirming the results obtained by x-ray diffraction analysis, the Ce present in the surface region was found to exist largely in an oxide form. For Ni species the oxidized $CeNi_5$ (C-4) exhibited the Ni $2p_{3/2}$ peaks at 853.9 and 856.6 eV. These binding energies are characteristic of Ni and NiO, respectively (19). Hence Ni is present in the surface region, consisting of several atomic layers, as metal and oxide. Since the ESCA peak intensity is directly correlated with the surface concentration, the composition of the surface can be roughly established from the ESCA information. The intensity ratio of Ni $2p_{3/2}$ to Ce $3d_{5/2}$, ~ 7.5, indicates that the surface is largely metallic Ni.

Table 1. Characterization of Catalysts Formed by Oxidation

Precursor Intermetallic Compound	O_2 Uptake (mmol/g)	Surface Area[a)] (m^2/g)	CO Chemisorption (μmol/g)	Particle Size (Å)
$LaNi_5$	-	0.10*	0.17*	
" (L-1)	1.71	0.55	1.2	90
" (L-2)	2.99	0.66	2.6	100
" (L-3)	6.57	3.5	7.1	100
$CeNi_5$	-	0.08*	0.13*	
" (C-1)	2.32	1.1	4.8	110
" (C-2)	3.74	15.7	31.7	300
" (C-3)	4.47	25.4	45.7	200
" (C-4)	5.14	23.7	51.8	350
$PrNi_5$	-	0.15*	0.10*	
" (P-1)	1.73	0.79	2.8	170
$NdNi_5$ (N-1)	1.71	1.1	1.2	140
$HoNi_5$ (H-1)	1.64	0.76	2.0	330
$ErNi_5$ (E-1)	1.61	1.0	2.0	280
$ThNi_5$	-	0.09*	0.2*	
" (T-1)	1.91	12.0	19.0	200
" (T-2)	3.35	18.0	105.7	270

a) Surface areas were measured at liquid nitrogen temperature by means of argon adsorption (17).

* These values were obtained for the original intermetallic compounds.

CO CHEMISORPTION

Although ESCA studies revealed existence of metallic Ni in the surface region, to obtain the information about the amount of metallic surface area or the number of active sites present on the surface room temperature CO chemisorption measurements were made. The results obtained are summarized in Table 1. It is informative to notice that the oxidized samples (L-1, C-1, P-1, N-1, H-1, E-1 and T-1) contain elemental oxygen corresponding to the complete formation of Ni/oxide assuming a stoichiometric reaction. It is evident that the oxidation led to an increase in the number of active sites along with a rise in the surface area. The extent of the increase was observed to be dependent upon the particular rare earth or actinide involved in the original compound. $CeNi_5$ and $ThNi_5$ exhibited striking changes in chemisorption during the stages of oxidation. CO chemisorption increases by up to 500-fold compared to the original compound were observed. In contrast, increases for $LaNi_5$ were much less pronounced. The differing behavior of $CeNi_5$ and $ThNi_5$ on the one hand and $LaNi_5$ on the other undoubtedly reflects important physicochemical differences. The most significant difference between $LaNi_5$ and the other two compounds is that La is tripositive and Ce and Th are quadripositive. This leads to a different electron concentration and perhaps a difference in chemical stability. This may be responsible for variation in

behavior of the systems produced by oxidation, but the precise factors and their operation are as yet unclear.

2. Reaction of CO and H_2

The reaction was carried out in the range of 150 to 300°C over the alloys, which had been oxidized to varying extents. The data obtained are summarized in Table 2. Activity for the present reaction was represented by the rate of CO

Table 2. Activity of Various Catalysts

Precursor Intermetallic Compound	CO Conversion (%)	Activity (ml/sec.g)	T.N.x10^3 (sec^{-1})
$LaNi_5$ (L-1)	1.2	$1.5x10^{-3}$	48
$CeNi_5$ (C-1)	2.0	$2.5x10^{-3}$	18
" (C-2)	1.0*	$1.2x10^{-3}$*	
" (C-3)	2.6*	$3.7x10^{-3}$*	1.7*
" (C-4)	5.0*	$6.1x10^{-3}$*	3.8*
$PrNi_5$ (P-1)	1.8	$2.2x10^{-3}$	26
$NdNi_5$ (N-1)	0.5	$6.1x10^{-4}$	19
$HoNi_5$ (H-1)	1.6	$2.0x10^{-3}$	31
$ErNi_5$ (E-1)	4.2	$5.2x10^{-3}$	59
$ThNi_5$ (T-1)	9.0*	$1.1x10^{-2}$*	10.6*
" (T-2)	7.0(at 190°C)	$3.5x10^{-2}$*	5.6*

* The values correspond to the results measured at 205°C; the others were obtained at 275°C, except as noted.

consumption per gram-catalyst. This kind of comparison seems valid since the catalysts were used under very similar conditions. Taking into account the fact that the catalytically active species is metallic Ni dispersed on the surface, it is also of interest to specify the turnover number (T.N.), representing the specific activity per site. The turnover number as molecules CH_4 produced per site per second was determined from CO chemisorption measurements assuming a 1:1 ratio of a CO molecule to surface Ni atom in the surface complex. Among the catalysts studied the oxidized $CeNi_5$ and $ThNi_5$ exhibited exceptional activity (Table 2). The oxidized $CeNi_5$ and $ThNi_5$ showed T.N. measured at 205°C about an order of magnitude higher than conventional silica- or alumina-supported Ni catalysts (15). It is therefore apparent that the supported catalysts derived using the oxidation treatment of intermetallics are exceptionally active for the conversion of CO and H_2 to methane. T. Inui et al. (20) have reported that activity for methanation was substantially enhanced when ∿3% rare earth oxide such as La_2O_3 or Ce_2O_3 was added to Ni-supported catalysts. It was found (21) that ThO_2 was also operative as a promoter for supported Ni catalysts.

It should be emphasized that the effectiveness of rare earth or actinide oxide-supported catalysts for syngas conversion is very dependent upon the preparation method. As noted in the Introduction, for example, a ThO_2-supported catalyst (6) prepared using the conventional impregnation procedure followed by calcining and reducing processes exhibited very poor activity compared to that obtained by the oxidation technique. It thus appears that the oxidation treatment of intermetallics plays a decisive role in formation of active catalysts and this method constitutes a new way of producing superior oxide-supported catalysts.

As shown in Table 2, for the oxidized $CeNi_5$ and $ThNi_5$ increase in the extent of oxidation results in an increase in the activity. There is a good correspondence between the CO chemisorption and activity and in this respect the present systems closely resemble behavior observed earlier for oxidized Ni_5Si_2 (22).

Hydrocarbon products in the reaction were largely methane. Small amounts of C_2 to C_4 hydrocarbons were also observed. Selectivity of hydrocarbon products over various oxidized alloys is listed in Table 3. The selectivity was determined in

Table 3. Selectivity of Catalysts

Precursor Intermetallic Compound	Conversion (%)	Composition (%) C_1	C_2	C_3	C_4
$LaNi_5$ (L-1)	1.8	92.0	7.0	1.0	-
$CeNi_5$ (C-1)	3.4	86.3	7.0	5.3	-
" (C-4)	5.0	77.3	15.9	6.8	-
$PrNi_5$ (P-1)	3.1	88.4	6.6	5.0	-
$NdNi_5$ (N-1)	1.8	91.3	4.3	4.3	-
$HoNi_5$ (H-1)	2.5	82.4	8.1	9.5	-
$ErNi_5$ (E-1)	4.2	74.0	10.9	15.0	-
$ThNi_5$ (T-1)	12.5	80.0	12.1	6.8	1.4

the conversion range below 10%. It is unclear from this study whether the selectivity is dependent upon extent of the total conversion. It is to be noted that the selectivity depends upon the nature of the rare earth or actinide in the precursor compound. Oxidized $LaNi_5$ revealed very high selectivity for methane formation. This accords with the observation of T. Inui et al. (20) referred to above.

References

1. V. T. Coon, T. Takeshita, W. E. Wallace and R. S. Craig, J. Phys. Chem. 80, 1878 (1976).
2. A. Elattar, T. Takeshita, W. E. Wallace and R. S. Craig, Science 196, 1093 (1977).
3. V. T. Coon, W. E. Wallace and R. S. Craig, in "The Rare Earths in Science and Technology," eds. G. J. McCarthy and J. J. Rhyne, Plenum Press, NY (1978), p. 93.
4. A. Elattar, W. E. Wallace and R. S. Craig, ibid., (1978), p. 87.
5. W. E. Wallace, in Hydrides for Energy Storage, A. F. Andressen and A. J. Maeland, eds., Pergamon Press Inc. (1978), p. 33.
6. A. Elattar, W. E. Wallace and R. S. Craig, Advances in Chemistry, in press.
7. V. T. Coon, Ph.D. Thesis, University of Pittsburgh, August, 1977.
8. C. A. Luengo, A. L. Cabrera, H. B. MacKay and M. B. Maple, J. Catal. 47, 1 (1977).
9. G. B. Atkinson and L. J. Nicks, J. Catal. 46, 417 (1977).
10. A. Elattar and W. E. Wallace, in "The Rare Earths in Modern Science and Technology" (1979), in press.
11. A. Elattar and W. E. Wallace, Science, submitted.
12. H. Imamura and W. E. Wallace, J. Catal, submitted.
13. A. G. Moldovan, A. Elattar, W. E. Wallace and R. S. Craig, J. Solid State Chem. 25, 23 (1978).

14. R. Chin, A. Elattar, W. E. Wallace and D. Hercules, J. Catal., submitted.
15. M. A. Vannice, J. Catal. 37, 449 and 462 (1975); 40, 129 (1975); 44, 152 (1976); 50, 228 (1977).
16. H. L. Gruber, Anal. Chem. 34, 1828 (1962).
17. F. M. Nelsen and F. T. Eggertsen, ibid., 30, 1387 (1958).
18. H. P. Klug and L. E. Alexander, in X-Ray Diffraction Procedures for Polycrystalline and Amorphous Materials, 2nd ed., p. 68, Wiley, NY (1974).
19. K. S. Kim and N. Winograd, Surf. Sci. 43, 625 (1974).
20. T. Inui, M. Funabiki, M. Suehiro and T. Sezume, J.C.S. Faraday I 75, 787 (1979).
21. S. Medsforth, J. Chem. Soc. 123, 1452 (1923).
22. H. Imamura and W. E. Wallace, J. Phys. Chem., in press.

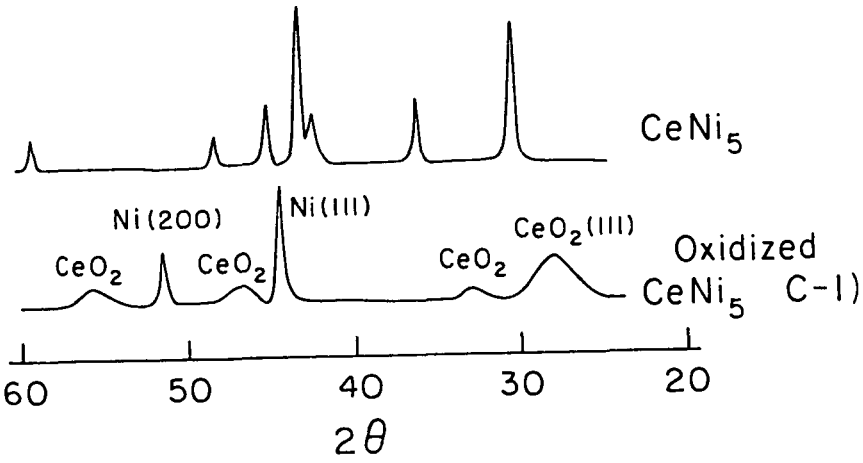

Fig. 1 Comparison of x-ray diffraction (Cu Kα radiation) of the oxidized and original $CeNi_5$.

CATALYTIC ASPECTS OF HIGH TEMPERATURE METHANATION

Karsten Pedersen, Allan Skov and J.R. Rostrup-Nielsen

Haldor Topsøe Research Laboratories
Nymøllevej 55, DK-2800 Lyngby, Denmark

INTRODUCTION

Methanation of synthesis gas mixtures is an essential step in the manufacture of substitute natural gas (SNG):

$$CO + 3H_2 = CH_4 + H_2O \quad (-\Delta H^o_{298} = 206 \text{ kJ/mol})$$
$$CO_2 + 4H_2 = CH_4 + 2H_2O \quad (-\Delta H^o_{298} = 165 \text{ kJ/mol})$$

The reactions are catalyzed by various metals of which supported nickel is preferred.

Methanation for SNG production is complex because the high concentrations of CO and CO_2 involved result in large potential temperature increases. This may cause sintering of the catalyst or for some cases a potential for carbon formation.

One solution is to include a recycle stream of product gas as a diluent. It is evident that this solution involves a loss of energy in the recycle operation, and that an economic process should allow minimum recycle. For an adiabatic process, however, this is equivalent to a large temprature increase.

Another solution is to carry out the methanation in a cooled reactor in which the heat of reaction is transferred from the reaction zone into a cooling medium, e.g. boiling water. For a cooled reactor, it appears advantageous to design for high "hot zone" temperatures, because this gives a better heat transfer.

When decreasing the operating temperature, the need for higher catalyst activity increases. Below a certain temperature the reaction will not "ignite". This problem may be aggravated because the catalyst having been exposed to the high temperature, may have to operate at the low temperature after ageing or poisoning of the catalyst at the reactor inlet.

Moreover, the steep temperature profile means that the operation temperature of a catalyst pellet may change 50-100°C within seconds in case of variations in load, recycle ratio and preheat temperature. This requires high mechanical stability of the catalyst.

Thus for adiabatic and for cooled reactors as well, in order to meet these process requirements, the catalyst should be active and stable both at high and low temperatures. This is a key problem to be solved when optimizing the methanation process for coal-based SNG.

The paper summarizes catalyst studies of important phenomena to be controlled in the development and use of an industrial catalyst meeting these requirements.

EXPERIMENTAL

The catalysts were studied in various test units. Sintering studies were performed in a tubular reactor (Di=32 mm) in which various catalyst samples were exposed simultaneously to sintering at given temperature, pressure and atmosphere. Low temperature deactivation phenomena were studied in differential flow reactors (Di=0.8 mm). The catalyst was used as 0.3 - 0.5 mm particles diluted with inert material. Standard activity tests, and determination of nickel surface areas were described earlier (1). The main part of the development work took place in a pilot plant with a 5 litre adiabatic reactor. The reactor had a full bed length (up to 2m) and operated at industrial mass velocities, leaving the reactor diameter as the only scale-up parameter. Catalyst samples from pilot tests were used for physical and catalytical examination.

RESULTS

Sintering

The methanation reaction on nickel requires a large ensemble of nickel atoms (2), and the specific activity is influenced by nickel crystallite size (3), by the composition of the support (4,5,6), and by non-linear poisoning effects (1). Therefore, the reaction appears sensitive to the structure of the catalyst and to its history of operation.

Sintering of the nickel crystals results in loss of surface area, and in principle recrystallization may change the nickel ensembles available, and hence cause a decrease of the specific activity. We showed previously (4,7) that heat treatment of nickel crystals on a stable low area ceramic support resulted in no sintering at 550°C over a period of 1000 hours, whereas the nickel surface area dropped to around 40 to 25% over the same period at 700°C and 850°C respectively, this result corresponds to the rule of Tammann, according to which sintering is expected above 0.5 times the melting point (°K) (8) of the metal. The growth mechanism of supported metal crystals appears very complex (9,10). The growth rate might be influenced by the wetting properties of the metal to the support, and by the micropores of the support material. It was illustrated that the diffusion of a metal crystallite is impeded, when the size of the metal crystallite is of the order magnitude of the diameter of the pore (11,12). In general, the metal particles may hardly grow to a size larger than the pore diameter of the support. This means that a stabilized micropore system of the support effectively prevents sintering of the nickel crystals.

Nickel catalysts designed for low temperature operation are normally based on high area supports such as gamma alumina, silica, chromia, etc. These supports suffer from significant sintering, which may be accompanied by weakening when exposed to temperatures above 500°C (4,13). The sintering may be accelerated by high steam partial pressure (14). Figure 1 shows results from sintering tests at conditions for accelerated sintering (i.e. H_2O/H_2=10, 30 atm). Three catalysts are compared: a low area steam reforming catalyst, a high area low

temperature methanation catalyst (Ni/γ Al_2O_3), and the Topsøe methanation catalyst MCR-type. The MCR catalyst maintains a high total surface area and mechanical strength, whereas the γAl_2O_3 based catalyst deteriorates. All catalysts show significant loss in nickel surface area at 800°C.

Carbon Formation

Thermodynamics predict carbon formation for methanation above a certain temperature, depending on feed composition and pressure. This may influence the minimum recycle ratio allowed, as illustrated in Figure 2. However, the thermodynamic data are influenced by the catalyst, because it modifies the structure of the carbon. This allows operation at conditions more critical than those, which correspond to the limit predicted on the basis of ideal graphite. We have shown previously (4,15) that this effect is favored by small nickel crystals in the catalyst.

In practice, this means that the so-called principle of equilibrated gas (1,4), (i.e. carbon formation when the gas shows affinity for carbon, after the establishment of the methanation and shift equilibria) predicts no carbon formation for methanation. The validity of this principle is indicated by the results in Table 1, obtained from thermogravimetric studies (1). The conclusion has been further confirmed by the experience in the pilot tests.

Low Temperature Problems

Low operating temperatures favor the adsorption of poisons, e.g. sulfur on the catalyst. We have shown that the effect of sulfur is strongly non-linear (1) reflecting that the methanation reaction is structure sensitive. This, and other studies (16,17), show that a sulfur content in the feed stream of less than 10 ppb is required to obtain a reasonable methanation activity after equilibration of the sulfur adsorption. Therefore, the effect of sulfur poisoning should rather be analysed in terms of a dynamic model for fixed bed adsorption (18).

The operation at a low recycle ratio or the straight-through operation in a cooled reactor, implies high partial pressures of carbon monoxide at the reactor inlet. This results in two problems.

At temperatures below 230°C, there is a substantial risk that carbon monoxide reacts with nickel, forming nickel carbonyl. Operation in this temperature range, with a partial pressure of carbon monoxide of 2.5 atm resulted in transport of nickel in the catalyst bed. Moreover, the formation of nickel carbonyl resulted in a drastic growth of the nickel crystals, up to particles of 20,000Å, thus exceeding, by large, the pore size of the catalyst support. This growth resulted in break-down of the catalyst. The forces involved appear much stronger than observed in thermal sintering of the nickel crystals, as described above.

Another result from operating with high partial pressure of carbon monoxide, appears to be a deactivation phenomenon, called β-deactivation developing slowly in some pilot tests, and being reflected by

the appearance of an inflection point in the axial temperature profile. Figure 3 illustrates the movement of the temperature profile, and that the β-deactivation disappears above a certain inlet temperature. The activity could be restored by treatment in hydrogen, as explained below.

The low temperature deactivation phenomena were further demonstrated by laboratory tests on a Ni/η Al_2O_3 catalyst in a differential reactor. As shown in Figure 4, no deactivation was observed if CO was replaced by CO_2. The deactivation rate increases significantly with the CO/H_2 ratio and by the presence of sulfur. The role of sulfur on other deactivation phenomena was indicated in our earlier studies (1).

The MCR-2X catalyst shows much less deactivation than the Ni/η Al_2O_3 catalyst. Analysis of the spent catalysts indicated by the growth of nickel crystals showed that the Ni/η Al_2O_3 catalyst had also been exposed to carbonyl formation in contrast to the MCR-2X catalyst. The large influence of catalyst composition on deactivation rate and carbonyl formation was also reported by Vannice and Garten (6).

The β-deactivation is probably due to the formation of a less reactive carbon state on the nickel surface, which might be the β-state identified by Wise et.al. (19,20).

The situation corresponds to the deactivation observed in steam naphtha reforming at low temperatures (21), and to a general model for carbon formation on nickel (22). The adsorbed intermediate (α'-carbon) may either be gasified to methane (2,19) or be dissolved in nickel as carbon and form carbon whiskers (1), or be transferred into encapsulating carbon (β-carbon). For the present case, apparently the conversion of α' into β is too slow at very low temperatures, e.g. 250°C, whereas at high temperatures the rate of hydrogenation of β-carbon exceeds the transformation rate of α' into β-carbon (20). These effects are overlapped by the influence of the surface concentration of α'-carbon such as the hydrogenation rate of α'-carbon and the parameters governing the chemisorption of carbon monoxide. The CO chemisorption depends on the partial pressure of CO and the temperature at a given position in the reactor, and it is also affected by the composition of the catalyst (5).

MCR-2X Catalyst

The development program for methanation catalysts at Topsøe's laboratories aimed specifically at solving the problem of operating over a wide temperature range. The work resulted in the MCR-2X catalyst. The support has a stabilized micropore system that effectively prevents sintering of the nickel crystals. The resulting high nickel surface area and the absence of alkali (sometimes added to prevent carbon formation) led to the desired high methanation activity. The catalyst is mechanically stable at high as well as low temperatures. The stability was proven in pilot tests with a total run-time amounting to 15,000 hours. This included 8,000 hours operation at the same catalyst filling at a maximum temperature of 600°C. Data in Table 2 demonstrates the thermo-stability of MCR-2X reflected by an almost unchanged mechanical strength and total surface area. The activity stabilized after 1,000-2,000 hours.

The mechanical and chemical properties of MCR-2X also offer flexibility in providing the capability for regeneration of spent catalysts. Table 3 shows results from regeneration tests performed on samples taken after 4700 hours operation in the pilot plant. The carbonaceous film responsible for the β-deactivation can be removed simply by treatment in hydrogen, whereas sulfur is more difficult to remove. However, the catalyst easily withstands a high temperature oxidation and re-reduction, which will not only remove sulfur, but also result in redistribution of any sintered nickel crystals. As shown in Table 3, more than 50% of the original activity of a new catalyst can be regained by this method.

The properties of MCR-2X can be utilized in different process schemes optimized for the feedgas in question. The critical step is the first methanation stage, where the full potential of MCR-2X is utilized, MCR-2X allowing maximum practicable temperature increase from ca. 300°C to 700°C.

The mechanical sintering problem could be solved by using steam reforming catalysts, which will, of course, be active also for methanation. However, the nickel surface areas in most steam reforming catalysts are too small to provide adequate low temperature activity, thus dictating operating at higher reactor inlet temperatures. This will not necessarily influence the overall conversion in the reactor, which is fixed by the exit temperature. However, for adiabatic operation, the reduced temperature rise means a higher recycle energy consumption. In principle this can be overcomed by increasing also the exit temperature, but this means a greater number of reactors because of the smaller conversion per reactor. This situation is illustrated in Figure 5, in which the operation, based on MCR-2X, is shown (solid line) in a simplified example involving three adiabatic reactors, corresponding to an overall conversion of 95%.

The process path, TREMP (Topsøe Recycle Methanation Process) is compared with alternative routes of high temperature methanation (dashed lines) based on a reforming type catalyst. A temperature of 450°C is assumed as the minimum inlet temperature for the reforming type catalyst. To achieve the same conversion of the first reactor as obtained in TREMP, a recycle ratio 2 times higher as in TREMP is required. This means higher energy consumption. If recycle is excluded, four reactor stages are necessary with reforming catalysts to obtain a conversion equivalent to that of the first TREMP reactor. Moreover, this solution is doubtful because of the excessively high exit temperature of the first reactor.

By the use of a combined bed of a non-nickel catalyst with MRC-2X, the inlet temperature can be decreased to 200°C, thus allowing a temperature increase of 500°C at a reduced recycle rate. The wide operating range of MCR-2X may be utilized in the design of boiling water reactors for methanation. With MCR-2X, design for "hot zone" temperatures of 700°C is realistic, since this leaves a good safety margin. An explorative test was made in the pilot plant in which MCR-2X was exposed to 780°C in the "hot zone". For simplicity the test was made in an air-cooled reactor. The inlet temperature was

300°C and after the hot zone, the reaction temperature was decreased to about 250°C. The tube wall temperature in the hot zone was between 300 and 400°C, which is close to the expected value in an industrial boiling water reactor. Measured and calculated temperature profiles are shown in Figure 6. No significant deactivation of the catalyst was observed at the test, which supports the possibility for designing for high hot spot temperatures, being important for optimum reaction and heat transfer conditions.

A special application of methanation is related to the Long Distance Energy Transport System NFE or ADAM/EVA system, which is being developed at the German Nuclear Research Center KFA-Jülich, in cooperation with Rheinische Braunkohlenwerke AG in Cologne. In this system (23,24), nuclear energy released in a helium-cooled high temperature reactor is transferred to steam reformer (EVA) with a hot helium as heating medium. The product is transported by pipeline to power plants in which the heat is recovered in a methanation plant (ADAM). The high exit temperature which can be accepted of MCR-2X makes it possible to raise superheated high pressure steam at the destination for electricity production as required in the NFE system. Topsøe has supplied the semi-commercial demonstration plant ADAM-1 to KFA - Jülich. The plant is based on three adiabatic methanation steps, and it is processing synthesis gas manufactured from up to 200 Nm^3 per hour of natural gas (23). Figure 7 shows temperature profiles from an ADAM I run which was made by KFA in cooperation with Topsøe (25). MCR-2X was installed in the first two methanation steps, whereas the third methanator operated on MCR-4 which is a highly active low temperature catalyst.

CONCLUSIONS

The use of a nickel catalyst for methanation is limited to a minimum operating temperature because of the risk of carbonyl formation and deactivation, and to a maximum operating temperature because of sintering and in certain cases the risk of carbon formation. Between these temperature limits, the activity and stability of the catalyst determines the optimum layout of the methanation process. The Topsøe MCR-2X catalyst allows operation in the temperature range 250°C to well above 700°C. By combination with a non-nickel catalyst, the operation range can, for certain cases, be extended to 200 to 700°C. This capability of high temperature methanation offers the possibility of design for low recycle, or for optimum boiling water reactors.

REFERENCES

1. Rostrup-Nielsen, J.R., and Pedersen, K., J.Catal. (in press).

2. Araki, M., and Ponec, V., J.Catal. 44, 439 (1976).

3. Coenen, J.W.E., Schats, W.M.T.M., and van Meerten, R.Z.C. Bull.Sco.Chim.Belg. (1979) (in press).

4. Rostrup-Nielsen, J.R., "Steam Reforming Catalysts", Teknisk Forlag, Copenhagen 1975.

REFERENCES (Cont'd)

5. Schoubye, P., J.Catal. 14, 238 (1969).

6. Vannice, M.A., and Garten, R.L., J.Catal. 56, 236 (1979).

7. Rostrup-Nielsen, J.R., J.Catal. 21, 171 (1971)

8. Garner S.W., "Chemistry of the Solid State", Butterworths, London 1955, p 307.

9. Ruckenstein, E., and Pulvermacker, B., AIChE Journal 19, 356 (1973).

10. Wynblatt, P., and Tae-Moon, Ahn, "Sintering and Catalysis", Materials Science Research 10, 83 (1975).

11. Ruckenstein, E., and Pulvermacker, B., J.Catal. 37, 416 (1975).

12. Borisova, M.S., Fenelonov, V.B., Dzisko, V.A., Simonova, L.G., Kinet.Katal. 17, 653 (1976).

13. Williams, W., Butler, G.A., and Hammonds, J., J.Catal. 24, 352 (1972).

14. Levy, R.M., Bauer, D.J., Roth, J.F., Ind.Eng.Chem.Prod. Res. Develop. 7, 217 (1968).

15. Rostrup-Nielsen, J.R., J.Catal. 27, 343 (1972).

16. McCarty, J.G., Wentrcek, P.R., Wise, H. and Wood, B.J. DOE Contract 76-C-03-115, Annual Report Oct. 26, 1978.

17. Fitzharris, W.D., PhD Thesis, University of Delaware, 1978.

18. Christiansen, L.J., and Andersen, S., Proc. 6th Int. Symp. on "Chemical Reaction Engineering", Nice 1980 (in press).

19. McCarty, J.G., and Wise, H., J.Catal. 57, 406 (1979).

20 McCarty, J.G., Wentrcek, P.R., and Wise, H., in "Proc.Amer. Chem.Soc.Symposium", Chicago, Aug. 28-Sept. 2, 1977", p 1315.

21 Moseley, F., Stephens, R.W., Stewart, K.D., and Wood, J., J.Catal. 24, 18 (1972).

22. Rostrup-Nielsen, J.R., and Trimm, D.L., J.Catal. 48, 155 (1977).

23. Harms, H.G., Höhlein, B., and Skov, A., Chem.Ing.Tech.(in press).

24. Boltendahl, V., Niessen, H.F., Theis, K.A., GWF-Gas/Erdgas, 117, 517 (1976).

25. Harms, H.G., Höhlein, B., and Skov, A., Oil and Gas J. (submitted).

Table - 1

Carbon Formation, Thermogravimetric Tests

Experimental conditions re ref (1)
Catalyst, 13wt% Ni, D_{Ni}= 300 - 3500 Å

Carbon limits calculated from "principle of equilibrated gas"

	1	2
CO/H_2	0,33	0,7
PCO atm	0,2	0,33
Temp. °C	400-470	400
Calc. carbon limits		
Carbon for (Temp.°C):		
Graphite	$415 < T < 800$	$T < 1069$
Catalyst (D_{Ni}=3500Å)	$600 < T < 350$	$T < 684$
Carbon Formation	No	Yes

Table - 2

High Temperature Stability of MCR2X
Results from Pilot Tests

Operation Time h	at Temp. °C	BET Area m^2/g	H_2 Area m^2/g	D_{Ni} Å
New MCR2X		52	7	220
8127	600	30	3	295
1895 followed by 860	600 700	35	3	345

Table - 3

Regeneration of MCR2X Catalyst

Samples from HTAS-run 5

Operating time at temp. h	°C	Regeneration Conditions	Activation Conditions	Intrinsic Activity relative to unused cat. Before	After
4800	290-385	H_2,15h,500°C	-	0.006	0.05
4800	290-385	H_2,4h,700°C	-	0.006	0.15
3900	280-300	H_2O,16h,700°C	800-850°C,2h	0.025	0.42
3900	600	H_2O,16h,700°C	800-850°C,2h	0.11	0.50

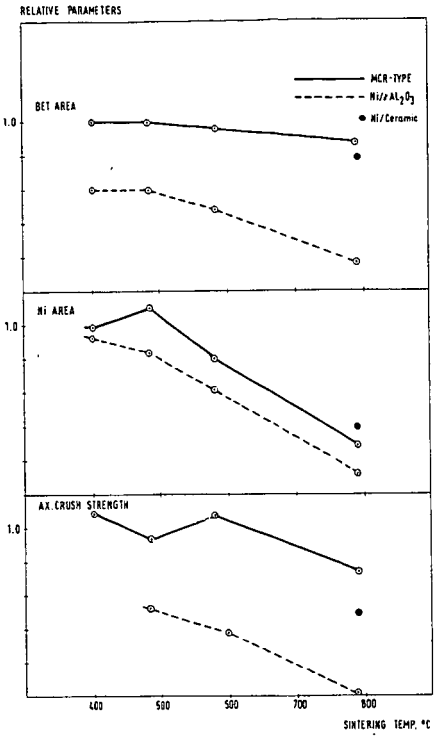

Figure 1

Sintering of Catalysts

30 kg/cm^{2}g, H_2O/H_2=10, 140-170 hours
MCR-type. BET-area = 33 m^2/g
Ni/γAl_2O_3. BET-area = 101 m^2/g
Ni/Ceramic. BET-area = 1.2 m^2/g

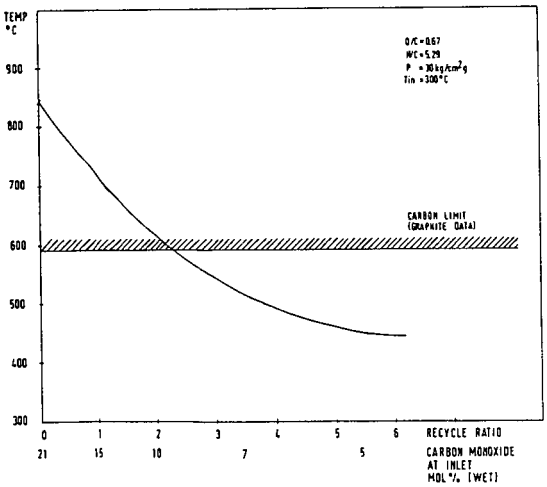

Figure 2

Carbon Limits

Recycle ratio and outlet temperature of adiabatic equilibration of gas. The example refers to a feed-gas containing 12 vol% CH_4. Correction for carbon-structure on catalyst moves carbon limits to 950-1050°C.

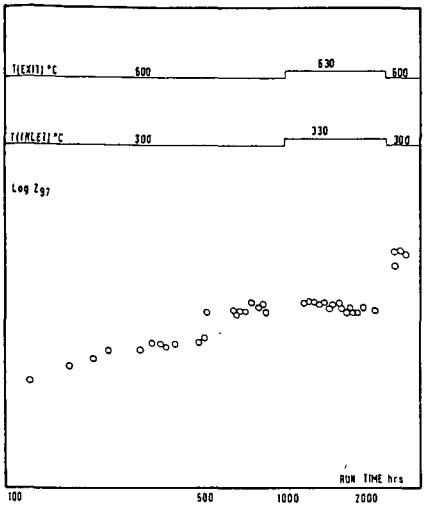

Figure 3

β-deactivation in Pilot Test

MCR-type catalyst.

O/C = 1., H/C = 6., P = 30 kg/cm^{2}g, PCO = 2 kg/cm^{2}g.

Z_{97} = axial distance from top of catalyst bed for 97% conversion of max. adiabatic ΔT obtained.

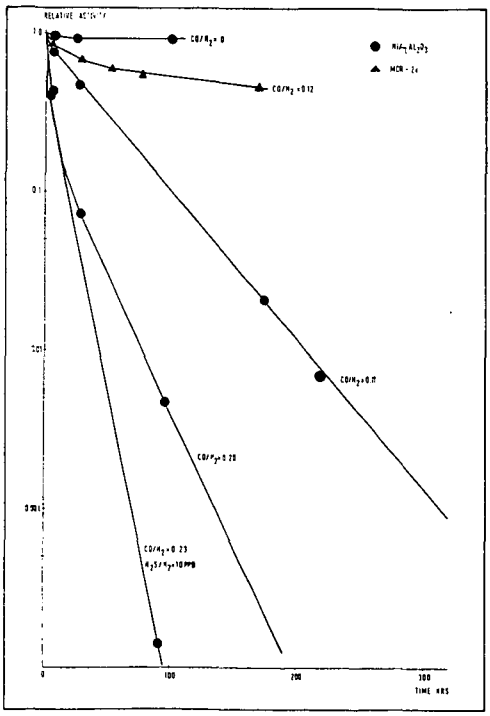

Figure 4

Low Temperature Deactivation Laboratory Tests

300°C, 21.2 kg/cm^{2}g, NHSV=$10^6 h^{-1}$

Feedgas (vol%):

H_2O (35)

CO (0-11)

CO_2 (5)

H_2 (rest)

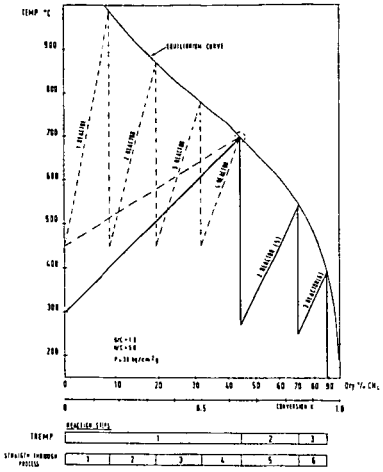

Figure 5

High Temperature Methanation

Simplified Example

Comparison of TREMP reaction steps (solid line) with reaction routes based on a reforming type catalyst (dashed lines).

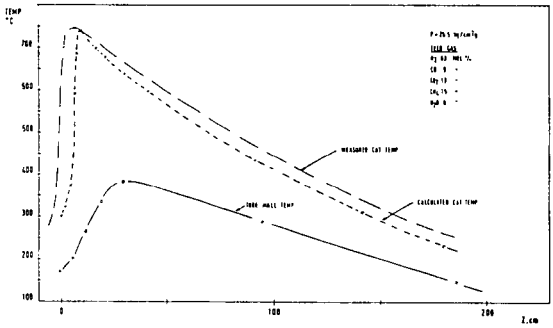

Figure 6

Explorative Pilot Test

with Air-cooled Reactor

Measured and calculated temperature profiles. The calculation model did not consider axial radiation in the bed, which explains the difference of the two profiles.

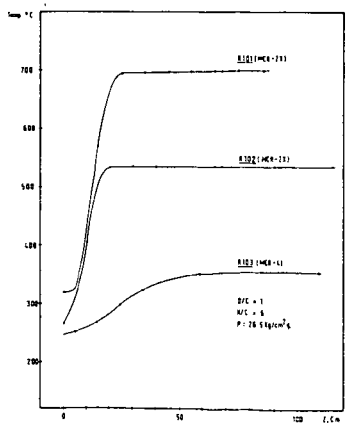

Figure 7

ADAM-1 Test Unit

Temperature Profiles

Applied Fischer-Tropsch Kinetics for a Flame Sprayed Iron Catalyst

W. J. Thomson, J. M. Arndt, and K. L. Wright

University of Idaho, Department of Chemical Engineering, Moscow, Idaho, 83843

INTRODUCTION

There has been a great deal of previous work done of Fischer Tropsch catalysis but until recently, very little rate data have been obtained other than semi-quantitative results. A great deal of the previous literature deals with the proposed and hypothetical mechanisms of Fischer Tropsch catalysis and its similarities/dissimilarities to SNG methanation. Despite the voluminous amount of work in this area there is still controversy as to whether deposited carbon or iron carbide (in the case of iron catalysts) is the active intermediate in the mechanistic scheme.[1] In addition to this there was a great deal of work accomplished at the Bureau of Mines in the 1940's and 50's concerning the behavior of Fischer Tropsch catalysis under various conditions.[2] Iron as well as cobalt and ruthenium have been proposed and studied as possible Fischer Tropsch catalysts.[3, 4] There has also been considerable interest in the incorporation of various promoters in Fischer Tropsch catalysis in order to alter olefin-to-paraffin ratios, minimize CO_2 make, etc. An interesting study being conducted at the University of Utah[5] is seeking to systematically alter various promoters in order to determine the best combination in order to achieve a maximum of C_2-C_5 hydrocarbons. A short review of Fischer Tropsch technology up to 1975 has been given by Shah and Perrotta.[6]

There have been two kinetic studies using iron catalysts for Fischer Tropsch applications.[7, 8] Dry et. al.[7] used a triple promoted iron catalyst in the pressure range of 10-20 atmospheres and at temperatures from 240-270C to determine the reaction orders of the CO consumption rate with respect to both hydrogen and CO. He employed a differential reactor with H_2-toCO ratios varying from 1 to 7. They found that the reaction order with respect to CO was effectively zero but the reaction order with respect to H_2 was first order. Between 225 and 265C they also determined an activation energy of 16.8 Kcal/mole. However all their data were obtained by measurements of the CO_2 and water-make in the exit stream. By assuming that there was minimal oxygenated products (reasonable for iron

catalysts), then the summation of the CO_2 and water-make should equal the total CO consumption rate. In all cases the ratio of CO_2-to-water was less than 1 except at the highest temperatures (265C, where it equaled 1.15). Since the effect of increasing space velocity was to dramatically decrease the CO_2/H_2O ratio, they concluded that CO_2 was a secondary reaction produced by the water gas shift reaction. A more recent kinetic study was conducted by Atwood and Bennett.[8] In this case they employed not only a tubular flow reactor but also an internally recirculated reactor (similar to the reactor employed here). They claimed in their paper that there was little difference in the reaction kinetics whether the recirculated reactor or the tubular flow reactor was employed. Based on our experience it would appear that this was due to their minimal H_2 consumption (H_2 in excess) and a zero order dependency of the reaction with respect to CO (as reported by Dry et. al.[7]). In this case they reported that with the iron catalyst, the CO_2/H_2O ratio was significantly greater than one but it should be pointed out that the temperatures employed in this study ranged from 250C to 315C; that is, signficantly higher than the temperatures used by Dry et. al.[7] They proposed a kinetic expression which is based on the rate being dependent on the hydrogen concentration and the fraction of reduced iron present.[9] A psuedo steady state balance between the oxidation of iron by H_2O and its reduction by CO leads to equation (1).

$$r_{CO} = \frac{k(P_{H_2})}{1 + b\, P_{H_2O}/P_{CO}} \qquad (1)$$

Experimental data at three temperatures were used to determine the constants k and b as a function of temperature. However it should be pointed out that the term involving the ratio of water to CO partial pressures in the denominator was only important for a very few data points. Also, since a constant feed mixture with a H_2 to CO ratio of 2.0 was used and the authors report that the mole fraction of H_2 in the product stream was essentially

independent of carbon monoxide conversion, the H_2 partial pressure was close to a constant for all runs. Although the authors show an excellent fit when equation (1) is rearranged to the linear form of equation (2), note that the essentially constant hydrogen partial pressures and a small

$$\frac{P_{H_2}}{r} = \frac{1}{k} + \frac{b}{k} \frac{P_{H_2O}}{P_{CO}} \qquad (2)$$

effect of the water-to-CO partial pressure would produce a constant rate at any temperature.

Two other rate expressions based solely on observation, have also been proposed.[9] In one, the rate was observed to depend only on the partial pressure of H_2 (for conversions less than 60%) and, in the other an adequate correlation for cobalt was obtained by equation (3).

$$r_{CO} = \frac{k\, P_{CO}\, P_{H_2}^{\,2}}{1 + K_1\, P_{CO}\, P_{H_2}^{\,2}} \qquad (3)$$

Fischer-Tropsch synthesis is highly exothermic and consequently a good deal of attention has been spent on reactor design considerations. Designs ranging from slurry reactors to fluidized beds have been proposed[2] and, in the latter case, actually constructed.[10] It is also common to utilize recycle reactors in order to restrict the temperature rise across the catalyst bed, but a heavy price must be paid in terms of compressor costs. A low pressure drop reactor utilizing parallel plates and inserts coated with catalyst was first proposed by DOE for the exothermic methanation reaction[11] and a similar design using iron catalysts for Fischer Tropsch has been discussed by Haynes, et. al.[12] The work reported here deals with an applied kinetics study utilizing this catalyst concept. While the scope of the project is concerned with product distributions as well as reaction rates, in this paper we will only focus on reactant and make-gas rates.

EXPERIMENTAL EQUIPMENT AND PROCEDURES

Berty Reactor System

All of the experiments were conducted in an internally recirculating reactor ("Berty" type) and a schematic of this equipment is shown in Figure 1. Hydrogen and CO are monitored separately via capillary flow meters equipped with pressure drop transducers and the flows are adjusted with the reactor on by-pass to obtain the desired inlet H_2-to-CO ratio and total flow. Once the desired ratio is obtained, a sample is sent for analysis via gas chromotography using a Carle Model 111 H gas chromotograph. The reactor is then put on stream and the H_2-CO mix is fed to the reactor. The exit stream leaving the reactor passes first through a "hot trap" (a condenser maintained at 120C) in order to condense waxes. The uncondensed portion of the stream then passes through a cold trap (at 0 C) where water and oil are condensed. The gas effluent from this condenser passes into a knock-out pot to remove entrained liquids and then proceeds via a wet test meter to vent. Provisions are made to sample this exit gas stream on line and again, analysis is done via a Carle 111 H gas chromotograph. The reactor pressure is adjusted and maintained by means of a needle valve at the reactor exit. Temperatures within the reactor are measured just above and below the catalyst sample. The mass velocity across the catalyst surface can be adjusted by means of regulating the RPM of the magnedrive unit equipped with the Berty reactor. Typically at RPM's above 750 the temperature difference across the catalyst is within 2C and all data reported here were obtained at 1500 RPM.

The Carle Analytical Gas Chromatograph is equipped with an on-line hydrogen transfer tube so that reasonably accurate hydrogen peaks are obtained as part of the analysis. A 2.5 m poropak Q column at 105C was placed in a series-bypass mode with a 2.5 m molecular sieve column maintained at 30C. With the columns connected in series, H_2, CO and CH_4 pass through the poropak column and into the molecular sieve column where they are temporarily retained. A valve is then switched so that the molecular

sieve is bypassed and CO_2, H_2O and C_2-C_4 compounds are separated and analyzed. With the columns placed in series once again, analysis of H_2, CO and CH_4 takes place.

The iron catalyst, supplied by the Pittsburgh Energy Technology Center (PETC) of DOE, consisted of taconite which was plasma-sprayed to an average thickness of 0.56 mm on flat plates of iron substrate. It had a BET area of 2 m^2/gm and a porosity of 0.48. The catalyst assembly consisted of 5 plates, each 7.6 cm high and of varying widths so as to be compatible with the draft tube size of the Berty reactor. The plates were bolted together with two threaded rods and the assembly and dimensions are shown in Figure 2. The catalyst was assembled, leak tested in He and then reduced by heating to 500°C in flowing H_2 over a 4-hour period and then holding at 450°C for 24 hours. Attempts were made to estimate the water make during reduction in order to determine the percentage reduction of the available iron. Unfortunately the slow reduction rate and consequent low H_2O concentrations did not allow for accurate measurements.

The need for a carburization pretreatment when using iron Fischer Tropsch catalysts has been the subject of a number of investigations.[13] In this case we utilized a H_2/CO feed of 1.5 at 300°C and 1.6 MPa and ran for a total of 30 hours on-stream. This corresponded to the time at which the activity and product distribution stabilized. It should be pointed out however, that the catalyst was idled in H_2 at 300°C and 1.6 MPa at the end of each day's running. In addition the conversions varied during this pretreatment and, since the reactor behaves as a CSTR, the catalyst was exposed to varying H_2/CO ratios. This will be discussed below in more detail.

RESULTS

Prior to entering into a discussion of the results, it is important to emphasize the behavior of a CSTR reactor such as the one used here.

First of all, in discussing reaction rates or product distributions, it is the reactor *exit* conditions which are the independent variables. These are brought about by independent control of the inlet flow rate, inlet composition, reactor pressure, and temperature. Consequently, in the subsequent discussion only the exit conditions will be referred to. Another important factor is that, since a fixed bed catalytic reactor ($\sim$ plug flow) will have catalyst exposed to both inlet and outlet conditions, it is important to obtain data over a wide range of conversions and inlet compositions. For example, in Fischer-Tropsch synthesis the H_2/CO ratio will generally increase as conversion increases. Thus it is important to vary the conversion as well as the inlet H_2/CO ratio so that a wide range of independent data are available for statistical analysis. In this work the CO conversions varied from 15% to 85% and the exit H_2/CO ratios were varied independently from 0.8 to 18. Total pressures ranged from 0.77 to 3.1 MPa and temperatures from 250C to 300C.

Induction Period

The fact that Fischer-Tropsch catalysts generally require an induction (or "carburization") period has already been mentioned. Proper carburization is thought to increase the catalyst lifetime and of course this is exceedingly important for commercial success. In our case, we wished to obtain rate data corresponding to the stable activity of the catalyst and we were unable to run continuously. Because of this latter restriction we followed a procedure of idling the catalyst in H_2 at 1.0 MPa whenever we were not running. Because of these differences we elected to utilize an alternate induction method which was more compatible with our day-to-day operation and which appeared to give the same stable activity[14] as the more typical complex carburization procedure.

The procedure employed during the first 24 hours of induction was to expose the catalyst at 300C and 1.6 MPa pressure to a 1.5 H_2/CO mixture at an "exposure velocity" (J, volumetric flow rate at standard condition per unit superficial catalyst area) of 2.6 m/hr. Some of the results obtained

during this period are shown in Figure 3. First of all it should be noted that the conversion was very high during the first four hours on stream. This points to the importance of conducting Fischer-Tropsch catalyst screening tests only after the catalysts have been exposed to synthesis gas for at least four hours. Note that during the first 20 hours of induction, the conversion starts off low and builds up during the day's run. It was hypothesized that the H_2 idling procedure was effecting reduction of the active iron carbide so that the first few hours of the run are spent reforming FeC at the expense of hydrocarbon production. As a result, the inlet conditions were changed at 24 hours time-on-stream (TOS) to 3.1 MPa and $H_2/CO = 2.0$. As can be seen from Figure 3, once this change was made, the variation in daily conversions was markedly reduced and the catalyst reached apparent stability after about 35 hours TOS.

While the results in Figure 3 show only the total CO conversion, some mention ought to be made of the selectivity to C_5^+ during this period. During the 24 hours TOS, the C_5^+ weight fraction of total hydrocarbon make gradually increased on a daily basis from about 0.05 to 0.20. After this period the fraction remained essentially constant at about 0.25.

Product Distribution

In principle either CO_2 or H_2O can be produced from the chain growth which occurs during Fischer-Tropsch synthesis. However, CO_2 can also be produced via the reversible water gas shift reaction

$$CO + H_2O \rightleftarrows CO_2 + H_2 \qquad (4)$$

Typically the CO_2 make was comparable to the CH_4 make at 250C and was 50 to 100% greater than CH_4 at 300C. If the CO_2 is produced from a side reaction such as equation (4), then one would expect an increasing CO/H_2 ratio with increased conversion. As Table I shows, this is indeed the case at both temperatures as long as the H_2/CO ratio is approximately constant. Also shown in Table I is the equilibrium parameter, ϕ, which is defined as

$$\phi = \frac{P_{CO_2} \; P_{H_2}}{K_{eq} \; P_{CO} \; P_{H_2O}} \qquad (5)$$

and will of course be equal to 1.0 at equilibrium (Keq is the equilibrium constant). It is apparent from the results shown in Table I that the water gas shift reaction is well removed from equilibrium at 250C but closer at 300C. Some measure of the reversible nature of the reaction rate can also be obtained from Table I. That is, at constant conversion the CO_2/H_2O ratio decreases as the H_2/CO ratio increases. This would indicate an inhibition of the forward reaction rate of equation (4) by increased product-to-reactant ratios.

Another important aspect of Fischer-Tropsch synthesis is the olefin-to-paraffin ratio of the hydrocarbon products. Table II shows the C_2H_4/C_2H_6 ratio as a function of the H_2/CO ratio and conversion at two temperatures. Note that this ratio decreases as conversion increases at both temperatures in agreement with Kugler's[15] hypothesis that the main elements in chain growth are olefins, not paraffins. As expected, higher H_2/CO ratios also lower the C_2H_4/C_2H_6 ratio since these would tend to promote hydrogenation. Comparing the data at two temperatures, it can also be seen that higher C_2H_4/C_2H_6 ratios are favored at the lower temperature.

The experiments conducted during this portion of the investigation were designed primarily to obtain reaction rate data and since a large number of separate runs were required to accomplish this goal, the run times were generally restricted to 3 hours or less. Unfortunately this is not a sufficient length of time to obtain large enough quantities of oil for accurate measurements (the oil make varied from about 0.2 to 4.0 ml/hr). Nevertheless, some insight into the parameters which favor oil make can be obtained from the data shown in Figure 4. Here the weight fraction of C_5^+ (C_5^+/total hydrocarbon make) is plotted as a function of conversion for different H_2/CO ratios at 250C. As expected, increasing conversions result in higher C_5^+ fractions (the chain has a chance to grow) and apparently higher H_2/CO ratios retard the formation of higher carbon numbers. Within the accuracy limitations of the data, the C_5^+ fraction did not appear to be a function of pressure at 250C. However this

was not the case at 300C where it was found that higher pressures tended to increase the C_5^+ fraction. Because of this, there were not enough 300C data at similar conditions in order to obtain a good comparison with the data at 250C. Nevertheless the results in Table III show a definite decrease in the C_5^+ fraction as the temperature increases from 250C to 300C.

Another parameter of interest in Fischer-Tropsch synthesis is the product distribution of the hydrocarbon make. During most runs a small but detectable wax was collected from the hot trap (see Figure 1) but the quantities were too small for accurate analysis. A number of oil-make samples were also subjected to GC-MS analysis and carbon numbers up to about 18 were detected with the highest weight fraction at C8 or C9. The major constituents of the oil were the normal paraffins with varying quantities of olefins and branched compounds at each carbon number. Little in the way of oxygenated compounds were detected.

A common analysis to which Fischer-Tropsch hydrocarbons are subjected is the so called "Schulz-Flory" distribution.[16] In this case the log of the mass fraction of each species divided by its carbon number would plot linearly as a function of carbon number if Fischer-Tropsch synthesis follows equal probability chain growth. Such a plot, typical of the data collected here, is shown in Figure 5. As can be seen, while linear plots are obtained at low and high carbon numbers, there is a transition region between C_4 and C_8 which does not plot linearly. Since the C_1-C_4 compounds essentially remain in the gas phase and the C_5^+ compounds are collected in the liquid phase, it was first thought that the behavior in Figure 5 was due to a material balance error. However when various arbitrary errors were added, either to the gas or liquid quantities, the same type of plot resulted. Evidently the Schulz-Flory distribution does not apply over the complete carbon number range. It is interesting to note that similar results with this catalyst have been obtained at PETC using a tubular flow reactor.[14]

Reaction Rates

Ideally we would like to measure intrinsic reaction rates (that is, rates in the absence of all transport limitations) under proposed commercial operating conditions such as those used here. For Fischer-Tropsch synthesis this is difficult to do because of the production of higher carbon number oils which could saturate the catalyst pores and lead to the necessity of gaseous reactants having to diffuse through liquid filled pores. Although the thickness of the catalyst used here was only 0.56 mm, the very low diffusivities of gases in liquids ($\sim 10^{-5}$ cm^2/sec) can still result in pore diffusion limited rates. This will be discussed in more detail below. For high reaction rates it is also possible to be limited by gas-solid transport phenomena. This was avoided in these experiments by increasing the reactor impeller speed until there was no separate dependency of the rate on impeller speed. This was found to occur at 750 rpm and, as mentioned earlier, all data were obtained at 1500 rpm.

Because of the possibility of pore diffusion limitations, the rate data were not subjected to thorough evaluations of various mechanistic kinetic expressions. In addition, because of the complexity of Fischer-Tropsch synthesis, it was decided to first attempt to analyze the rate of consumption of CO, independent of the species, produced. Consequently a simple power law model in terms of CO and H_2 partial pressures was evaluated but it did not provide for a sufficiently accurate correlation. Although a number of more complex models were found to give adequate correlations of the data it was found that the rate expression given by equation (1) gave as good a correlation as any. Specifically

$$r_{CO} = \frac{k\, P_{H_2}}{1 + b\, P_{H_2O}/P_{CO}} \qquad (1)$$

with

$$k = 7.6\times10^3 \exp\left[\frac{-8820}{RT}\right] \qquad (6)$$

$$b = 0.40 \exp\left[\frac{1430}{RT}\right] \qquad (7)$$

In these quations r_{CO} is expressed in terms of the superficial area of the catalyst, g moles/m^2-hr, pressure is in atmospheres and temperature is in degrees Kelvin.

In comparing these values with those given previously by Atwood and Bennett[8] for a potassium promoted fused iron catalyst, the major difference is in the apparent activation energy for k. Atwood and Bennet reported a value of 20.3 Kcal/mole whereas we observe a much lower value of 8.8 Kcal/mole. Again this might be due to strong pore diffusion effects since it is well known that for near first order kinetics, pore diffusion rate limitations will produce an apparent activation energy equal to one-half its true value. If this were the case, one would expect that equation (1) would not give as good a fit at the higher temperature. Figure 6 shows a plot of the predicted versus the measured values of r_{CO} and, as can be seen, the data scatter is definitely larger at 300C. In fact the average deviation at 250C was approximately 10% whereas it was 20% at 300C.

As already mentioned, CH_4 was the most signficant product under all conditions. Consequently a separate determination was made of a rate expression which would describe its rate of formation. Due to the fact that CH_4 is only one of many products, no attempt was made to base the rate expression on kinetic mechanisms. Instead a simple power low model was employed and the results are shown in equation (8)

$$r_{CH_4} = 5.7\text{x}10^4 \exp\left[\frac{-13,120}{RT}\right] P_{CO}^{-\frac{1}{2}} P_{H_2} \qquad (8)$$

Here again the rate is given in moles/m^2hr and the pressure in atmospheres. As expected, an increased rate of CH_4 production is favored by higher temperatures and higher H_2/CO ratios.

A similar attempt was made to obtain a suitable correlation for the rate of CO_2 production. Since it is hypothesized that the CO_2 is produced via the water gas shift reaction, it was anticipated that the rate here would depend on the partial pressures of CO and H_2O. Surprisingly however,

the rate was found to be independent of P_{CO} but rather to be dependent on the H_2O/H_2 ratio as shown in equation (9).

$$r_{CO_2} = 6.58\times10^7 \exp\left[\frac{-15,500}{RT}\right] \left(\frac{P_{H_2O}}{P_{H_2}}\right)^{1.3} \quad (9)$$

This could be explained in two ways: the reverse reaction rate is significant and strongly dependent on P_{H_2}; and CO is in excess (since H_2O is a product of the primary synthesis reactions). The first portion of this explanation can not be proven but seems to be reasonable (strong H_2 adsorption could produce the same effect). Although the data used in obtaining equation (9) covered a wide range of CO/H_2O ratios (0.2-12), there were only three runs (out of 62) with CO/H_2O less than one. Since these runs had very high CO_2 production rates and high CO conversions, it is conceivable that the rate of CO_2 production does depend on P_{CO} when it is less than or equal to P_{H_2O}.

Diffusion Limitations

The possibility of strong pore diffusion effects has already been mentioned and the data for the CO consumption rate gives some evidence of its existence. However the rate expression for CO_2 production had an activation energy more typical of kinetic reations and since it was found to depend on P_{H_2O}, the primary product of Fischer-Tropsch synthesis, it is somewhat surprising that it did not have a lower apparent activiation energy. A possible explanation could be that the dominant reaction is methanation and, if it were much faster and in parallel with the other slower reactions, it could be the only pore diffusion limited reaction. Since equation (1) is based on the total CO consumption rate and CH_4 is the major product, this would explain the apparent discrepancy in the apparent activation energies in equations (6) and (9). Some support of this argument is given by the low activation energy associated with CH_4 production [equation (8)].

Whereas separate experiments to quantify the role of pore diffusion were not conducted, estimates of the effectiveness factor can be made provided there is some knowledge of the value of the effective diffusivity. Atwood and Bennett,[8] assuming that CO diffusion in the liquid filled pores was limiting, used a value of 1.6×10^{-5} cm^2/sec for a fused iron catalyst. Using this value and rearranging equation (1) to give an effective first order reaction, we estimate the effectiveness factor be about 0.30 at 300 C. Thus it appears that we have strong pore diffusion effects with respect to the CO consumption rate. This is probably due to the high rate of formation of CH_4 which was the major product (selectivity $\sim$ 60%).

ACKNOWLEDGE

The financial support of this work by DOE under contract No. DE-AS22-78ET00260 is gratefully acknowledged.

REFERENCES

1. Ponec, V., CATAL. REV. - SCI. ENG., 18, p. 151 (1978).

2. Storch, H. H., N. Golumbic, and R. B. Anderson, "The Fischer-Tropsch and Related Syntheses," John Wiley & Sons, New York (1951).

3. Dent, A. L. and M. Lin, ACS Preprints, Div. of Petr. Chem., Anaheim, CA., 23, No. 2, p. 502, March 1978.

4. Everson, R. C., E. T. Woodburn, and A. R. M. Kirk, J. CATAL., 53, p. 186 (1978).

5. Yang, C. H. and A. G. Oblad, Preprints, Div. of Petr. Chem., Anaheim, CA., 23, No. 2, p. 513, March 1978.

6. Shah, Y. T. and A. J. Perrotta, I & EC PROD R & D, 15, p. 123 (1976).

7. Dry, M. E., T. Shingles, and L. J. Boshoff, J. CATAL., 25, p. 99 (1972).

8. Atwood, H. E. and C. O. Bennett, I & EC PROC. DES. DEV., 18, p. 163 (1979).

9. Anderson, R. B., in "Catalysis", p. 257, Vol. IV, Ed. by P. H. Emmett, Rheinhold Pub. Co., N.Y., 1956.

10. Chemical and Engineering News, Sept. 17, p. 13, 1979.

11. Demeter, J. J., Youngblood, A. J., Field, J. H., and Blenstock, D., U. S. BUR. MINES REPT. INV. 7033 (1967).

12. Haynes, W. P., Baird, M. J., Schehl, R. R. and Zarochak, M. F., Preprints, Div. Petr. Chem., ACS, 23, No. 2, p. 559, 1978.

13. Sancier, K. M., Isakson, W. E., Wise, H., Preprints, Div. of Petr. Chem., ACS, 23, No. 2, p. 545, 1978.

14. Schehl, R. R., Pitts Energy Tech Ctr., private communication.

15. Kugler, E. L., paper presented at the ADVANCES IN CATALYTIC CHEMISTRY, Snowbird, UT, Oct. 2-5, 1979.

16. Henrici-Olive, G., Olive, S., Angem. Chem. Int. Ed. Engl., 15, p. 136, 1976.

TABLE I

CO_2/H_2O MAKE AT TWO TEMPERATURES

	H_2/CO	X_{CO}	CO_2/H_2O	ϕ
250 C	2.24	.26	.14	.004
	2.25	.34	.25	.01
	2.16	.50	.37	.01
	5.9	.79	.42	.016
	8.9	.74	.27	.027
300 C	1.2	.60	1.9	.057
	2.8	.59	1.1	.077
	5.5	.62	0.6	.083
	3.6	.75	1.0	.091
	6.1	.79	1.0	.153
	7.3	.74	0.6	.110
	9.3	.76	0.45	.11

TABLE II

ETHYLENE/ETHANE MAKE AT TWO TEMPERATURES

	H_2/CO	X_{CO}	C_2H_4/C_2H_6
250 C	1.5	.15	.14
	1.2	.21	.13
	2.24	.26	.092
	2.25	.34	.076
	2.16	.50	.050
	5.9	.79	.020
	8.9	.74	.012
300 C	1.05	.26	.096
	1.20	.41	.079
	1.20	.60	.028
	2.80	.59	.023
	5.50	.62	.012
	9.30	.76	.005

TABLE III

COMPARISON OF C_5^+ FRACTION AT TWO TEMPERATURES

T(C)	X_{CO}	H_2/CO	P_T(MPa)	C_5^+ Fraction
250	.50	2.5	1.47	.31
300	.51	1.7	1.47	.12
250	.55	4.0	2.15	.18
300	.58	3.3	2.02	.10
250	.65	6.7	2.84	.13
300	.76	8.3	2.84	.07

FIGURE 1: SCHEMATIC OF EXPERIMENTAL EQUIPMENT

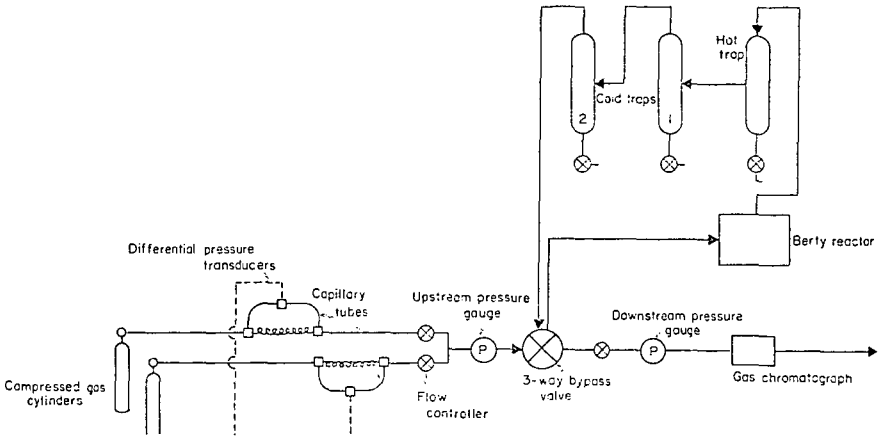

FIGURE 2: CATALYST ASSEMBLY

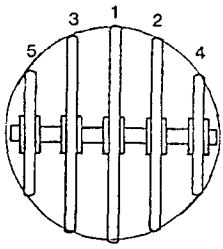

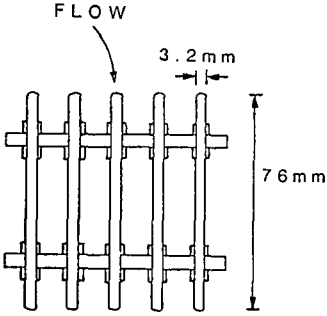

FIGURE 3: INDUCTION PERIOD: CONVERSION VERSUS TIME

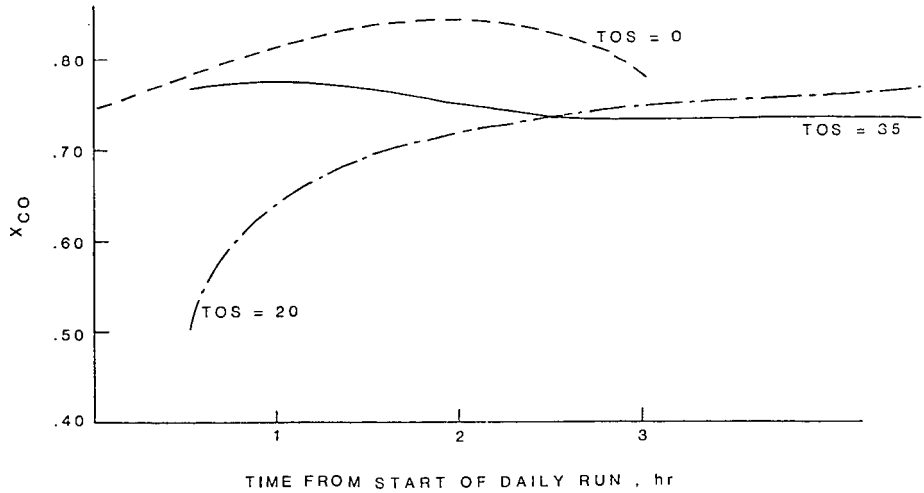

FIGURE 4: WEIGHT FRACTION C_5^+ VS. X_{CO} (250C)

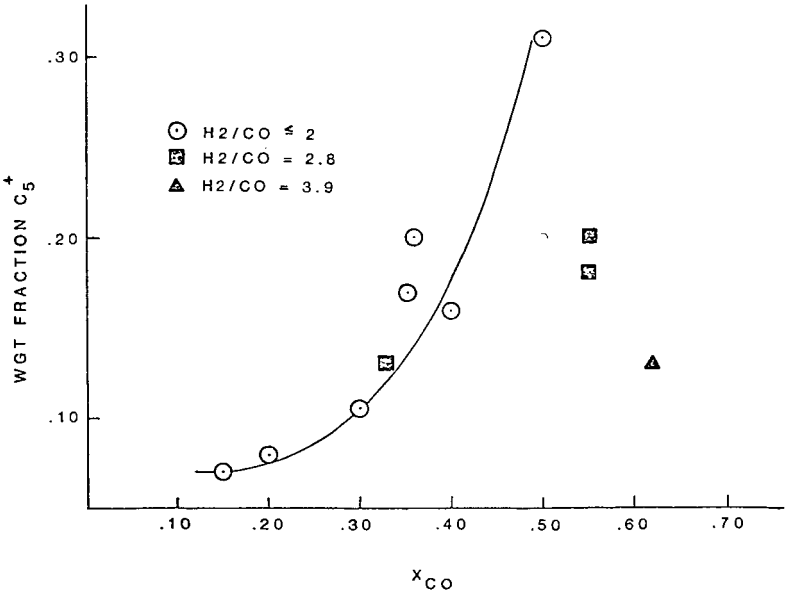

FIGURE 5: TEST OF SCHULZ-FLORY DISTRIBUTION

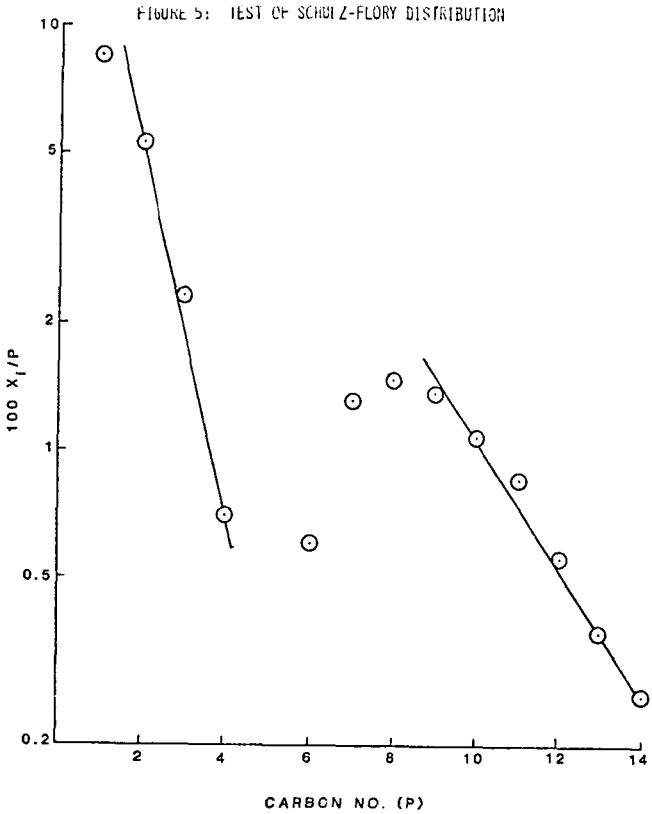

FIGURE 6: PREDICTED VS. MEASURED VALUES OF R_{CO}

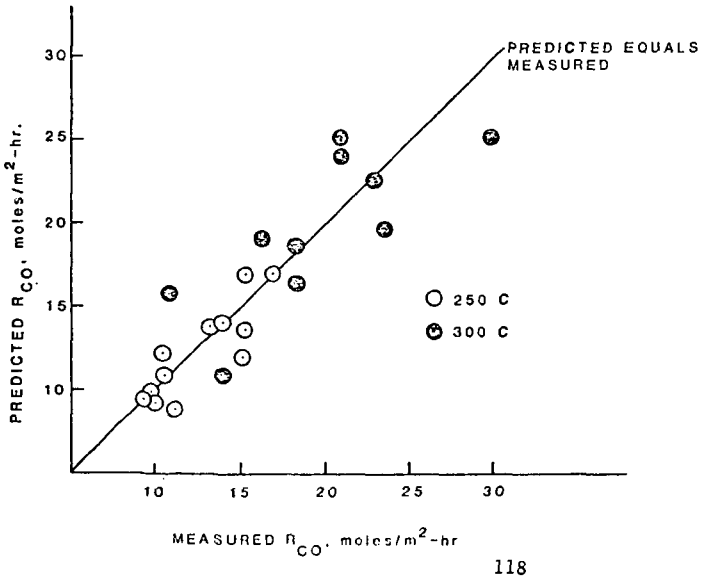

Synthesis Gas Conversion to Gasoline Range Hydrocarbons over Medium Pore Zeolite Catalysts Containing 3d-Metals and Bimetallics

V. U. S. Rao, R. J. Gormley, H. W. Pennline, L. C. Schneider and R. Obermyer*

Pittsburgh Energy Technology Center
4800 Forbes Avenue
Pittsburgh, PA 15213

and

*Department of Physics
Pennsylvania State University
McKeesport, PA 15132

Introduction

There is much current interest in the conversion of synthesis gas to gasoline range hydrocarbons using bifunctional zeolite catalysts (1,2). The medium pore (dia 6Å) zeolite ZSM-5 in combination with Fe was shown to yield a high fraction of aromatics in the product, resulting in a favorable octane number (≈ 90). The transition metal (TM) component catalyzed the hydrogenation of CO while the acid function of the zeolite led to an aromatic product. Owing to the medium size pores of ZSM-5 there was a fairly sharp cut-off, in the product distribution near the end of the gasoline range for the aromatic fraction.

In order to explore further the role of the TM component and the acidity of the zeolite on the product composition, experiments were performed in our laboratory on ZSM-5 impregnated with Fe and Fe-Co, and on Silicalite impregnated with Fe. Silicalite is a molecular sieve form (3) of SiO_2.

A comparison of the crystallographic studies (4,5) on ZSM-5 and Silicalite, shows that the two zeolites possess very similar crystal structures. While the Si/Al ratio in ZSM-5 can be varied from 3 to ∞, Silicalite has essentially no Al. Hence, it appears that Silicalite is the limiting form of ZSM-5 when the Al concentration is vanishingly small. Owing to the lack of cations which can be exchanged with protons, Silicalite has no acidity, while HZSM-5 is a highly acidic zeolite. Our investigations sought to find the difference in selectivity for synthesis gas conversion by ZSM-5 (Fe) and Silicalite (Fe) catalysts resulting from the above mentioned difference in acidity.

A further aim of the investigation was to investigate possible difference in selectivity between ZSM-5 (Fe) and ZSM-5 (Fe-Co) catalysts, resulting from the different 3d-electron concentration of the TM component. Magnetic studies (TMA) were performed to characterize the TM component and particularly to detect the formation of bimetallic Fe-Co clusters.

Experimental

The zeolites were prepared using methods described in the literature (3,6). The metal component was introduced by gradually adding the metal nitrate solution to the zeolite until incipient wetness was reached. The impregnation with the metal nitrate solution was carried out for an hour under vacuum in order to enable the nitrate solution to enter the pores of the zeolite. The material is initially dried with constant stirring over a boiling water bath, and further dried in air at 110° C for 12 hours. It is then pelleted to yield tablets 3mm in diameter. In the case of the Silicalite based catalysts, about 10% by weight of an amorphous silica such as Ludox AS-40 was added as a binder before the pelletization step.

The catalysts were tested for synthesis gas conversion in both a fixed bed microreactor and a Berty (continuous flow stirred tank) reactor (7). The latter is shown in Figure 1. The catalyst pellets were loaded into the 2-inch diameter CFSTR chamber and retained by glass wool with a screen. Impeller speed was 1240 rpm. Excellent bed temperature control was obtained by a modification which involved the installation of a coil in the head of the reactor through which air could flow for faster heat removal.

A schematic diagram of the reactor system is shown in Figure 2. Synthesis gas with a H_2/CO-ratio of either 2/1 or 1/1 would pass through a carbon trap and enter the reactor. Liquid and solid hydrocarbon products are collected in a hot trap usually maintained at 150° C and in an ice trap. This series of traps are alternated and drained periodically. Product gases are metered and then flared.

The tablets of the zeolite impregnated with TM were reduced in flowing H_2 at 21 bar and 450° C for 24 hrs. They were then carbided with synthesis gas at 7 bar and 250° C for 24-48 hrs to yield the active catalyst. The gas phase product (C_1-C_4 hydrocarbons) was analyzed by gas chromatography. The liquid product was separated into paraffins, olefins, aromatics and oxygenates by column chromatography using FIA detection.

Results and Discussion

(a) Influence of Zeolite Acidity:

The results obtained in the Berty reactor on the catalysts ZSM-5 (11.1 wt% Fe) and Silicalite (13.6 wt% Fe) are shown in Table 1. It is apparent that a high percentage of aromatics is obtained from the ZSM-5 (11.1% Fe) catalyst, while the product from the Silicalite (13.6% Fe) catalyst has a low aromatic fraction but much higher olefin and oxygenate fractions. It is thus apparent that the acid function of ZSM-5 based catalyst is responsible for the conversion of the olefins and oxygenates to aromatics. The aromatic fraction imparts a high octane number to the product.

(b) High Olefin Yields from Silicalite Based Catalysts:

The interesting aspect of the product slates from the Silicalite based catalysts was the high percentage of olefins in both the gas and liquid phase products. When promoted with potassium, the Fe containing Silicalite catalyst yielded a large C_2-C_4 olefin fraction as seen in Table 2. The C_2-C_4 olefin fraction from Silicalite (7.8% Fe, 0.9% K) in a fixed bed microreactor is compared with that from a precipitated Fe-Mn catalyst of Kolbel et al (8), known for its very high olefin yield. It is seen that the olefin yields from the two catalysts are quite comparable. The Silicalite (7.8% Fe, 0.9% K) catalyst yields a much higher C_2-C_4 olefin/paraffin ratio than the precipitated Fe-Mn catalyst and hence is of potential commercial interest. The mechanism for the enhancement of olefin production on adding K as a promoter has been discussed by Dry et al. (9).

(c) Influence of Transition Metal Component on Product Composition:

The addition of cobalt to Fe containing ZSM-5 catalyst was found to result in a marked change in product composition as seen from the Berty reactor study results in Table 3. It is seen that the incorporation of cobalt into the catalyst results in (a) reduction in the wasteful shift conversion as seen from the decrease in CO_2 in the product (b) lowering of the aromatic fraction to about 10% of the C_5^+ fraction. However, the octane number remained at a relatively high value of 81, despite the decrease in the aromatic fraction. Hence, the impregnation of zeolites with bimetallic TM clusters provides a promising means of altering the extent of shift conversion and the composition of the liquid product. Changes in the aromatic fraction with TM component was an unexpected result since aromatization is normally associated with the acidity of the zeolite. It is possible that some of the cobalt is attached to the Al sites in the zeolite, reducing its acidity. Further studies on this subject are necessary.

(d) Magnetic Studies:

The magnetic properties of TM impregnated zeolite catalysts have been investigated between 77K and 923K in applied fields up to 21 kOe. Samples of ZSM-5 (11.1% Fe), ZSM-5 (5.6% Fe, 4.5% Co) and Silicalite (13.6% Fe) were magnetically analyzed after each of the impregnation, reduction and carburization steps and after use as a catalyst.

The reduced samples of ZSM-5 (11.1% Fe) and Silicalite (13.6% Fe) indicate that Fe is in the metallic state with 86% and 85% reduction, respectively. Thermo-magnetic analysis (TMA) of carbided ZSM-5 (11.1% Fe), show it to be in the high Curie point form (10) of the Hagg carbide. TMA analysis reveals the used ZSM-5 (11.1% Fe) to be the hexagonal close packed (hcp) carbide form of Fe_2C, and the used Silicalite (13.6% Fe) to be the high Curie point form of the Hägg carbide.

The TMA of ZSM-5 (5.6% Fe, 4.5% Co) shows that the reduced, carbided, and spent samples have large magnetic moments (1.94, 2.04 and 2.61μ_B per TM atom respectively, at room temperature) and high Curie points (> 900° C), which cannot be accounted for on the basis of individual Fe and Co particles. The magnetic data indicate the composition to be that of a Fe-Co alloy (11). Hence, we conclude that the difference in selectivity between ZSM-5 (11.1% Fe) and ZSM-5 (5.6% Fe, 4.5% Co) catalysts can be attributed to the presence of bimetallic TM clusters in the latter, with consequent changes in the average number of 3d-electrons per TM atom.

(e) TM Cluster Size and Bifunctional Catalysis:

To determine TM particle size in the bifunctional catalysts CO adsorption studies were performed to determine the TM surface area. These studies showed that the TM clusters had an average diameter of 100-110 Å. Owing to the limitations connected with CO adsorption for estimating metal surface areas, the above may be considered to be approximate values of the TM cluster diameter. Hence, the majority of the TM clusters must reside outside of the pores of the zeolite. We believe that the bifunctional catalytic behavior of these catalysts results from high interparticle diffusivity relative to intracrystalline diffusivity (12).

Conclusions

Our experiments lead to the following conclusions:

(1) Zeolite acidity plays an important role in the formation of aromatics from synthesis gas by bifunctional catalysts as strikingly evidenced in a comparison of the product slates from ZSM-5 (11.1% Fe) and Silicalite (13.6% Fe).

(2) The transition metal component impregnated into the zeolite plays an important role in selectivity as seen from the liquid phase products from ZSM-5 (11.1% Fe) and ZSM-5 (5.6% Fe, 4.5% Co). In this context, zeolites containing bimetallic clusters are of special interest.

(3) Silicalite impregnated with Fe and promoted with K has an exceptionally high selectivity for the production of C_2-C_4 olefins from synthesis gas.

Acknowledgements

We wish to thank R. R. Schehl and B. D. Blaustein for useful discussions, S. S. Pollack for x-ray diffraction analyses, M. F. Ferrer for FIA chromatographic studies, A. Elattar of the University of Pittsburgh for CO adsorption measurements, and W. Picking of Gulf Research for measuring octane numbers.

Table 1. - Comparison of Products from ZSM-5 (11.1% Fe) and Silicalite (13.6% Fe) Catalysts with $H_2/CO=2$, and P=21 bar.

Catalyst	ZSM-5 (11.1% Fe)	Silicalite (13.6% Fe)
Temperature, °C	300	280
CO Conversion, %	68.2	39.4
H_2 Conversion, %	38.7	16.5
Space Velocity (h^{-1})	1500	1350
Product Composition (%)		
CO_2	52.0	51.1
H_2O	19.4	22.1
CH_n + oxygenates	28.6	26.9
Hydrocarbon and Oxygenate Composition (%)		
CH_4	54.1	26.5
C_2H_4, C_2H_6	1.1, 15.0	2.5, 15.0
C_3H_6, C_3H_8	2.1, 6.3	10.8, 7.2
C_4H_8, C_4H_{10}	0.0, 4.5	4.8, 4.8
C_5+ and oxygenates	16.9	25.0
Composition of C_5+ and oxygenates (%)		
Aromatics	72	4
Olefins	3	41
Saturates	24	33
Oxygenates	1	22
%Gasoline range (BP <204° C)	75	77
Research octane No.	96	36

Table 2. - Conversion of Synthesis Gas to Olefins in Fixed Bed Reactors, Using Silicalite (7.8% Fe, 0.9% K) Compared with That Using a Precipitated Fe-Mn Catalyst of Kolbel et al (8).

Catalyst	Silicalite (7.8% Fe, 0.9% K) (our)	Precip. Fe-Mn (Kolbel et al)
Pressure (bar)	21	14
Temperature (°C)	280	290
H_2/CO Ratio	0.9	0.8
Space Velocity (h^{-1})	1300	353
Product Composition (CH_n + Oxygenates) %		
CH_4	8.6	12.1
C_2H_4	8.2	7.6
C_2H_6	0.4	4.9
C_3H_6	19.3	17.3
C_3H_8	<0.2	2.1
C_4H_8	8.6	15.2
C_4H_{10}	<0.2	3.1
C_2-C_4 Olefins	36.1	40.1
C_2-C_4 Paraffins	<0.8	10.1
C_5+ and oxygenates	55.1	47.8
$\frac{C_2\text{-}C_4 \text{ Olefins}}{C_2\text{-}C_4 \text{ Paraffins}}$	>45.1	4.0

Table 3. - Product Compositions from the Catalysts ZSM-5 (11.1% Fe) and ZSM-5 (5.6% Fe, 4.5% Co), in a Berty Reactor, Showing the Influence of cobalt addition to the Catalyst. Process Condition: $H_2/CO = 2$, P = 21 Bar and GHSV = 1000 hr^{-1}

Catalyst	ZSM-5 (11.1% Fe)	ZSM-5 (5.6% Fe, 4.5% Co)
Temperature	300	280
CO Conversion, %	68.2	37.8
H_2 Conversion, %	38.7	41.3
Space Velocity	1500	1400
Product Composition (%)		
CO_2	52.0	9.8
H_2O	19.4	51.8
CH_n + Oxygenates	28.6	38.4
Hydrocarbon and Oxygenate Composition (%)		
C_1-C_4 hydrocarbons	83.1	74.3
C_5+ and Oxygenates	16.9	25.7
Composition of C_5+ and Oxygenates (%)		
Aromatics	72	10
Olefins	3	46
Saturates	24	37
Oxygenates	1	7
% Gasoline range (BP 204° C)	75	94
Research octane No.	96	81

References

1. C. D. Chang, W. H. Lang and A. J. Silvestri, J. Catal. 56, 268 (1979).

2. P. D. Caesar, J. A. Brennan, W. E. Garwood and J. Ciric, J. Catal. 56, 274 (1979).

3. R. W. Grose and E. M. Flanigen, U. S. Patent 4,061,724 (1977).

4. G. T. Kokotailo, S. L. Lawton, D. H. Olson and W. M. Meier, Nature 272, 437 (1978).

5. E. M. Flanigen, J. M. Bennett, R. W. Grose, J. P. Cohen, R. L. Patton, R. M. Kirchner and J. W. Smith, Nature 271, 437 (1978).

6. R. J. Argauer and G. R. Landott, U. S. Patent 3,702,886 (1972).

7. J. M. Berty, Chem. Engr. Prog. 70, 68 (1974).

8. H. Kolbel, M. Ralek and K. D. Tillmetz, Proc. 13th Intersoc. Energy Conv. Eng. Conf., Society of Automot. Engineers (1978), p. 482.

9. M. E. Dry, T. Shingles, L. J. Boshoff and G. J. Oosthuizen, J. Catal. 15, 190 (1969).

10. K. M. Sancier, W. E. Isakson and H. Wise, Preprints, Div. of Petroleum Chemistry, ACS, 23 (2), 545 (1978).

11. R. M. Bozorth, "Ferromagnetism", Van Nostrand, New York, 1951, pp. 190-209.

12. P. B. Weisz, Adv. Catal. 13, 137 (1962).

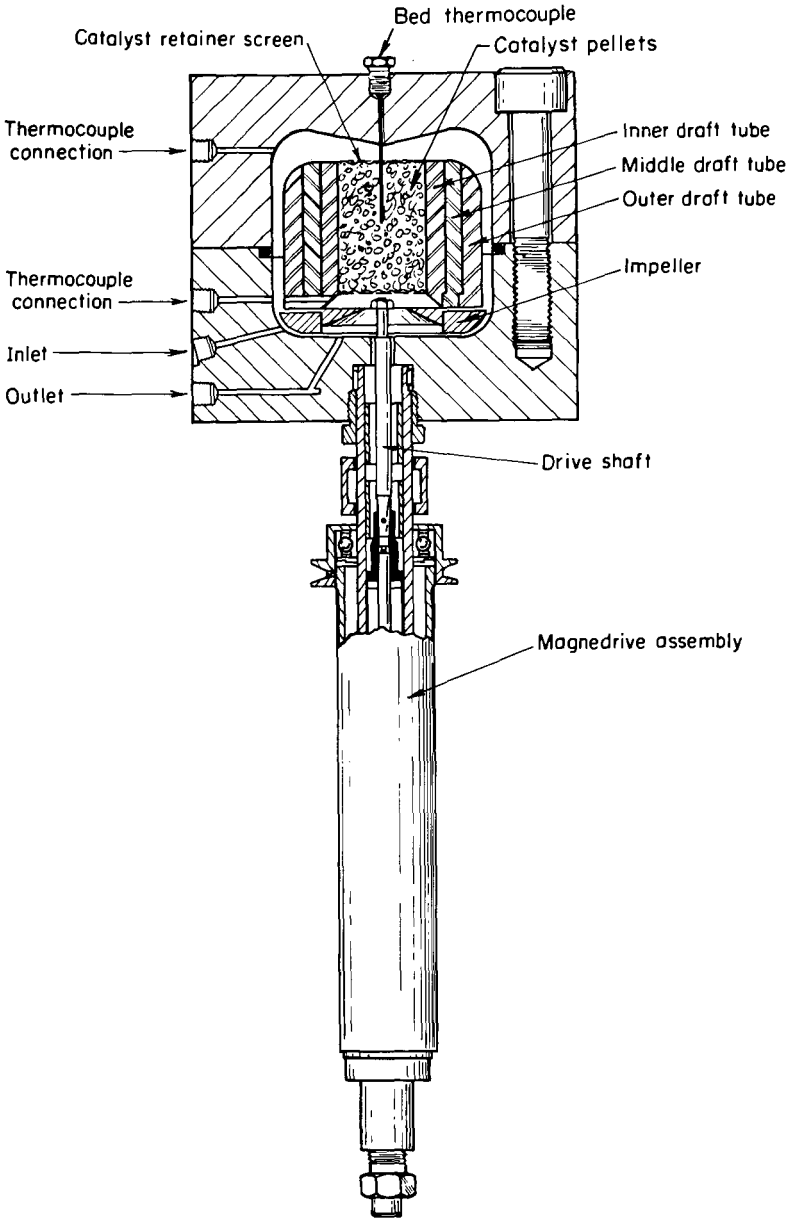

Figure 1. - Berty Reactor (CFSTR)

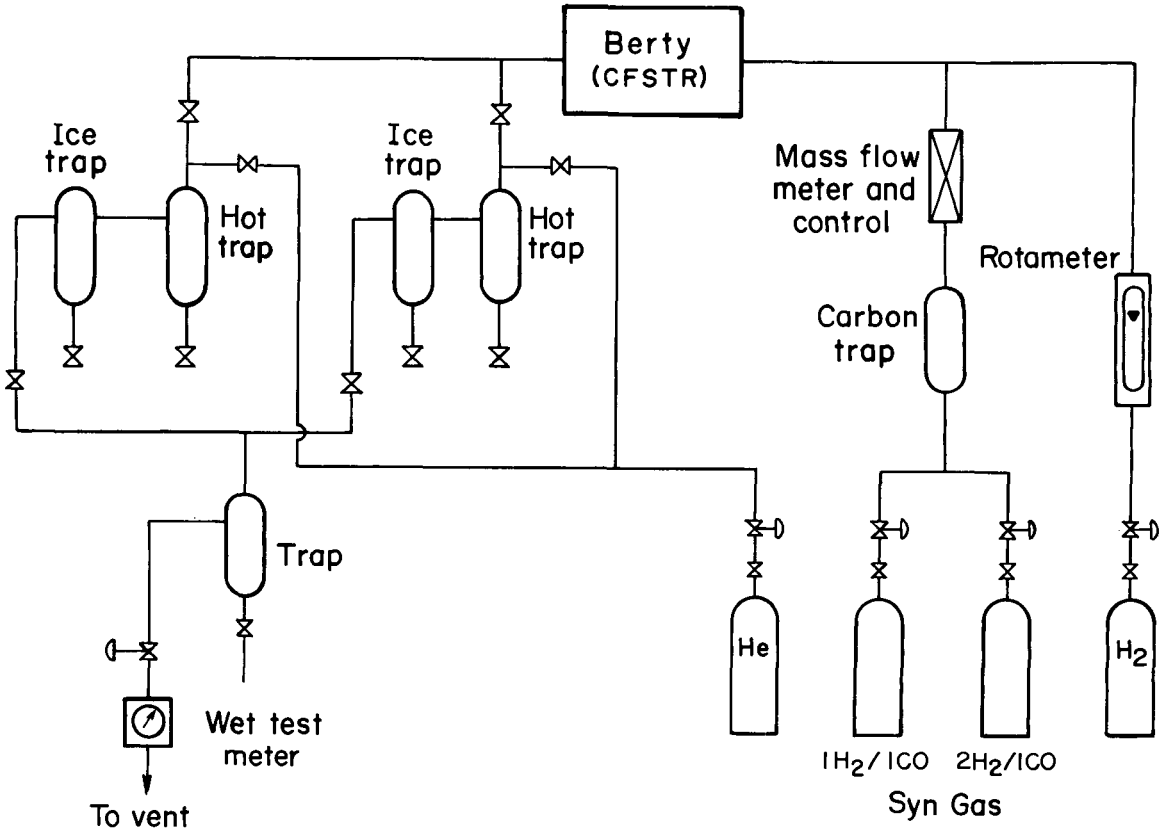

Figure 2. - Flow Diagram for Berty Reactor System

THE HYDROGENATION OF CARBON MONOXIDE OVER UNSUPPORTED IRON-MANGANESE CATALYSTS FOR THE PRODUCTION OF LOW-MOLECULAR WEIGHT OLEFINS. Y. S. Tsai, A. G. Oblad and F. V. Hanson, Department of Fuels Engineering, 320 W. C. Browning Building, University of Utah, Salt Lake City, Utah 84112.

The hydrogenation of carbon monoxide for the production of low molecular weight (C_2-C_4) olefins has been investigated over unsupported iron-manganese catalysts. A series of fifteen catalysts of different iron/manganese ratio were prepared and evaluated.

The screening tests were conducted in a fixed-bed, bench-scale reactor. The standard catalyst evaluation conditions were 473-523 K, 500 psig, 2/1 H_2/CO ratio and a gas hourly space velocity 1.08 $cm^3g^{-1}s^{-1}$. The most promising catalyst with regard to the C_2-C_4 hydrocarbon yield was composed of 2.2 parts of manganese per 100 parts of iron.

Four of the catalysts, Mn/Fe=2.2, Mn/Fe=8.4, Mn/Fe=63 and Mn/Fe=278 were selected for an extended process variable investigation. The olefin yield increased with increasing reaction temperatures, with decreasing space velocity and with decreasing H_2/CO ratio. The dependence of the olefin yield on reactor pressure reported in the literature was not observed in this investigation. The activation energy in the temperature range 473-523 K was 20-30 kcal mol^{-1}.

A MODEL FOR THE ISOTHERMAL PLASTOMETRIC BEHAVIOR OF COALS

William G. Lloyd, Henry E. Francis, Morgan R. Yewell, Jr.

Institute for Mining and Minerals Research, University of Kentucky,
P. O. Box 13015, Lexington, KY 40583

Raymond O. Kushida and Vega D. Sankur

Jet Propulsion Laboratory, California Institute of Technology
Pasadena, CA 91103

Introduction

The plasticity of bituminous coals in the range 350-500°C is of critical importance in thermomechanical fluidization such as is required for coal pumping by heated screws (1-3) and in hydrogenolysis in the absence of added solvent (4,5). The fact that the optimum reaction temperatures for three major current liquefaction technologies are nearly identical (6) and are close to the fluidity maxima for many plastic coals suggests that the processes comprising coal "melting" are critically important to hydroliquefaction. More generally, coal plasticity is obviously involved in caking problems (7-10).

The most widely used method of measuring coal plasticity was developed by Gieseler (11). With minor modifications this remains a standard procedure (12); its relationship to other measurements has been discussed elsewhere (13). This method measures the resistance of a mass of well-packed pulverized coal to the rotation of a rabble-arm stirrer which is driven through a constant-torque clutch. At low temperatures the solid mass completely immobilizes the stirrer shaft. In the standard Gieseler procedure the coal is heated at a uniform rate of 3°C/min. As the coal begins to soften -- typically at about 390°C -- the stirrer shaft commences to turn slowly. As temperature increases the coal becomes more fluid and the shaft turns more rapidly, eventually achieving a maximum rate. The coal melt -- actually a heterogeneous mixture of solids, molten phase and gaseous pyrolyzate -- then undergoes a thickening or "coking"; the stirrer shaft turns progressively more slowly, and eventually stops. Gieseler data are recorded in units of dial divisions per min (ddpm), where 100 ddpm = 1 shaft rotation per min. For three bituminous coals of varying plasticity the standard Gieseler data are shown in Table 1.

The Isothermal Model

It is often useful to study phenomena under isothermal conditions. Gieseler plastometry lends itself to such studies, since sample warmup time in the standard crucible (2-3 min.) is short in comparison with the usual melting/coking time scale (20-120 min.). Isothermal Gieseler plastometry has been explored by Fitzgerald (14,15) and by Van Krevelen and coworkers (16,17). A plot of log(ddpm) against time shows a long linear coking region (14,15).

Figure 1 (open circles) shows the isothermal plastometric curves at 410-2°C obtained with the three coals described in Table 1. Both the maximum fluidities

and the periods of fluidity are seen to vary substantially among these coals.

The linearity of the coking slopes has been interpreted to imply a sequence of first-order reactions (14-17):

$$C \rightarrow M \qquad k(init) \qquad \text{(first-order melting)} \qquad (1)$$

$$M \rightarrow S \qquad k(coke) \qquad \text{(first-order coking)} \qquad (2)$$

where C, M and S represent the meltable portion of the original coal, the fraction which is molten (metaplast), and the fraction which is resolidified (coked). This scheme gives rise to the rate law:

$$d[M]/dt = k_i[C] - k_c[M] \qquad (3)$$

There are two problems with this scheme. First, it does not generate model curves which resemble observed curves. Specifically, it predicts the rate of increase of fluidity during the softening process to decelerate progressively, while in fact this increase is exponential with time over most of the melting period. Second, this scheme specifically assumes that Gieseler fluidity is a linear measure of the molten fraction or metaplast; but that assumption is mistaken, as we will show.

For the purpose of more closely modeling the actual isothermal curves we propose a second melting process, such that the rate of increase of fluidity is dependent upon the concentrations of both metaplast and unmelted fraction:

$$C + M \rightarrow 2\,M \qquad k(melt) \qquad (4)$$

The rate law now acquires a third term:

$$dF/dt = k_i[C] + k_m[C][M] - k_c[M] \qquad (5)$$

(We use F for fluidity, rather than [M] for metaplast, on the left-hand side). The virtue of Equation 5 is that, for most isothermal runs, it can provide a fairly good fit to the experimental data, and therefore can define the experimental curves in terms of numerical constants associated with the melting and coking processes. The solid points in Figure 1 are values generated by the Equation 5 model, using the values given in Table 2. It is a characteristic of this model that the experimental points in the vicinity of maximum fluidity tend to be higher than those generated by the model. This may reflect formation of gas bubbles, which lead to anomalously high experimental readings.

In applying this model, the least-squares melting and coking slopes are calculated from the experimental data; we use all data between 1 ddpm and one fourth the maximum observed fluidity. The extrapolated maximum fluidity (emf) and the time of maximum fluidity are taken from the intersection of these slopes.

From these determinations, approximate values for the model constants can be estimated empirically from the cubic equations:

$$\frac{m(melt)}{k(melt)} = -0.3179 + .71507 \times R - .15991 \times R^2 + .012348 \times R^3 \quad (6)$$

$$\frac{m(coke)}{k(coke)} = -0.6934 + 1.1504 \times R - .26779 \times R^2 + .020826 \times R^3 \quad (7)$$

$$\ln[k(init)] = -16.127 + 2.8478 \times P - .25098 \times P^2 + .005726 \times P^3 \quad (8)$$

where m(melt) and m(coke) denote the melting and coking slopes, R = m(melt)/m(coke), and P = [(m(melt) + m(coke)) x t(max flu)]. These equations give fairly good fits when k(melt) is in the range 0.5 to 4 $min.^{-1}$ and k(coke) is in the range 0.2 to 1.5 $min.^{-1}$. To relate the conceptual molten fraction [M] to the observed ddpm, the emf from a model curve is compared with that from the experimental curve. For example, Ohio #9 seam coal at 411° has an experimental emf of 81.3 ddpm, and a calculated emf (using the k values of Table 2) of [M] = 0.683. When each datum in the model curve is multiplied by the factor 81.3/0.683, the model fluidities are converted to units of ddpm. [Detailed procedures and programs for these estimates are available from the authors.]

Effect of Temperature

Isothermal curves were obtained upon Kentucky #11 seam coal at five additional temperatures, in the range 400-460°C. Values of the model constants are given in Table 3. An Arrhenius plot of the model constants k(melt) and k(coke) is shown in Figure 2. For this coal the value of the apparent E_a for k(melt) (best 5 of 6 data) is 173 ± 13 kJ; that for k(coke) (also best 5 of 6) is 228 ± 6 kJ. Viscosities commonly show an analogous "activation energy of viscosity" (18,19). The apparent E_a of maximum fluidity is approximately 600 kJ, high when compared with those for asphalt (120-150 kJ) and glass (390-400 kJ) (20,21).

When the temperature dependencies for the parameters of this model have been estimated from the data of Table 3, isothermal curves may be calculated for any interpolated temperature, or for any extrapolated temperature close to the range of experimental data. Figure 3 shows a family of fluidity envelopes for the Kentucky #11 seam coal, based upon data calculated for the range 392-468°C. Each curve is an "isofluidity" envelope, open at the top. Figure 3 is read along horizontal (isothermal) lines. At 430° this coal exhibits a plastic period (fluidity greater than 1 ddpm) from 2 to 30 min., and has a fluidity exceeding 100 ddpm from 5 to 20 min. This projection, which will afford markedly different envelopes for different coals, may find use in applications in which the plastic properties of bituminous coals are important.

Discussion

The organic structures of coals are numerous and varied. Bonds which thermally cleave at useful rates at 390-400°C (dissociation energies of 210-230 kJ) are not the same as those cleaved at 460° (240-260 kJ). A major reason for isothermal measurements is to control this variable.

Gieseler fluidity can be related to viscosity units by calibrating with standard fluids. Measurements with the plastometer used in this study and with

appropriate standards (22) in the range 500 - 10,000 poise yield a linear calibration:

$$\ell n(\text{poise}) = 16.2789 - 0.96787\ \ell n\ (\text{ddpm}) \tag{9}$$

with a correlation coefficient of .9997. Actual coal melts are heterogeneous (7,16), pseudoplastic (23), and viscoelastic in their later coking stages (24). It is nevertheless useful to interpret Gieseler fluidities as estimates of true viscosities.

Nicodemo and Nicolais (25) and Fedors (26) have shown the viscosity of Newtonian suspensions of solids to conform to the expression:

$$\eta/\eta_o = \exp(a\phi) \tag{10}$$

where η, η_o, and ϕ are the suspension viscosity, solvent viscosity, and solids fraction. Data obtained by Lee (27) show the <u>logarithm</u> of the maximum fluidity of coal blends to vary linearly with composition. These observations are telling us the same thing: that the logarithm of fluidity, not fluidity itself, is a direct measure of the molten fraction. If we assume that a fluidity of 1 ddpm corresponds to the maximum solid fraction ϕ_{max}, we can project the relationship:

$$\ell n(F) = \ell n(F^\circ)\cdot[1 - \frac{\phi}{\phi_{max}}] \tag{11}$$

To use Equation 11 we need estimates of ϕ_{max} and of the fluidity of pure metaplast, F°. The maximum solid fraction in a random dispersion of monodisperse spheres is 0.63 (28,29). This fraction is higher for polydisperse spheres (30) and for some size distributions may be as high as 0.9 (31). For coal melts we will assume a value of ϕ_{max} of 0.80. If the extrapolated maximum fluidity of the Pittsburgh #8 seam sample at 412° (1.0×10^6 ddpm) is taken as a rough estimate of F°, we can estimate solid fractions in other coals from fluidities at this temperature. Fluidities of 10, 100, 1,000 and 10,000 ddpm indicate solid fractions of approximately .67, .53, .40 and .27. The minimum values of ϕ for Ohio #9 and Kentucky #11 samples in Table 2 are approximately 0.55 and 0.41.

The linearity of log(F) with ϕ has mechanistic implications as well. The left-hand of Equation 3 is more accurately expressed as $d\ \ell n[M]/dt$. The curves of Figure 1 show linear increases of metaplast with time in the early stages, and linear decreases of metaplast with time (zeroth order kinetics) in the later coking stages.

Extrusion pumping of coals in the plastic state entails substantially isothermal operations for residence times of a few minutes in the screw (1-3). Several coals, including those of the present study, have been extruded with no difficulty in JPL's 1.5-in. coal pump. Two coals which showed very little plasticity (less than 2 ddpm) were not extrudable (3). The isothermal plastometry profiles may prove to be a useful tool in predicting behavior in coal pumps. Recent evidence of the substantial effect of pressure upon observed plasticity (10) indicates that this variable should be considered in future work.

Acknowledgments

Christopher England (Jet Propulsion Laboratory) first suggested this study. This work was performed for the coal pump development project, Jet Propulsion Laboratory, California Institute of Technology, under Contract no. 954920. The coal pump project is supported by the Department of Energy through an agreement with the National Aeronautics and Space Administration.

References

(1) P. R. Ryason and C. England, Fuel, 57, 241 (1978).

(2) V. Kevorkian and F. J. Cumings, U. S. Patent 4,106,997 (1978).

(3) W. J. Schatz, E. G. Carpenter, C. S. Daksla, C. England, S. P. Feinstein, R. O. Kushida, D. W. Lewis, W. G. Lloyd and V. D. Sankur, "Coal Pump Development - Phase I Feasibility Report", JPL 5030-235, Jet Propulsion Laboratory, California Institute of Technology, Pasadena, September 1978.

(4) H. E. Mehesch, Erdoel, Kohle, Erdgas, Petrochem., 31, 323 (1978).

(5) Y. Sato, K. Imuta and T. Yamakawa, Fuel, 58, 322 (1979).

(6) B. Gates, Chemtech, 1979, 97.

(7) D. W. Van Krevelen, "Coal", Elsevier Publishing Co., Amsterdam, 1961, pp 263ff.

(8) R. Loison, A. Peytavy, A. F. Boyer and R. Grillot, in H. H. Lowry, ed., "Chemistry of Coal Utilization", supplementary vol., John Wiley & Sons, New York, 1963, pp 177ff.

(9) S. V. Sobolev and E. M. Taits, Khim Pererab. Topl., 30, 68 (1974).

(10) M. Kaiho and Y. Toda, Fuel, 58, 397 (1979).

(11) K. Gieseler, Gluckauf, 70, 178 (1934).

(12) ASTM Method D 2639-74, Amer. Soc. for Testing and Materials, Philadelphia, PA, 1974.

(13) R. Loison, et al., ref. (8), pp 152-69.

(14) D. Fitzgerald, Trans. Faraday Soc., 52, 362 (1956).

(15) D. Fitzgerald, Fuel, 35, 178 (1956).

(16) D. W. Van Krevelen, F. J. Huntjens and H. N. M. Dormans, ibid., 462 (1956).

(17) H. A. G. Chermin and D. W. Van Krevelen, ibid., 36, 85 (1957).

(18) E. N. da C. Andrade, Nature, 125, 309 (1930); E. N. da C. Andrade, "Viscosity and Plasticity", Chemical Publishing Co., Inc., New York, NY, 1951.

(19) S. Glasstone, K. J. Laidler and H. Eyring, "The Theory of Rate Processes", McGraw-Hill Book Co., Inc., New York, 1941, pp 480ff.

(20) P. B. Macedo and A. Napolitano, J. Chem. Phys., 49, 1887 (1968).

(21) H. E. Schweyer and R. W. Lodge, Ind. Eng. Chem., Prod. Res. Develop., 13, 202 (1974).

(22) Cannon Instrument Co., State College, PA 16801.

(23) P. L. Waters, Fuel, 41, 3 (1962).

(24) D. Fitzgerald, ibid., 36, 389 (1957).

(25) L. Nicodemo and L. Nicolais, Polymer, 15, 589 (1974).

(26) R. F. Fedors, ibid., 16, 305 (1975).

(27) H. C. Lee (Kaiser Steel Corp.), private communication.

(28) G. D. Scott, Nature, 188, 908 (1960).

(29) R. F. Fedors, J. Colloid Interface Sci., 46, 545 (1974).

(30) R. F. Fedors, Polymer, 20, 225 (1979).

(31) S. Feinstein (Jet Propulsion Laboratory), private communication.

Table 1

Properties of Three Bituminous Coals

Seam	Ohio #9	Kentucky #11	Pittsburgh #8
source	Noble Co.	Webster Co.	(from METC)
Proximate:[1]			
moisture	2.15%	1.97%	0.79%
ash	18.87	8.34	8.65
vol. matter	39.40	41.19	40.85
fixed carbon	39.58	48.50	49.71
Ultimate:[2]			
carbon	79.41	82.21	84.83
hydrogen	5.30	5.43	5.49
nitrogen	1.13	1.36	1.44
sulfur	5.38	3.52	2.92
oxygen[3]	8.78	7.48	5.33
Heating value[2]	14,010 Btu/lb	14,770 Btu/lb	15,290 Btu/lb
Free swelling index	3	7	7½
Petrographic analysis[1]			
exinoids	2.1%	5.1%	4.0%
vitrinoids	70.1	76.3	75.3
other reactives	1.9	1.2	0.9
inert macerals	12.9	11.0	13.7
ASTM Gieseler plastometry			
softening T	398°C	392°C	372°C
coking T	462°	474°	485°
max flu T	435°	435°	(414-459°)
max fluidity	114 ddpm	6240 ddpm	>>25000 ddpm

[1] As received. [2] Moisture- and ash-free basis. [3] By difference.

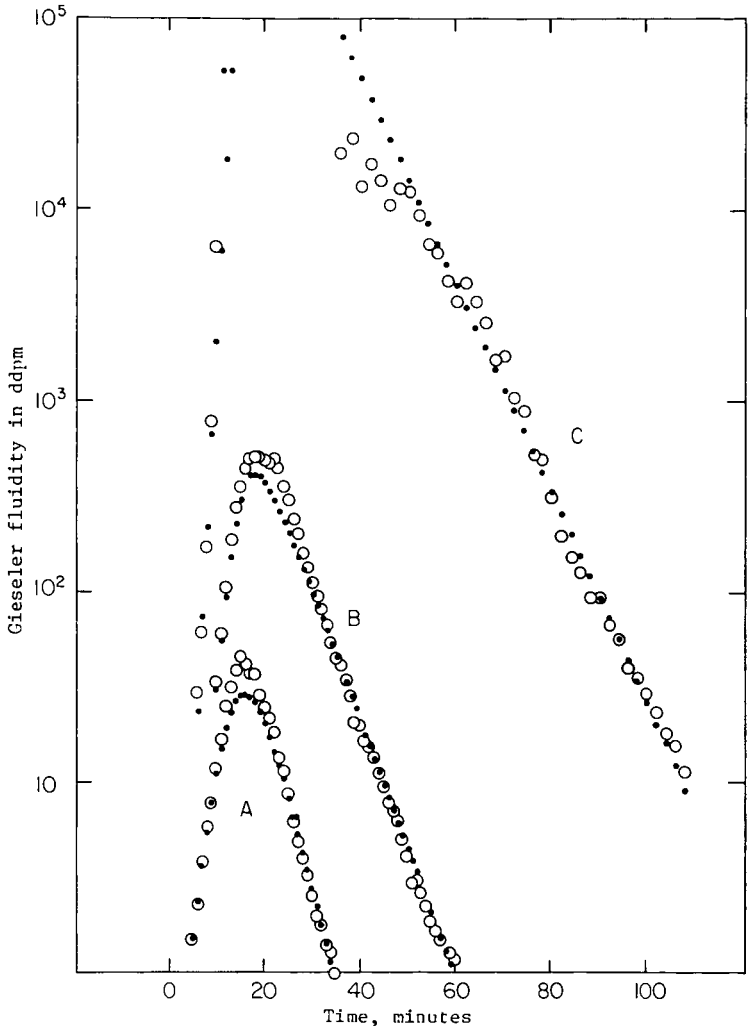

Figure 1. Isothermal plastometric curves of three bituminous coals. A - Ohio #9 seam (Noble Co.) at 411°C. B - Kentucky #11 seam (Webster Co.) at 410°C. C - Pittsburgh #8 seam (from METC) at 412°C. Open circles are experimental data; solid points are calculated by the three-parameter model (values given in Table 2).

Figure 1

Table 2

Characteristics of Three Isothermal Plastic Curves at 410-412°C

	Ohio #9 411°C	Kentucky #11 410°C	Pittsburgh #8 412°C
Melting slope	0.425	0.621	1.084
Coking slope	-0.216	-0.151	-0.125
Maximum fluidity, ddpm[1]	81	896	1.0×10^{6}
Time of maximum fluidity[1]	14.3_4	15.4_2	15.7_5
Calculated values:[2]			
k(init)	6.0×10^{-4}	4.3×10^{-5}	3.4×10^{-8}
k(melt)	0.77	0.79	1.24
k(coke)	0.35	0.16	0.125

[1] By extrapolation of melting and coking slopes.
[2] Using the three-parameter model described in text. Dimensions of k(init) and k(coke) are min^{-1}; k(melt) is min^{-1} mass $fraction^{-1}$.

- -

Table 3

Effect of Temperature upon the Isothermal Plastic Curves of Kentucky #11 Seam Coal (400-460°C)

Temperature, °C	400.	410.	425.5	440.	449.9	460.
Melting slope	0.172	0.621	1.35	1.60	2.57	$5._3$
Coking slope	-0.069	-0.151	-0.325	-0.67_9	-1.11	-1.5_6
Maximum fluidity, ddpm[1]	44	896	2.58E4	3.34E4	8.89E4	2.21E6
Time of maximum fluidity[1], min.	25.8_2	15.4_2	11.1_4	8.1_2	6.3_0	4.1_3
Calculated values:[2]						
k(init)	1.2E-3	4.3E-5	1.9E-6	3.0E-6	6.5E-7	4.3E-7
k(melt)	0.26	0.79	1.74	2.49	4.05	$7._1$
k(coke)	0.083	0.158	0.339	0.84_8	1.40	1.6_6

[1] By extrapolation of melting and coking slopes.
[2] See Table 2, footnote 2.

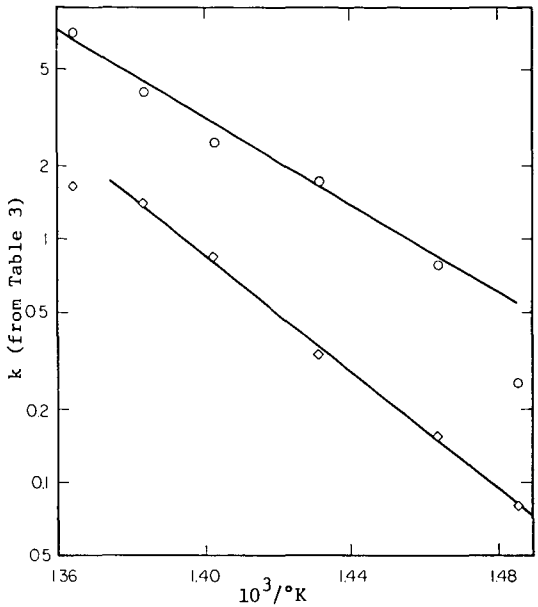

Figure 2. Arrhenius dependency of the model constants k(melt) (circles) and k(coke) (diamonds) for Kentucky #11 seam coal

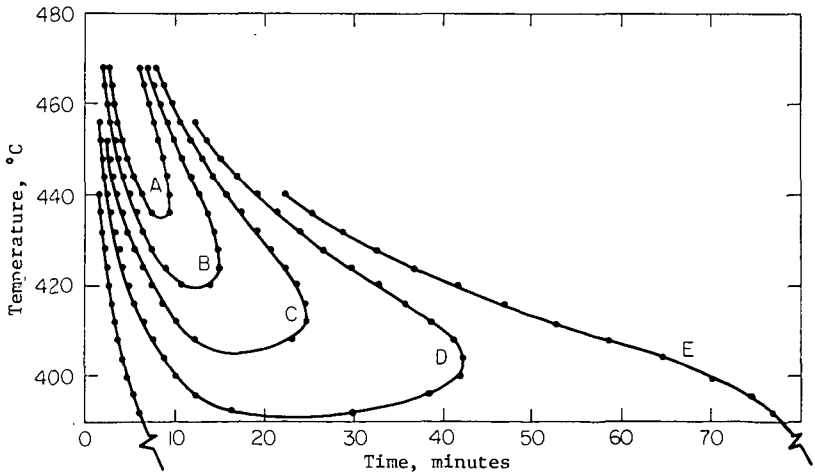

Figure 3. Isothermal fluidity envelopes for Kentucky #11 seam coal
A - 10^4 ddpm. B - 10^3 ddpm. C - 10^2 ddpm. D - 10 ddpm. E - 1 ddpm